Overexpression, Purification and Characterization of Potential Iron-Trafficking Proteins from a Phenol-Degrading Pseudomonad

Amy Ho Yee Wong

A Thesis

in

The Department

of

Chemistry and Biochemistry

Presented in Partial Fulfillment of the Requirements

for the Degree of Master of Science (Chemistry and Biochemistry) at

Concordia University

Montreal, Quebec, Canada

April 2006

Your file Votre référence
ISBN: 0-494-14232-4
Our file Notre référence
ISBN: 0-494-14232-4

Abstract

Overexpression, Purification and Characterization of Potential Iron-Trafficking Proteins from a Phenol-degrading Pseudomonad

Amy Ho Yee Wong

Frataxin is a small protein implicated in intracellular and mitochondrial iron trafficking. Some studies of frataxin have suggested that it can act as an iron donor for iron-sulfur cluster assembly and heme assembly. We are interested in iron-binding proteins involved in phenol degradation by *Pseudomonas sp.* strain CF600, and the possible involvement of frataxin and other proteins in their assembly.

One of the goals of this research was to overexpress, purify, and to characterize the stability, metal iron binding properties, and subunit structure of CyaY, the frataxin homologue from *Pseudomonas sp.* strain CF600. *CyaY* was successfully overexpressed and CyaY purified to homogeneity using Fast-Flow DEAE-Sepharose, Sephacryl S-300HR Gel Filtration, and High-Performance Phenyl Sepharose chromatographies. Analytical ultracentrifugation studies indicated that CyaY exists mainly as a monomer and that it does not aggregate in the presence of Fe(II). Isothermal titration calorimetry results were consistent with the binding of 1 Fe(II) or 1 Mn(II) per monomer of CyaY, with Fe(II) binding with a higher affinity. These and other results were similar to the reported iron-binding properties of CyaY from *E. coli.* Additional studies showed that CyaY significantly retarded oxidation of Fe(II), helping to keep it available for incorporation into other proteins.

A second goal was to overexpress and purify a putative iron-sulfur protein (CyaZ) that is encoded in the *Pseudomonas putida* genome adjacent to CyaY. This was successfully

accomplished, and the resulting preparation appears to contain an iron-sulfur cluster. As was demonstrated for CyaY, CyaZ significantly retarded oxidation of Fe(II) in the presence of both proteins. CyaY and CyaZ are currently being tested for their ability to affect assembly of iron-containing proteins involved in phenol degradation.

Acknowledgements

First and foremost, I would like to take this opportunity to thank my M. Sc. supervisor Dr. Justin Powlowski for his patience and guidance throughout these two years. His endless advice and insights have helped me develop a foundation that will guide me through the rest of my life journey.

I am grateful for having Dr. Paul Joyce and Dr. Joanne Turnbull as my committee members who were eager to give valuable suggestions for my project.

I would also like to thank my labmates Dr. Lena Sahlman and Yu Lei who were always prepared to help when asked.

Special thanks to my parents, sister and Connie Wong for their undying support.

Last, but not least, Bonny Choy for being a true best friend for 13 years through both thick and thin times.

Table of Contents

Materials and Methods

Results

List of Figures

List of Tables

List of Abbreviations and Symbols

ACN: Acetonitrile

Ala: Alanine

Asn: Asparagine

Asp: Aspartate

Arh1: Putative ferredoxin reductase

AUC: Analytical ultracentrifugation

BCA: Bicinchoninic acid

BIPY: α,α'-Bipyridine

BSA: Bovine serum albumin

cDNA: Complementary Deoxyribonucleic Acid

$CaCl_2$: Calcium chloride

CD: Circular dichroism

2'-CMP: Cytidine 2'-monophosphate

$CoCl_2$: Cobalt (II) chloride

CyaY: *E. coli* frataxin

CyaZ: Putative iron-sulfur protein

Cys: Cysteine

DNA : Deoxyribonucleic Acid

DnaK: *Escherichia coli* heat shock protein

DnaJ: *Escherichia coli* heat shock protein

Dps: DNA-binding proteins from starved cells

DTT: Dithiothreitol

E.coli: Escherichia coli

EDC: 1-Ethyl-3-(3-dimethylaminopropyl)carbodiimide Hydrochloride

EDTA: Ethylenediaminetetraacetic acid

EMPO: 5-ethoxycarbonyl-5-methyl-1-pyrroline-*N*-oxide

EndA1: Endonuclease deficient

EPR: Electron paramagnetic resonance

ESI-MS: Electrospray ionization mass spectrometry

FA: Formic acid

Fdx: Ferredoxin

Fe^{2+}: Iron(II)

Fe^{3+}: Iron(III)

$FeCl_3$: Iron (III) chloride

$Fe(NH_4)_2(SO_4)_2 6H_2O$: Ferrous ammonium sulfate hexahydrate

FRDA: Friedreich's ataxia

Fxn: Frataxin

Glu: Glutamic acid

Gln: Glutamine

Gly: Glycine

Gu·HCl: Guanidine hydrochloride

H: Helix

H_2O_2: Hydrogen peroxide

HCl: Hydrochloric acid

HEPES: 4-(2-hydroxyethyl)-1-piperazineethanesulfonic acid

His: Histidine

Hfra: Human frataxin

HscA: Homolog of Hsp70 chaperone (encodes chaperone Hsp66)

HscB: Encodes co-chaperone Hsp20

Ile: Isoleucine

IPTG: Isopropyl-1-thio-β-D-galactopyranoside

IscA: Iron-sulfur cluster assembly protein

ISC: Iron-sulfur cluster

IscS: Cysteine desulfurase

IscU: Iron-sulfur cluster scaffold protein

Isu1/Isu2: Scaffold protein

Isu1p: Putative scaffolding protein

ITC: Isothermal titration calorimetry

Jac1: Mitochondrial J-type chaperone

K_d: Dissociation constant

KCl: Potassium chloride

KOH: Potassium hydroxide

Leu: Leucine

LB: Luria broth

LMW: Low molecular weight marker

Ssq1p: Chaperone protein

m-fxn: Mature frataxin

MALDI : Matrix assisted laser desorption ionization

$MgCl_2$: Magnesium chloride

$MnCl_2$: Manganese (II) chloride

$MnSO_4 \cdot 4H_2O$: Manganese (II) sulfate tetrahydrate

MS: Mass spectrometry

MW: Molecular weight

NaCl: Sodium chloride

NADH: Nicotinamide dinucleotide

$Na_2S_2O_4$: Sodium dithionite

NATA: N-acetyl-L-tryptophanamide

NAYA: N-acetyl-L-tyrosinamide

Nfs1: Cysteine desulfurase

NMR: Nuclear magnetic resonance

OH: Hydroxide

$OH^{\cdot}$: Hydroxyl radical

pI: Isoelectric point

PCR: Polymerase chain reaction

Pro: Proline

Q-ToF: Quadrupole Time-of-Flight

RE: Restriction enzyme

RecA1: Recombination deficient

RNA: Ribonucleic Acid

ROS: Reactive oxygen species

S: Strand

SDS-PAGE: Sodium dodecyl sulfate-polyacrylamide gel electrophoresis

Ser: Serine

Ssq1: Mitochondrial Hsp70-type molecular chaperone

TBE: Tris base-Borate-EDTA

TCA: Trichloroacetic acid

TCEP: Tris(2-carboxyethyl)phosphine

Thr: Threonine

Tris: Tris(hydroxymethyl)aminomethane

Trp: Tryptophan

Tyr: Tyrosine

UV: Ultraviolet

Val: Valine

Vis: Visible

Yah1: Putative ferredoxin

Yfh1: Yeast frataxin

Introduction

The intracellular distribution of metal ions is an important process that is increasingly found to be carried out by proteins that sequester and distribute metal ions to their ultimate destinations. Although bacterial iron import and storage is reasonably well understood, there are many aspects that are unclear in the distribution of iron to sites in metalloproteins (*1, 2*). Free iron in cells is problematic for a number of reasons. Fe(II) oxidizes to produce toxic reactive oxygen species (ROS), and Fe(III) forms insoluble oxides (*2, 3*). Iron also has a tendency to bind tenaciously to biomolecules, so that it has a hard time finding its way to target proteins. *E. coli* synthesizes a number of proteins, which have been implicated in intracellular iron metabolism (*4-6*).

Dps, bacterioferritin and ferritin are known to sequester and regulate iron in bacterial systems (*4-6*). They are composed of 12 (Dps) or 24 (ferritin and bacterioferritin) identical subunits that assemble to form a 24-mer spherical protein shell which surrounds a central cavity where iron is stored. These iron storage proteins take up ferrous iron and deposit the iron in the ferric form in the central core; bacterioferritin contains heme in addition to iron oxides (*2*). The iron storage cavities of ferritin and bacterioferritin can accommodate up to 4500 iron atoms (*7, 8*). Ferritin and bacterioferritin are both expressed in bacterial cells, although bacterioferritin is more common than ferritin. They are synthesized to store iron when there is a high iron concentration inside the cells and when iron is readily accessible in the environment (*9*). Ferritin and bacterioferritin both donate stored iron when required, although the donation process is not clearly defined. Mutants that lack ferritin and bacterioferritin stop growing when iron is scarce, in contrast to cells expressing wild-type ferritins which continue to grow (*10*). The mutants are also more sensitive to oxidant. Dps

proteins are non-specific DNA-binding proteins from starved bacterial cells that accumulate to high levels under nutritional and oxidative stress conditions (*11, 12*). Dps proteins are believed to play a central role in binding DNA and sequestering iron in response to oxidative conditions.

Although iron storage proteins are quite well characterized, less is known about how iron gets from storage into metallocenters that require it. A relative newcomer in the area of intracellular iron trafficking is a protein called frataxin. Frataxins are low molecular weight proteins that have been demonstrated in the past few years to play important roles in assembly of iron into metallocenters of various proteins.

I. *In Vivo* Studies of Frataxin

I.1. Defective Frataxin Causes Friedreich's Ataxia

It has been known for many years that defects in human frataxin, a small mitochondrial protein, are associated with the progressive neurodegenerative disease, Friedreich's ataxia (FRDA) (*13, 14*). Frataxin normally is present in the highest concentrations in the spinal cord, dorsal root ganglia and the heart, all tissues that are highly dependent on oxidative respiration. Friedreich's ataxia is the most commonly inherited recessive ataxia, and strikes 1 in 50 000 people (*15*). The disease is associated with the expansion of the GAA trinucleotide repeat in the first intron of the gene χ25 on human chromosome 9q13 (*13, 14, 16-18*). This repeat reduces the levels of frataxin available, leading to problems such as degeneration of large sensory neurons and spinocerebellar tracts, cardiomyopathy, progressive gait and limb ataxia, dysarthria, pyramidal weakness of the legs, increased probability of diabetes and premature death (*19-25*). Numerous studies have implicated human frataxin in iron homeostasis (*21, 23*).

I.2. Frataxin Deficiencies Have Been Studied in Human Cells, Mammals, Yeast and Bacteria

Deficiencies in frataxin have been studied in several different cell types and linked to mitochondrial dysfunction and increased sensitivity to oxidative stress. FRDA-CH individuals contain one allele with a GAA expansion and a point mutation on the other allele. FRDA-CH lymphoblasts lacking frataxin expression were found to be more sensitive to oxidative stress (*26*). Transfection with cDNA encoding human frataxin restored frataxin to near-physiological levels and returned sensitivity towards oxidant to a normal level. In mice, frataxin knockouts die during early embryonic life, indicating that frataxin is necessary for normal development (*27-29*). In yeast, the frataxin gene, *YFH1*, was knocked out to create a strain that showed a severe growth defect on fermentable carbon sources despite a high iron concentration in the medium (*30, 31*). This strain, Δ*yfh1*, was unable to grow on medium containing ethanol and glycerol as the carbon source which suggests that it cannot carry out oxidative phosphorylation. The deletion of *YFH1*, resulted in an accumulation of mitochondrial iron and in hypersensitivity to oxidant (*30*). Together, these data indicate that *YFH1* is involved in mitochondrial function (*32-34*).

The importance of frataxin to bacteria is less well established. CyaY is the frataxin orthologue in *E. coli*, and the corresponding gene has been knocked out by homologous recombination. Somewhat surprisingly considering the results with yeast and human cells, the *cyaY* knockout did not appear to affect the intracellular iron concentration or sensitivity to oxidants (*35*). This suggests that CyaY proteins in bacteria could have a different function from other frataxin orthologues despite the fact that they share many structural similarities.

I.3. Phylogenetic Evidence Suggests CyaY is Involved in Iron-Sulfur Cluster Assembly

Sequencing of genomes makes it possible to deduce the possible functions of a protein using comparative genomic analysis (*36*). *CyaY* seems to have identical phylogenetic distribution as *hscA* and *hscB/JAC1 (37).* This suggests a role for *cyaY* in the assembly of iron-sulfur proteins since *hcsA* and *hscB/JAC1* in bacteria are part of the iron-sulfur cluster (*isc*) assembly operon. In *E. coli*, this operon encodes nine proteins: IscA, IscS, IscU, HscA, HscB, fdx (2Fe-2S ferredoxin), a hypothetical RNA methylase (EC2532), a hypothetical helix-turn-helix containing transcriptional regulatory protein (EC2531), and a hypothetical protein (EC2524) (*38*).

Biosynthesis of iron-sulfur proteins in eukaryotes is assisted by a corresponding set of conserved components located in mitochondria (*39*). The ISC-assembly machinery requires Isu1/Isu2 (scaffold protein), that bind Fe(II), and Nfs1 (cysteine desulfurase) which supplies the sulfur for *de novo* synthesis of iron-sulfur clusters. Other proteins such as ferredoxin Yah1, ferredoxin reductase Arh1, DnaK, DnaJ, Ssq1 and Jac1 also play essential roles in the complex assembly machinery of the ISC. Interactions of the yeast frataxin homologue with components of the ISC machinery have been studied using pure proteins and will be discussed in more detail later (*39*).

I.4. Molecular Functions of Frataxin and its Orthologues

In addition to roles in iron-sulfur cluster assembly and repair, frataxin has also been implicated in heme assembly as well as maintaining intracellular iron in a soluble, nontoxic and bioavailable form (*23, 40, 41*). Much of the evidence for these functions comes from experiments using purified proteins and their interaction(s) with iron in various forms.

Thus, the next section will review the structural properties of frataxin orthologues and possible structural insights into iron binding properties and potential interactions with other proteins.

II. Structures of Frataxin Orthologues

II.1. Primary Amino Acid Sequence Comparison of Frataxin Orthologues

Frataxins are proteins that are conserved throughout evolution, from bacteria to humans (Fig. 1) (*42-45*). The percent identities of CyaY from *E. coli* to frataxins from selected organisms are summarized as follows: CyaY from *Yersinia pestis* (71%) (*46*); CyaY from *Yersinia intermedia* (71%) (*46*); CyaY from *Erwinia chrysanthemi* (68%) (*47*); CyaY from *Haemophilus influenzae* (46%) (*48*); yeast frataxin (34%) (*49*); CyaY from *Rickettsia prowazekii* (29%) (*50*); mouse frataxin (26%) (*27*); frataxin from *Schizosaccharomyces pombe* (26%) (*51*); human frataxin (25%) (*52*). Frataxin has little amino acid sequence conservation with other known proteins that are involved in iron or heme metabolism.

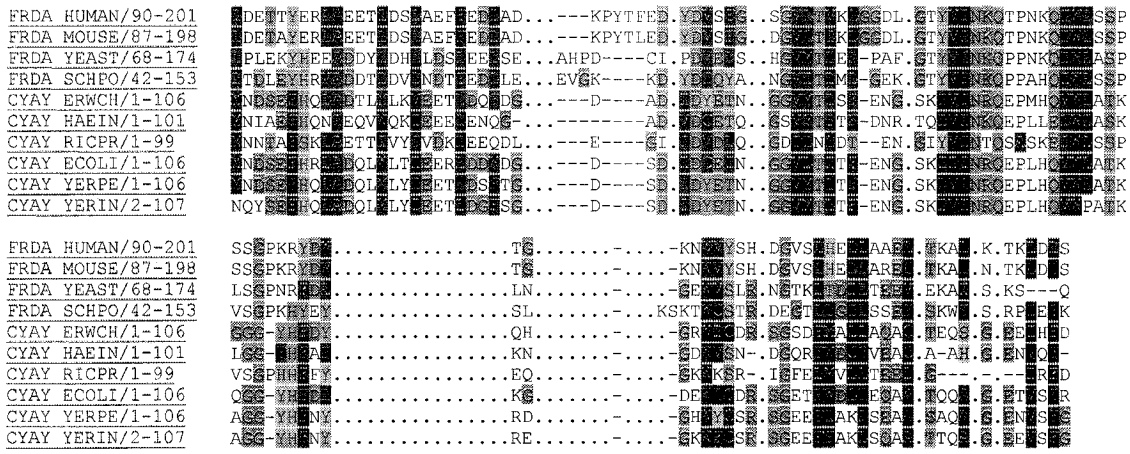

Figure 1: Sequence alignment of 10 members of the frataxin family generated using Pfam. Alignments were created by Jalview. Orange: (G); yellow: (P); blue: small or hydrophobic amino-acids (A, V, L, I, M, F, W); green: hydroxyl and amine amino-acids (S, T, N, Q); red: charged amino-acids (D, E, R, K); cyan: (H) and (Y). Dashes indicate gaps to better align the amino acids at these positions whereas dots correspond to absence of amino acids at these positions.

II.2. Three-Dimensional Structures of Frataxin Orthologues

There are three published three-dimensional structures of frataxin: *E. coli (43),* human (*44*) and yeast (*53*). The structures of *E. coli* (*43, 45*) and human (*20, 44*) frataxins have been resolved using x-ray diffraction and NMR, whereas, only the NMR structure of yeast frataxin has been determined (*53*). Nuclear magnetic resonance (NMR) spectroscopy revealed well-defined resonances and dispersioned in the spectra for CyaY (*E. coli*) and Hfra (human) which indicates well–folded globular proteins in solution (*43, 44*). However, NMR studies of the yeast orthologue, Yfh1, indicated that well-dispersed, sharp resonances coexist with a dense overlapping cluster of poorly dispersed broad peaks at values that are expected for random coil conformations (*16*). Consequently, the solution structure of Yfh1 has regions that are not well resolved as compared to the other known structures of frataxins.

II.2.1. ***E. coli Frataxin (CyaY):*** The crystal structure of *E. coli* CyaY has been determined at 1.4 Å resolution (*43, 54*). It consists of 6 consecutive anti-parallel β-strands ((S1) residues 30-35, (S2) residues 38-43, (S3) residues 48-53, (S4) residues 60-63, (S5) residues 69-73, and (S6) residues 78-80), flanked by a long N-terminal α-helix and a shorter C-terminal α-helix (Fig. 2) (*45*).

Knowledge of the tertiary structure makes it possible to locate the positions of conserved residues and possible iron binding sites. Comparison of the primary amino acid sequences of three frataxin orthologues (Hfra, Yfh1 and CyaY) shows that there are 17 invariant residues (*43*). The invariant residues are: Ala10, Asp31, Gly37, Val38, Thr40, Ile51, Asn52, Gln54, Pro56, Gln59, Trp61, Leu62, Gly67, Asp72, Trp78, Gly84 and Leu91 (using the numbering of the CyaY sequence) (*43*). When CyaY is aligned with 10 members of the frataxin family (Fig. 1), seven of the seventeen residues are conserved: Asp31, Ile51, Asn52,

Gln54, Trp61, Gly67, and Trp78. Of these, the hydrophobic core contains residues Ile51 and Trp78 while the other 5 conserved residues are located on the surface and exposed to the solvent.

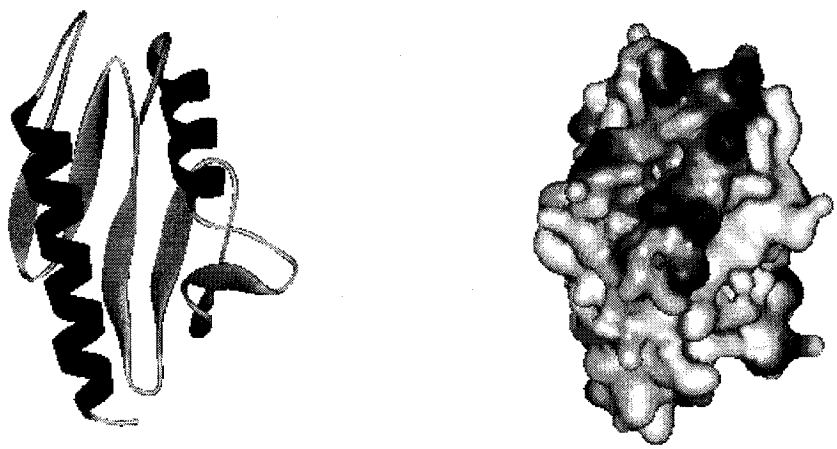

Figure 2: Ribbon structure of CyaY (PDB code: 1EW4), helix red and strand blue (left). Electrostatic potential surface of CyaY (right). Acidic residues are red and basic residues are blue. Structures were created using Swiss-PDB (*55*) and WebLab Viewers (*56*) .

NMR spectroscopy was used to probe the potential binding site of iron to CyaY (*45*). The amide resonances of Arg20, Leu21, Asp22, and Asp23 vanished at an Fe^{2+}:CyaY ratio of 1:1 (*45*). When the ratio was increased from 1:1 to 2:1, more peaks shifted and broadened. The strong perturbation of resonances for residues 20-23 suggested the occupancy of the Fe(II) binding sites and perturbations seen in other areas indicate the transient population of secondary Fe(II) binding sites. When the Fe^{2+}:CyaY ratio was increased to 6:1, the spectrum was perturbed further with disappearance and broadening of additional residues. Upon titrating CyaY with Fe(III), the same three amino acid residues (Arg20, Asp22 and Asp23), were affected. The peaks continued to broaden upon addition of higher amounts of Fe(III). It thus can be deduced that CyaY can bind both Fe(II) and Fe(III) using the same region on the protein surface. The surface of the protein is mostly

negatively charged with an overall pI of 4.2, and therefore can mediate the role in binding to the positively charged iron ions (Fig. 2).

The CyaY fold has no significant similarity to any other known iron binding protein (*45*). A unique attribute of the CyaY structure (Fig. 2), shared with other frataxin orthologues is that, unlike some other non-heme iron binding proteins, it does not appear to enclose any cavities or hydrophilic pockets to which iron can be bound or stored. The CyaY structure is highly asymmetric in charge distribution and although the α-helical side is negatively charged, there are no negative charges on the β-sheet side. This structural feature suggests that the β-sheet of CyaY may be involved in protein-protein interactions (*45*).

II.2.2. ***Human Frataxin (Hfra):*** Hfra is expressed in the cytoplasm as a larger precursor that is cleaved upon entering the mitochondrion to generate a mature protein (mHfra, residues 88-210) (*44*). The Hfra structure is a compact αβ sandwich (Fig. 3). It consists of five antiparallel β-sheets flanked by two parallel α-helices and a second smaller β-sheet between the C-terminus of β5 and strands β6 and β7. Elements of secondary structure and the core structure of Hfra are very similar to those of CyaY from *E. coli.* Hydrophobic side chains such as Leu198, Leu200 and Leu203 of the C-terminal tail of Hfra point inwards toward the hydrophobic core, probably playing a significant role in stabilizing the protein (*44*). The hydrophobic core itself is dominated by aromatic residues (Trp173 surrounded by Tyr95, Trp168 and Tyr205). There is a grouping of twelve acidic amino acid on the surface of Hfra that forms an anionic patch, with a pI of 4.72 for the complete structure (*20, 44*). The clustering of the twelve acidic amino acids residues resembles the surface of the well-known iron storage protein ferritin (*8, 57*). Since Hfra binds iron, it possibly does so by first

assembling with itself or other mitochondrial proteins to use the anionic patch as is observed with ferritin (*57*).

Hfra crystals were soaked in ferrous sulfate and ferric chloride to establish whether iron binds to Hfra. X-ray diffraction data revealed that one iron (Fe(II) and Fe(III)) atom can bind per Hfra via His177: the iron appears to have displaced a water molecule to form a 2.08 Å bond to N^{ε} of His177 (*44*). The Fe(II) or Fe(III) is also bound very loosely (>4 Å) to the backbone carbonyl oxygen of Ala114, Asp115, and to the carboxylate side chain of Asp115 of an adjacent molecule. The His177 is not a conserved residue in the CyaY protein sequence and is not close to the potential iron-binding region of residues 20-23 in CyaY. The His177 residue is highly exposed to the solvent and does not interact with the acidic patch of twelve amino acids. The outer surface of the β-sheet is highly conserved among the known eukaryotic frataxins and as with CyaY, is predicted to mediate protein-protein interactions (*44*).

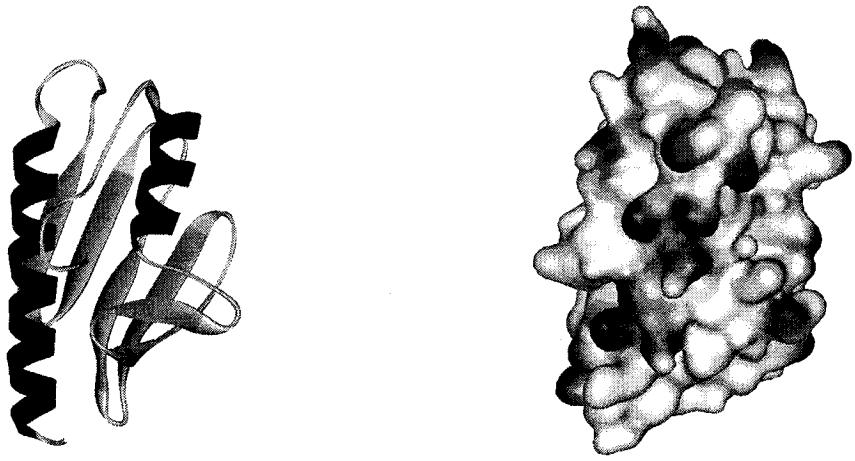

Figure 3: Ribbon structure of Hfra (PDB code: 1EKG), helix red and strand blue (left). Electrostatic potential surface of Hfra (right). Acidic residues are red and basic residues are blue. Structures were created using Swiss-PDB (*55*) and WebLab Viewers (*56*).

II.2.3. ***Yeast Frataxin (Yfh1):*** The solution structure of yeast frataxin also shows an αβ-sandwich motif, with molecular dimensions very similar to those of CyaY and Hfra (Fig. 4). Yfh1 has an overall acidic pI of 4.34, and the surface is mainly composed of acidic residues such as Asp and Glu, which are particularly concentrated in the H1-S1 interface.

The addition of Fe(II) to NMR samples of Yfh1 under strict anaerobic conditions at a ratio of 2:1 Fe(II) to protein led to broadening of amide line widths, which indicated either that protein oligomerization occurred or the iron bound nonspecifically to the protein (*53*). These results are consistent with the observation that Yfh1 assembles to a multimer of ~1.1 MDa in the presence of iron atoms (*58*). These analyses are also consistent with previous observations of weak iron binding affinity to both human and yeast frataxin with K_d of 55 μM and 3.8 μM, respectively (*23*). In summary, the acidic H1-S1 interface gives the yeast frataxin quite a negatively charged surface that makes it a good candidate to bind to positively charged iron(II). The iron-binding site thus appears to be different in all three orthologues, which could be consistent with different mechanisms for regulating cellular iron.

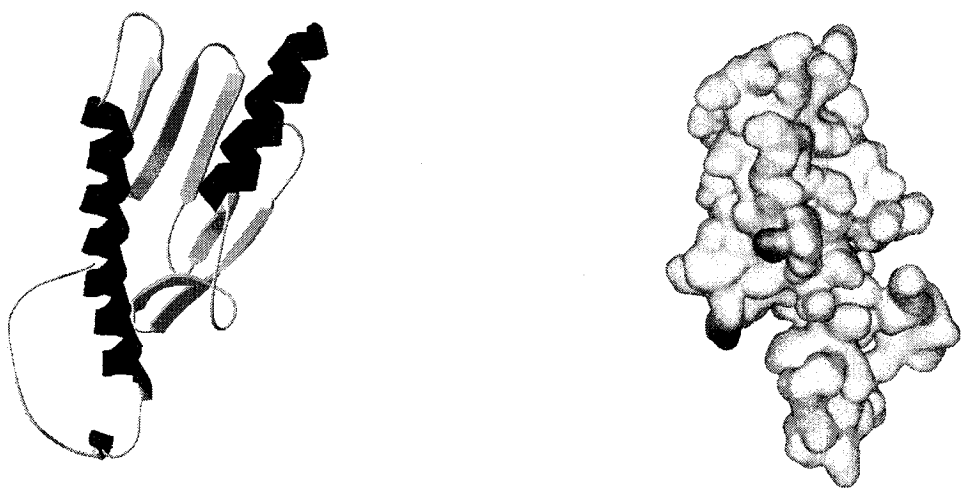

Figure 4: Ribbon structure of Yfh1 (PDB code: 1XAQ), helix red and strand blue (left). Electrostatic potential surface of Yfh1 (right). Acidic residues are red and basic residues are blue. Structures were created using Swiss-PDB (*55*) and WebLab Viewers (*56*).

III. Structural Stabilities of Frataxin Orthologues

The three orthologues (Hfra, Yfh1 and CyaY) have been characterized for their thermal stability using circular dichroism to monitor unfolding. Although the three orthologues have similar secondary and tertiary structures, they exhibit distinctive thermal denaturation curves. Thus, CyaY, Hfra, and Yfh1 display melting points of 50.1 ± 0.7°C, 69.4 ± 0.04°C and 35.8 ± 1.2°C, respectively (*16, 42*).

Structural contributions to the stabilities of the three frataxin orthologues have been examined in some detail (*16*). The length of the C-terminal end of the protein appears to have a significant effect on the stability. Mature human frataxin, the most thermally stable frataxin orthologue, has the longest N- and C-termini in comparison to the other two orthologues: Hfra has the longest C-terminus, followed by CyaY and Yfh1. As mentioned above, the C-termini of Hfra and CyaY insert into the groove between helices 1 and 2, whereas the C-terminal tail of Yfh1 is too short to do so. Leu198 and Leu200 of Hfra are two conserved hydrophobic residues near the C-terminus end of the protein that are missing in the Yfh1 sequence. These two hydrophobic residues anchor the C-terminus of Hfra to the groove by positioning directly into the hydrophobic core, thus providing a stabilizing effect (*16*). By contrast, the amino-terminus of Hfra appears to be involved in subunit-subunit interactions (*59*). CyaY from *E. coli* is less stable than Hfra since additional stabilizing hydrophobic residues Leu203 and Tyr205 are missing from the CyaY sequence. However, a number of structural features help to stabilize the tertiary structure of CyaY (*45*). The last seven C-terminal residues insert into the groove between H1 and H2 to help form a well ordered hydrophobic core. Salt bridges between Arg8 and Arg11 and between Arg106 and Glu77/Asp89 contribute to additional stability of the overall fold. Trp14 and Trp88 also form stabilizing interactions with nearby Arg53 and Arg20/Arg106. Yfh1 lacks these

hydrophobic residues in this region, which renders it the least stable structure among the three orthologues.

IV. Quaternary Structures of Frataxin Orthologues in the Absence of Iron

Frataxin homologues exist in different oligomeric forms that are correlated with the presence or absence of iron. In the absence of iron, the monomer usually predominates. Sedimentation velocity/equilibrium measurements of CyaY in the absence of iron showed a molecular mass of 12.5 kDa, consistent with a monomer (*40*). A molecular weight of 17 kDa for the mitochondrial (mature) form of Hfra (m-Hfra) was estimated using SDS-PAGE. The protein was purified using ion-exchange chromatography, which yielded two different m-fxn fractions, of which one (~17 kDa, as estimated by Superdex 200 gel filtration) eluted at low salt concentration and the other (>60 kDa, as estimated by Superdex 200 gel filtration) at high salt concentration (relative amounts of each forms were not reported) (*23, 60*). Electrospray ionization mass spectrometry (ESI-MS) confirmed that the predominant species is 17 252 Da in the low molecular weight pool (does not assemble), which is consistent with the full-length mature form of Hfra with the N-terminal methionine cleaved off during expression in *E. coli*. ESI-MS detected a second species of 14 663 Da in the low molecular weight pool, indicating some proteolysis of m-Hfra. The high molecular weight pool is an assembled form of Hfra. Yfh1 is originally translated in the cytoplasm as a larger precursor protein, which is then imported into mitochondria to yield the mature Yfh1. The purified protein expressed in *E. coli* had a molecular mass of ~20 kDa, as estimated by SDS-PAGE, but microelectrospray ionization mass spectrometry indicated a mass of 13 783 Da which is the molecular mass expected for mYfh1 (*61*). Superdex-200 gel filtration column chromatography indicated a molecular mass of ~18 kDa, consistent with a monomer.

V. Iron Binding Properties of Frataxin Orthologues

Extensive studies have been carried out on different frataxin orthologues using isothermal titration calorimetry (ITC) and ultrafiltration techniques to examine iron binding. It was shown using anaerobic ITC that CyaY monomer binds two ferrous ions/monomer with a dissociation constant of 3.8 μM (*40*). Additional weak binding sites for Fe(II) on CyaY have been detected in ultrafiltration experiments, but the much weaker binding affinities make it difficult to accurately determine stoichiometry and binding affinity for Fe(II) (*40*). Nonetheless, CyaY is believed to bind Fe(III) with a stoichiometry of 1:6 protein to iron ratio at the first stage of iron oxidation, which could probably lead to the sequestration of up to 26 Fe(III) atoms per monomer of CyaY (*40*).

Iron binding to Hfra has been quantitated using ITC, yielding K_d=10.2 μM (6.5 Fe^{3+}:Hfra), and using fluorescence titration, yielding K_d=11.7 μM (6.4 Fe^{3+}:Hfra) and K_d=55.0 μM (6.4 Fe^{2+}:Hfra) (*23, 62*).

Isolated mYfh1p (mature yeast frataxin) monomers contained no iron, but the addition of ferrous iron resulted in assembly of a multimer (1.1 MDa) that can take up over 3000 atoms of iron in a nonspecific, soluble and stable form (*61*). The yeast frataxin orthologue thus displays ferritin-like behaviour *in vitro* in the presence of a large excess of iron (*61*). Iron binding is observed only at very low ionic strength and is competed out at salt concentrations that are close to physiological conditions (*16*). Therefore, the ability to bind iron and the stability of the structure is influenced by ionic strength.

V.1. Quaternary Structure Changes in the Presence of Iron

Gel filtration and other experiments have been conducted to investigate quaternary structure changes accompanying iron binding to the three frataxin orthologues, CyaY, Hfra

and Yfh1 (*42*). In the absence of iron, the three proteins showed a single peak at a position that corresponded to a monomer. After incubating under aerobic conditions with Fe^{2+}:protein at a ratio of 20:1, Hfra showed no tendency to aggregate except under extreme conditions such as incubation at 57°C in the presence of 20-fold excess of ferrous ammonium sulfate (*42*). On the other hand, Yfh1 and CyaY formed high molecular weight aggregates in the presence of a 20-fold excess of ferrous ammonium sulfate (*58, 61*).

The CyaY samples exhibited three peaks: a monomer, intermediate and high-molecular weight species depending on the relative ratio of iron to protein. At a ratio of 1:1 Fe^{2+}:CyaY, CyaY was mainly in the monomer form with a minute amount of intermediate species being detected. When the ratio of Fe^{2+}:CyaY increased further to 40:1, the high molecular weight peak sharpened with the disappearance of both the monomer and intermediate species. CyaY precipitated out of solution at a ratio of 60:1 of Fe^{2+}:CyaY. When CyaY was titrated with $FeCl_3$ instead, the formation of the high molecular weight aggregate was detected, but the titration lacked the intermediate species, suggesting that a different kinetic mechanism occurs in the presence of ferric ions (*42*). Although aggregation occurred upon addition of Fe(II) and Fe(III) to CyaY, it did not seem to affect the secondary or tertiary structures of CyaY, as monitored using far-ultraviolet CD spectroscopy (*42*).

Another question of interest is whether other cations can bind and compete with iron for CyaY. Ca(II) was found to reduce CyaY aggregation, suggesting that Ca(II) can compete with Fe(II) for the same binding site on CyaY (*16, 40*). There was also a strong stabilizing effect of Ca(II) on the thermal stability of CyaY. Aggregation itself seems to be iron-specific, although Al(III) and Co(II) appeared to have a minor ability to cause aggregation (*42*). Aggregation was also studied using competition experiments with citrate and EDTA, two known chelators of Fe(II) (*42*). When citrate was incubated with Fe(II) at

the same time, the protein remained as a monomer which implies that aggregation can be competed out with chelators.

Recombinant yeast frataxin (mYfh1) was incubated with excess Fe(II) and analyzed on a Superdex-200 gel filtration column (*61*). Recombinant yeast frataxin existed in a monomer form in the absence of Fe(II), but converted into a high-molecular weight species in the presence of excess Fe(II) under aerobic conditions. This observation was seen with $Fe(NH_4)_2(SO_4)_2$. Incubation with $CaCl_2$, $CoCl_2$, $MgCl_2$ or $MnCl_2$ did not cause any self-association of mYfh1. As the concentration of Fe^{2+}:mYfh1 was increased from 1:1 to 20:1, the monomer peak intensity decreased and the high-molecular weight species (~1.1 MDa) increased. Analytical ultracentrifugation experiments (sedimentation equilibrium) confirmed the presence of two predominant forms, which contain 6 and 60 mYfh1 subunits per macromolecule, respectively (*61*). Electron micrographs and atomic force spectroscopy showed that the 1.1 M Da multimer is a regular spherical particle (*61*). It has been proposed that the iron-dependent self-assembly of mYfh1 suggests a physiological role in mitochondrial iron sequestration and bioavailability (*61*).

V.2. Yeast Frataxin Couples Protein Assembly with Iron Oxidation

In *in vitro* studies, the mature forms of yeast frataxin homologues have a distinctive mechanism to regulate iron oxidation and availability. It has been suggested that there is stepwise assembly of mYfh1 into a multimer with the following mechanism: $\alpha_3 \rightarrow \alpha_6 \rightarrow \alpha_{12} \rightarrow \alpha_{60}$. In this mechanism,Yfh1p assembly is first driven by a ferroxidase reaction ($\alpha \rightarrow \alpha_3$), followed by a slower autoxidation reaction that is associated with the assembly of oligomers (α_{48}) (*63, 64*). The following mechanism is the summary of yeast frataxin activation by Fe(II) and O_2 (Equation 1-2) (*65*):

Ferroxidation $2Fe^{2+} + O_2 + 2H^+ \rightarrow 2Fe^{3+} + H_2O_2$ (1)

Autoxidation $4Fe^{2+} + O_2 + 4H^+ \rightarrow 4Fe^{3+} + 2H_2O$ (2)

The assembled Hfra is believed to also have ferroxidase activity (*66*) but ferroxidase activity is absent in CyaY (*40*).

VI. Mutagenesis for Characterization of Surface and Iron-Binding Properties in CyaY

VI.1. ***Mutant Designed to Affect the Electrostatic Surface Potential of CyaY (CyaY-_181922):*** Site-directed mutants have been used to help identify the surfaces responsible for both aggregation and iron binding. Four variants of CyaY were designed and studied. In one variant, Glu18, Glu19, and Asp22 (CyaY_181922 triple mutant, the numbers represent the residue being changed) were changed to lysines with the intention of altering the electrostatic property of the protein surface (*42*). These mutations did not affect the tertiary structure of CyaY and this mutant was primarily in the monomeric form up to a protein to iron ratio of 1:20. Mutant CyaY_181922 had a thermodynamic stabilizing effect. This could be due to the introduction of the positively charged lysine residues in a negatively charged environment, thus triggering the formation of salt bridges (data not shown). This mutant remained monomeric up to an Fe^{2+}:protein ratio of 20:1 though a small amount of aggregation was observed at 10:1 estimated using calorimetry on column fractions. It was concluded from these observations that the conserved negatively charged patch involving Glu18, Glu19, and Asp22 is involved in iron binding and aggregation.

VI.2. ***Mutants Designed to Mimic Hfra Behavior and Iron Binding (CyaY_1833 and CyaY_776):*** Two other mutants were designed to affect residues that are common only to CyaY and Yfh1. Glu18 and Glu33 were converted to Ala and Ser (CyaY_1833) (*42*). The

purpose of introducing these two mutations was to try to mimic the behavior of the human protein, which has Ala and Ser at positions 18 and 33, respectively. Mutant CyaY_776 involved converting of His7 and Asp76 to lysines. These two residues are believed to be involved in iron binding (secondary iron binding site) (Fig. 5). The stabilities of Cya_776 and CyaY_1833 were lower than the stability of the wild-type protein. However, CyaY_1833 showed similar behaviour to CyaY_181922 such that aggregation was strongly diminished but not completely abolished. CyaY_776 had a propensity to aggregate even at low iron:protein ratio (1:1). The alteration of Glu18 and Glu33 seems to be adequate to eliminate the aggregation that was characteristic of Hfra. Mutant CyaY_776 incorporated the highest amount of iron among all the mutants, thus, this mutant appears to have affected the iron binding property.

VI.3. ***Mutant Designed to Affect a Conserved Residue in CyaY (CyaY_61):*** Mutant CyaY_61 was designed to convert Trp61 to an arginine. An American patient with Friedreich's ataxia was found to have a W155R mutation (*67*). This residue is highly conserved and exposed at the centre of the β-sheet surface. Mutant CyaY_61 (W61R), which is equivalent to W155R in Hfra, causes disruption of π-interactions between a positive charge and aromatic ring caused by the proximity of Arg, and also electrostatic repulsion between the two positively charged amino acids (*42, 67*). The properties of aggregation are indistinguishable between mutant CyaY_61 and the wild-type frataxin. It can be deduced from these observations that aggregation cannot be achieved by formation of an unstructured aggregate in which each monomer is surrounded by the others. There is an ordered spherical assembly of frataxin in the presence of iron, a property that is reminiscent of ferritin (*68*).

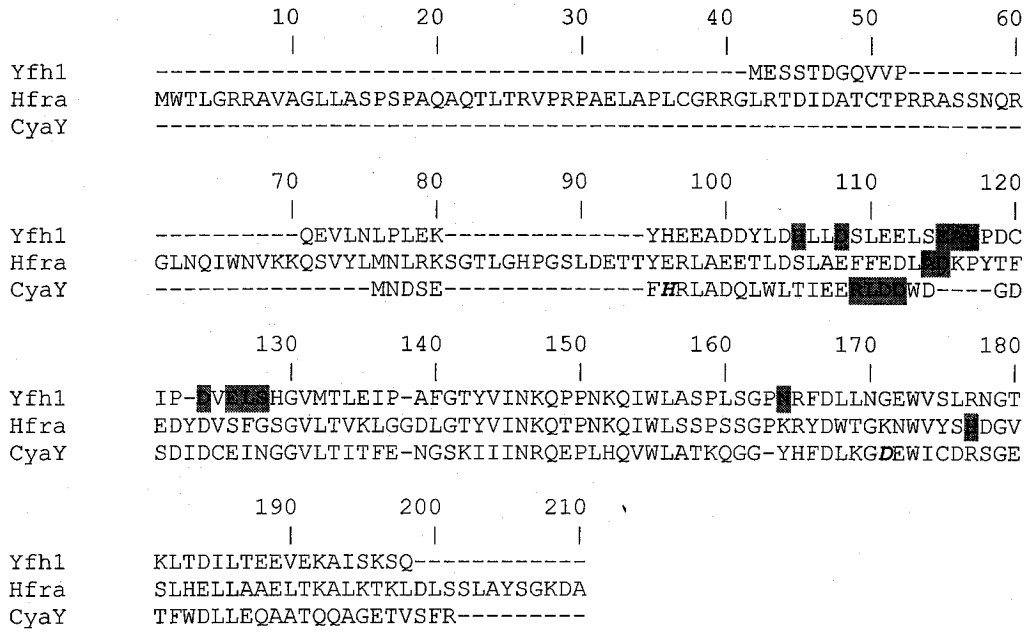

Figure 5: Sequence comparison of the primary and secondary iron binding sites of Yfh1, Hfra and CyaY using CLUSTALX (*69*). Primary binding sites (based on perturbation of resonances in NMR) are bolded and shaded. Secondary binding sites are bolded and italicized. It is clear that the iron binding sites are different for all three orthologues.

VI.4. Common Mutations in FRDA Patients

Clinically important mutants associated with Friedreich's ataxia have been studied to provide insight into the biochemical function of Hfra. The mutants D122Y, W155R and R165C are at the surface sites that affect severely the conserved surface residues of Hfra. Hfra with point mutations I154F or W155R were expressed in *E. coli.* The melting points of these variants were found to be lower than that of the wild-type protein, which suggests that these mutants were destabilized (*20*). I154F is the most common mutation occurring in several families and the mutation introduces steric hindrance at this position (*70, 71*). The I154F mutation significantly reduced the thermodynamic stability and refolding ability of the protein. These properties may lead to reduced amounts of functional Hfra in the cell due to the inability of the I154F mutant to refold properly after import into mitochondria. W155R was chosen because Trp155 is an exposed and extremely conserved residue. Both the

refolding pathway and ligand binding site has been disrupted in the W155R mutant, which could possibly explain the cause of the disease FRDA.

VII. Roles of Frataxin in Iron-Sulfur Cluster Assembly, Heme Biosynthesis, Iron Detoxification and Iron Bioavailability

Biochemical studies using purified proteins have provided evidence that frataxins play important roles in iron-sulfur cluster assembly, heme biosynthesis, and iron bioavailability. Defects in these processes would be expected to result in the kinds of symptoms observed *in vivo* (see above), such as mitochondrial dysfunction, iron accumulation and increased oxidative stress. For example, two non-related FRDA patients with hypertrophic cardiomyopathy exhibited complete cellular aconitase and mitochondrial iron-sulfur dependent respiratory chain (Complex I, II and III) enzyme deficiency in endomyocardial biopsies (*72, 73*).

VII.1. ***Iron-Sulfur Cluster Assembly:*** IscU for prokaryotes and ISU for eukaryotes are homologous families of proteins involved in assembly of [2Fe-2S] centers, which can then deliver the [2Fe-2S] centers to apo forms of iron-sulfur proteins. Complex formation between holo-Hfra (human frataxin with Fe(III) bound) and apo-human ISU was demonstrated using ITC and fluorescence quenching experiments (*23*). Holo-frataxin was obtained by addition of at least a 10-fold excess of ferric ion to the apo-protein, with excess iron removed by gel filtration chromatography. A K_d of ~0.15 μM between holo-frataxin and apo-human ISU was estimated using ITC. Apo-Hfra did not bind to apo-ISU, so it appears that the interaction is associated with delivery of iron from holo-Hfra to apo-ISU. The fluorescence emission of the three tryptophan residues in Hfra was strongly quenched

by the presence of both Fe(II) and Fe(III). Assembly of the iron-sulfur cluster on purified human ISU was achieved using holo-frataxin (6Fe(II) or 6Fe(III)) as the iron source and inorganic sulfide, resulting in formation of ~70% holo ISU.

Aconitase, which contains an iron-sulfur cluster, is a citric acid cycle enzyme that catalyzes the stereo-specific isomerization of citrate to isocitrate via *cis*-aconitase (*74*). Frataxin deficiency leads to accumulation of iron in mitochondria and reduced activity of a variety of mitochondrial iron-sulfur proteins including aconitase (*75, 76*). The $[4Fe\text{-}4S]^{2+}$ cluster of aconitase reacts directly with the enzyme substrate (*75, 76*). Purified aconitase is vulnerable to oxidant-induced inactivation due to the release of solvent-exposed Fe-α and formation of inactive $[3Fe\text{-}4S]^{1+}$ containing enzyme. Frataxin plays a role in protecting and stabilizing aconitase from cluster disassembly and acts as a donor of iron to the $[3Fe\text{-}4S]^{1+}$ cluster during pro-oxidant induced modulation of the aconitase activity.

VII.2. ***Heme Biosynthesis:*** Human frataxin was shown to donate iron to ferrochelatase and mediate the terminal step in mitochondrial heme biosynthesis (*62, 77, 78*). Human ferrochelatase is the terminal enzyme in the heme biosynthetic pathway, catalyzing the insertion of Fe(II) into protoporphyrin IX (*62, 74*). ITC experiments indicated complex formation between human ferrochelatase and human holo-frataxin (Fe(II)) with K_d = 17 nM. Fluorescence quenching experiments also showed that there is high affinity binding of holo-frataxin and ferrochelatase (*62*). Together, these experiments support a role for frataxin in recruiting iron and mediating its delivery to ferrochelatase.

VII.3. ***Iron Detoxification:*** EPR experiments were performed in order to determine the ability of CyaY to efficiently manage the toxicity of Fe(II) and H_2O_2 (Fenton chemistry) and

in protection against oxidative stress (*40*). The spin trap EMPO was used. Control experiments with EMPO + Fe(II) + H_2O_2 showed a stoichiometry of 1:1 H_2O_2/Fe(II) with an intense signal from trapped $OH^{\cdot}$ radical being observed. An intense EPR spectrum was also observed for another control experiment with albumin + EMPO+ Fe(II) + H_2O_2 with 6 Fe(II) binding per albumin (*40*). These results imply that iron(II) oxidation by H_2O_2 in the presence of albumin occurs via a two step process in which in the $OH^{\cdot}$ is trapped with EMPO before further Fe(II) can react (Equations 3-5):

$$Fe^{2+} + H_2O_2 \rightarrow Fe^{3+} + OH^- + OH^{\cdot} \quad (3)$$

$$Fe^{2+} + OH^{\cdot} \rightarrow Fe^{3+} + OH^- \quad (4)$$

Overall reaction: $$2\,Fe^{2+} + H_2O_2 \rightarrow 2Fe^{3+} + 2OH^- \quad (5)$$

On the other hand, upon incubation of CyaY with 6 Fe(II) or 20 Fe(II), the hydroxyl radical production was attenuated compared to buffer with 6 Fe(II) and albumin with 6 Fe(II) (*40*).

VII.4. ***Iron Bioavailability and Detoxification:*** The previous sections have reviewed evidence that frataxin interacts with proteins to which it apparently donates iron. More generally, different forms of frataxin appear to interact with iron and maintain it in a form that keeps it available for cellular processes and not non-specific side-reactions (*66*). Mature human frataxin assembles into a regular homopolymer during expression in *E. coli* and purified mature frataxin monomer is stable and does not associate into a multimer upon iron addition. Assembled mature frataxin (isolated from high-salt fraction when overexpressed in *E. coli (60)*) and monomer mature frataxin were analyzed for the ability to make Fe(II) bioavailable in the presence of oxygen and at neutral pH: these conditions normally promote the oxidation of Fe(II) to insoluble iron oxides (*66*). Calmodulin, a calcium binding protein, and apo-ferritin, a 24-subunit shell that promotes iron oxidation and mineralization were

used as controls. Bipyridine (BIPY) is an iron-chelator that preferentially binds to Fe(II) and forms a colored complex, allowing it to be used to monitor the stability and availability of Fe(II). At an Fe(II):subunit ratio of 10:1, the monomeric and assembled mature frataxin kept Fe(II) available to BIPY or ferrochelatase more efficiently than compared to the two controls and buffer alone (*64*).

Oxidative damage to DNA was also studied upon exposure to Fe(II) in the presence of assembled or monomeric mature frataxin to see if frataxin could protect against oxidative damage (*66*). Supercoiled DNA was converted to an open circular form upon addition of Fe(II), but the amount of residual supercoiled DNA was higher in fractions containing increased levels of assembled mature frataxin in comparison to buffer only. Thus, assembled mature frataxin, which exhibits ferroxidase activity, exhibited a protective effect against the oxidative damage of DNA (Fig. 6). The protective effect of the assembled mature frataxin is probably due to its ability to sequester Fe(II) from the solution and formation of a stable mineral core similar to that of ferritin.

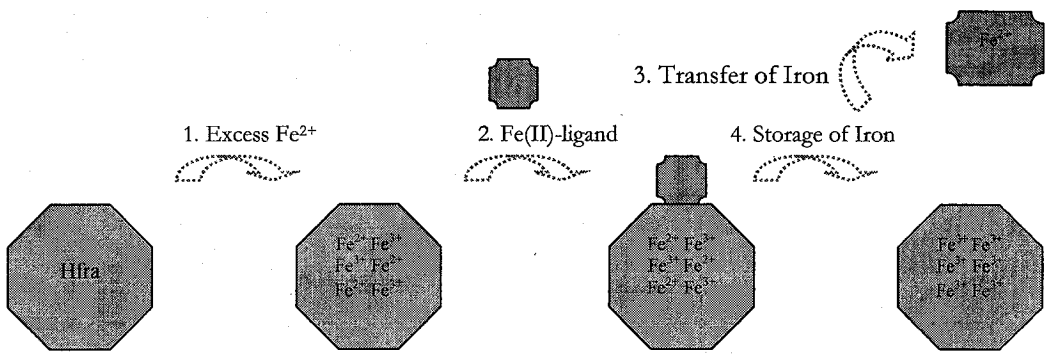

Figure 6: Proposed mechanism of human frataxin in high Fe(II) flux. Step 1: Assembled Hfra is incubated in the presence of excess Fe(II). Step 2: An Fe(II)-ligand (protein) can form a complex and accept Fe(II) (Step 3). Step 4: Excess iron will be stored in the form of Fe(III) (oxidation) (*66*)

VII.4.1. ***Similarity of Assembled Human Frataxin to Ferritin:*** Ferritin is an iron-storage protein that releases iron in a controlled fashion. Ferritins have 24 protein subunits arranged as a hollow shell with an 80 Å-diameter cavity that can acquire up to 4500 Fe(III) atoms. Iron is stored in the protein shell of ferritin as a hydrous ferric oxide nanoparticle that resembles ferrihydrite. Ferritin acquires Fe(II) from solution, catalyzes its oxidation ("ferroxidase activity") and induces mineralization within the cavity (*8*, *57*). Assembled frataxin resembles ferritin in function in that it stores iron and releases it in time of need. Human frataxin assembles during expression in *E. coli* to form individual particles of ~1 MDa, and rod-shaped polymers of these particles. After purification, the assembled human protein exhibits ferroxidase activity, which is characteristic of ferritin. Spectroscopic studies indicate that the iron core of human frataxin is composed of ferric iron that is coordinated by six oxygen atoms (*65*).

Unlike monomer Hfra, the assembled Hfra exhibits ferroxidase activity and the ability to limit oxidative damage to DNA. Though there is ferroxidase activity in assembled Hfra, it is much slower than that of mammalian ferritin (minutes vs. seconds). It is hypothesized that Hfra (monomeric and assembled forms) serve different physiological roles depending on the level of the mitochondrial iron flux (Fig. 6 & 7).

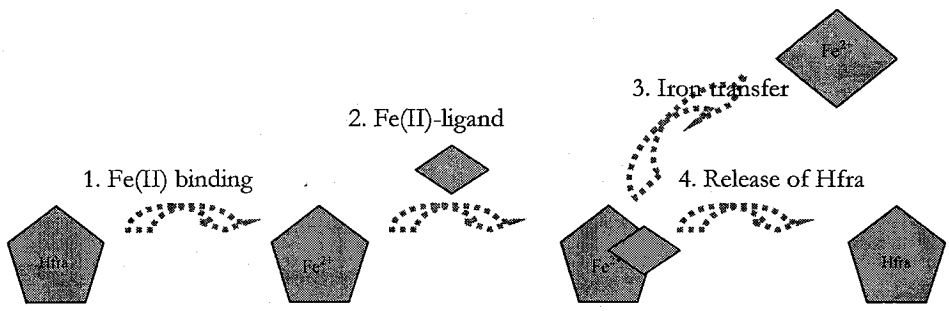

Figure 7: Proposed mechanism of human frataxin in limited Fe(II) flux. Step 1: Monomeric Hfra is incubated with limited Fe(II). Step 2: An Fe(II)-ligand (protein) can form a complex and accept Fe(II) quickly to prevent oxidative damage (Step 3). Step 4: Hfra is released and available to bind more Fe(II) (*66*).

VIII. Thesis Objectives

The aim of this research was to purify, and to characterize the stability, metal iron binding properties, subunit structure, and function of CyaY, the frataxin homologue from *Pseudomonas sp.* strain CF600. Iron binding properties were examined under aerobic and anaerobic conditions using a combination of techniques, and compared with the reported iron-binding properties of frataxin from *E. coli.* The iron binding stoichiometry of frataxin under aerobic and anaerobic conditions was determined using a colourimetric assay and ITC. CyaY was tested for the ability to make Fe(II) available to iron-containing proteins involved in phenol degradation. Interaction of CyaY with a putative iron-sulfur protein (CyaZ) encoded just upstream of CyaY in the *Pseudomonas sp.* strain CF600 genome was also examined.

Materials and Methods

I. Materials

Oligonucleotide primers were synthesized by BioCorp (Montreal, Que.). Restriction enzymes were purchased from Promega or MBI Fermentas. The Wizard Genomic DNA Purification and Wizard Plus Miniprep DNA Purification kits were from Promega. The High Pure PCR Product Purification Kit and Rapid DNA Ligation Kit, purchased from Roche-Applied Science, and the Qiaex II Agarose Gel Extraction Kit from Qiagen were used in DNA extraction and purification. DNA sequencing was performed by Bio S&T (Montreal, Que.).

All chemicals were reagent grade or of the highest available purity.

Strain or Plasmid	Properties	References
Strains		
E. coli XL2-Blue	**endA1recA1*	Stratagene
E. coli DH5α (*79*)	r^-m^+ *recA1*	(*79-81*)
E. coli BL21 (DE3) (*80*)	Protease⁻ strain expressing T7 RNA Polymerase under the control of the *tac* promoter	(*80*)
Pseudomonas sp. strain CF600	Phenol, 3,4-dimethyl phenol degrader	(*82*)
Plasmid (vector)		
pET3a	Ampicillin resistant T7 promoter expression vector	(*81*) Novagen
pGEM-T Easy	Cloning PCR products T7 and SP6 RNA polymerase promoters flanking a multiple cloning region Blue/white screening for recombinants	Promega
pGEM-T(*cyaY*)	Cloning construct	This study
pET3a(*cyaY*)	Expression construct	This study
pGEM-T(*cyaZ*)	Cloning construct	This study
pET3a(*cyaZ*)	Expression construct	This study
	Luria Broth	(*83*)
	M9 minimal medium	(*83*)

Table 1: Strains, plasmids, and media used in this study. r and m refer to host restriction and modification systems respectively (*81*).

II. Agarose Gel Electrophoresis

Agarose gel electrophoresis was used to separate and analyze DNA (*84*). For a 0.8% gel, agarose (0.24 g) was weighed and dissolved by heating gently in 30 mL 1x TBE buffer, followed by addition of ethidium bromide (1.67 μg/mL) (*85*). Samples were diluted using 6x (4 μL) blue/orange loading dye (Promega) and loaded into wells. Electrophoresis was carried out at 80-100V until the loading dye reached near the end of the gel. Gels were then soaked in a solution of ethidium bromide (1.67 μg/mL) in water for 30 min with agitation to improve visualization of smaller bands. Bands were visualized using a UV-transilluminator. The standard marker used was the Gene Ruler 1 kb DNA ladder (MBI Fermentas). The DNA Ladder contains the following 14 discrete fragments (in base pairs): 10 000, 8000, 6000, 5000, 4000, 3500, 3000, 2500, 2000, 1500, 1000, 750, 500, and 250.

III. Genomic DNA Extraction from *Pseudomonas sp.* Strain CF600

Pseudomonas sp. strain CF600 from a permanent culture was grown on minimal medium (M9) agar with 3 mM phenol at 30°C for 24 h. Single colonies were picked and inoculated into Luria broth (LB) or LB (3-5 mL) containing 3 mM phenol, and then grown for 12-16 h at 37°C with shaking (200 rpm). The Wizard Genomic DNA Purification Kit was used for the isolation of DNA from the overnight culture, following the manufacturer's instructions. The genomic DNA was analyzed for concentration and purity using the A_{260}/A_{280} ratio and by agarose (0.8%) gel electrophoresis.

III.1. PCR Amplification of *cyaY* from *Pseudomonas sp.* Strain CF600

CyaY was amplified using PCR following the protocol suggested by the *Pfu* polymerase manufacturer (Stratagene). The primers were (underline represents *Nde*I or *Bam*HI sites, the start codon is italicized):

Frataxin1 -IG1094: 5'GGTTCCTCAT*ATG*AGTTTGAGTGAAGC-3' (Forward)

Frataxin2 -IG1095: 5'CTTAGGATCCGCTACTCATGTCAGATTTCG-3' (Reverse)

PCR reactions were prepared with the following components: native *Pfu* DNA polymerase (2.5 U/μL, 1 μL), 10x native *Pfu* buffer (10 μL), dNTPs (10 mM each NTP, 2 μL), DNA template (0.92 μg), forward primer (2.5 μg), reverse primer (2.5 μg) and distilled water (to a final volume of 100 μL). Conditions of PCR were: segment 1: 1 cycle (95°C) for 45 sec; segment 2: 16 cycles of denaturation (95°C) for 45 sec, annealing (55°C) for 45 sec and extension (72°C) for 2 min; segment 3: 1 cycle (72°C) for 10 min.

The PCR amplification product was purified using the High Pure PCR Product Purification Kit, and the purified DNA was stored at -20°C until ready for ligation.

III.2. Construction of pET3a(*cyaY*) Expression Plasmid

Construct pVI203 was digested with *Bam*HI and *Nde*I to remove the *dmpK* fragment (*81*). After electrophoresis on an agarose gel (0.8%), the pET3a vector (Novagen) fragment was purified from the gel using the High Pure PCR Purification Kit. The PCR-amplified *cyaY* fragment was first ligated into the pGEM-T Easy vector (Promega) with the addition of A tails to the *cyaY* fragment end, using the protocol suggested by the manufacturer, and then cut out of this vector using *Bam*HI and *Nde*I: fragments were separated using agarose gel electrophoresis. The 350 bp fragment was extracted from the agarose gel and ligated into *Nde*I-*Bam*H1-digested pET3a vector. The ligation reaction was performed using the Rapid

DNA Ligation Kit. The molar ratio of vector DNA to insert DNA in a final volume of 10 μL was 1:10-1:20.

Ligation mixtures were used to transform DH5α competent cells. Transformation mixtures were plated onto LB agar containing carbenicillin (100 μg/mL) (*83*). After overnight incubation at 37°C, single colonies were picked and grown overnight in LB (5 mL) containing carbenicillin (100 μg/mL). The Wizard Plus Miniprep DNA Purification Kit was used to isolate plasmid DNA from these cultures. Plasmid DNA was digested with *Hinc*II and electrophoresed on an agarose gel (0.8%) to check that the correct plasmid DNA was obtained. This was also confirmed by sequencing of the insert (Bio S&T).

III.3. Expression of CyaY in *E. coli*

The pET3a(*cyaY*) construct was transformed into *E. coli* BL21(DE3) (Novagen). Transformation mixtures were spread onto LB agar containing carbenicillin (100 μg/mL) and grown overnight at 37°C. Cells were scraped from these plates and used to inoculate LB (4 L) containing ampicillin (100 μg/mL). Cultures were grown for 2-3 h until an OD_{600} of 0.8-1.0 was reached. At this point, IPTG (0.5 mM) was added to each flask and cultures were grown for an additional 3 h. Cells were harvested by centrifugation at 14 300 x g at 4°C for 15 min. Cell pellets were washed with 20 mM Tris-HCl, pH 8.0, containing 50 mM NaCl. The supernatant was discarded and the cell pellet (~6 g from 4 L culture) was stored at –80°C until ready for purification.

IV. Gel Electrophoresis

IV.1. SDS-PAGE Electrophoresis

Sodium dodecyl sulfate-polyacrylamide gel electrophoresis was used to analyze the purity of protein preparations and to estimate the molecular masses under denaturating conditions. The gel system included a separating gel (12% acrylamide) and a stacking gel (3.9% acrylamide) (*86*). Proteins were visualized by staining with a solution containing 50% methanol, 10% acetic acid and 0.1% Coomassie Blue G250 (*85*). Destaining was carried out with 7% acetic acid in 50% methanol. Sample buffer and sample preparation were identical in all cases unless stated otherwise (*86*). The standard protein markers (Low Molecular Weight, Amersham Biosciences) used were: phosphorylase b (97 400 Da), serum albumin (66 200 Da), ovalbumin (45 000 Da), carbonic anhydrase (31 000 Da), trypsin inhibitor (21 500 Da) and lysozyme (14 400 Da).

A Tris-Tricine gel electrophoresis system was used to separate proteins in the range of 5-20 kDa at a higher resolution (*87*). Samples were prepared by diluting with an equal volume of 2x Tricine sample buffer (*88*). The stacking and separating gels (30% acrylamide/0.8% bisacrylamide) were prepared according to procedures described in *Current Protocols in Molecular Biology* (*88*). Separate cathode and anode running buffers were used. Electrophoresis was performed at 30 V for 30 min and then at 150 V for ~120 min or until the tracking dye reached the bottom of the separating gel. Proteins were visualized by staining with a solution of 10% (v/v) acetic acid, containing 0.025% (w/v) Coomassie Blue G250. Destaining was carried out with 10% (v/v) acetic acid. The standard protein marker (LMW, as above) was used, with the addition of aprotinin (6500 Da, 2.4 μg) to the mixture (10 μL).

In some cases, gels were silver-stained. The procedure was based on that of the modified Morrisey protocols (*89*). Gels were fixed for 30 min in 50% methanol containing 12% TCA. The gels were then thoroughly rinsed with distilled water (3 times, 60 min). The gels were then agitated in water containing dithiothreitol (5 μg/mL) for 30 min. The DTT solution was removed and replaced with a solution of 0.2% silver nitrate without rinsing the gels. After 30 min, the gels were briefly rinsed with distilled water followed by a rinse with 3% sodium carbonate. Colour was developed by continuous agitation in a solution of 3% sodium carbonate containing 37% formaldehyde (50 μL/100 mL). Development was stopped by immersing the gel in a solution of 15% acetic acid followed by gentle agitation. Gels were stored in 10% ethanol containing 3% glycerol.

IV.2. Native or Non-Denaturing Gel Electrophoresis

The procedure for non-denaturing discontinuous electrophoresis was to omit SDS and DTT from the standard Laemmli SDS-PAGE protocol. Samples and sample buffers did not contain SDS or DTT and were not heated (*86, 88*).

V. UV-Visible Spectrophotometry

A Cary50 spectrophotometer was used to measure all absorbances.

VI. Purification of CyaY

VI.1. ***Preparation of Crude Extract:*** A suspension of cells in 20 mM Tris-HCl, pH 8.0 containing 50 mM NaCl ("TN50 Buffer") (~2 mL of buffer/1 g weight of cell paste) was sonicated for ten bursts of 15 sec each with cooling in an ice/saltwater bath. The temperature was not allowed to rise above 8°C. This was followed by centrifugation at 70

500 x g for 60 min. The supernatant ("crude extract") was decanted and used for further purification.

VI.2. ***Fast-Flow DEAE-Sepharose Column Chromatography:*** A Fast-Flow DEAE-Sepharose (GE Healthcare) ion-exchange column (30 x 2.6 cm) was equilibrated with TN50 Buffer. The crude extract from the previous step (~22.5 mL) was loaded onto this column which was then washed with TN50 Buffer (~150 mL). Proteins was eluted using a linear gradient (1000 mL) of 50-550 mM NaCl in 20 mM Tris-HCl pH 8.0 buffer, and absorbance of the fractions (9 mL) at 280 nm was monitored. A prominent peak detected near the middle of the gradient was found using SDS-PAGE to contain large quantities of a 12.6 kDa protein. These fractions were combined and concentrated to ~3-5 mL via ultrafiltration with an Amicon YM-10 membrane. The protein was exchanged into 50 mM HEPES-KOH buffer, pH 7.4, via repeated ultrafiltration with an Amicon YM-10 membrane before loading onto a gel filtration column.

VI.3. ***Sephacryl S-300HR Gel Filtration Column Chromatography:*** The concentrated sample from the previous step was loaded (1.0 mL/min) onto a Sephacryl S-300HR (GE Healthcare) gel filtration column (78 x 2.6 cm) that was equilibrated with 50 mM HEPES-KOH, pH 7.4, containing 50 mM NaCl. Fractions (10 mL) were collected and monitored for the presence of protein by SDS-PAGE and absorbance at 280 nm. Fractions from a large peak containing a 12.6 kDa protein were pooled and brought to 1 M ammonium sulfate. This sample (150 mL) was then loaded onto the Phenyl-Sepharose High Performance column for further purification.

VI.4. ***Phenyl-Sepharose High Performance Column Chromatography:*** The preparation from the previous step was loaded (2.0 mL/min) onto a Phenyl-Sepharose High Performance column (36 x 2.5 cm) that was equilibrated with 50 mM HEPES-KOH, pH

7.4, containing 1 M ammonium sulfate. The column was then washed with 50 mM HEPES-KOH, pH 7.4, containing 1 M ammonium sulfate (50 mL). Proteins were eluted using a decreasing linear gradient (500 mL) of 1-0 M ammonium sulfate in 50 mM HEPES-KOH, pH 7.4. Fractions (7 mL) were collected and proteins were detected using SDS-PAGE and the absorbance at 280 nm. The 12.6 kDa protein did not bind to this column, and eluted in the wash and first few fractions of the gradient. These fractions were pooled, desalted, and concentrated to a final volume of ~3-5 mL using repeated ultrafiltration over an Amicon YM10 membrane with 50 mM HEPES-KOH pH 7.4. The purified protein was stored in aliquots at -80°C until use.

VII. PCR Amplification of *cyaZ* from *Pseudomonas sp.* Strain CF600

CyaZ was amplified using PCR following the protocol suggested by the *Pfu* polymerase manufacturer (Stratagene). The primers were (underline represents *Nde*I and *Bam*HI sites and the start codon is italicized):

Iron-Sulfur Forward: JH2313 5'-CGAAATCTCAT*ATG*AGTAGCGCCCAGGCCCG-3'

Iron-Sulfur Reverse: JH2314 5'-CTTAGGATCCCCTGCGCTCAGTGTGCCTTAGCC-3'

PCR reactions were prepared with the following components: native *Pfu* DNA polymerase (2.5 U/μL, 2 μL), 10x native *Pfu* buffer (10 μL), dNTPs (10 mM each NTP, 2 μL), DNA template (0.92 μg), forward primer (2.5 μg), reverse primer (2.5 μg) and distilled water (to a final volume of 100 μL). Conditions of PCR were: segment 1: 1 cycle (95°C) for 45 sec; segment 2: 30 cycles of denaturation (95°C) for 45 sec, annealing (55°C) for 45 sec and extension (72°C) for 2 min; segment 3: 1 cycle (72°C) for 10 min.

The PCR amplification product was purified using the High Pure PCR Product Purification Kit, and the purified PCR amplified DNA was stored at -20°C until ready for ligation.

VII.1. Construction of pET3a(*cyaZ*) Expression Plasmid

Construct pET3a(*cyaY*) was digested with *Bam*HI *and Nde*I to remove the *cyaY* gene from this construct. The digest was run on an agarose gel (0.8%), and the pET3a vector fragment was purified from the gel using the Qiaex II Gel Extraction Kit. The PCR-amplified *cyaZ* fragment was first ligated to the pGEM-T Easy vector with the addition of A tails to the *cyaZ* fragment ends, using the protocol suggested by the manufacturer, and then cut out of this vector using *Bam*HI and *Nde*I. Fragments were separated using agarose gel electrophoresis. The 250 bp fragment was extracted from the agarose gel and ligated to the *Nde*I-*Bam*H1-digested pET3a vector fragment. The ligation reaction was performed using the Rapid DNA Ligation Kit. The molar ratio of vector DNA to insert DNA in a final volume of 10 μL was 1:10-1:20.

Ligation mixtures were used to transform XL2-Blue competent cells. Transformation mixtures were plated onto LB agar containing carbenicillin (100 μg/mL) (*83*). After overnight incubation at 37°C, single colonies were picked and grown overnight in LB (5 mL) containing carbenicillin (100 μg/mL). The Wizard Plus Miniprep DNA Purification Kit was used to isolate plasmid DNA from these cultures. Plasmid DNA was digested with *Nru*I or *Bgl*II and run on an agarose gel (0.8%) to check that the correct plasmid DNA was obtained. This was also confirmed by sequencing of the insert.

VII.2. Expression of CyaZ in *E. coli*

The pET3a(*cyaZ*) construct was transformed into *E. coli* BL21(DE3). Transformation mixtures were spread onto LB agar containing carbenicillin (100 μg/mL) and grown overnight at 37°C. Cells were scraped from these plates and used to inoculate LB (6 L) containing ampicillin (100 μg/mL). Cultures were grown for 3-4 h until an OD_{600} of 0.8-1.0: IPTG (1 mM) was added to each flask and cultures were grown for an additional 16 h at 20°C. Cells were harvested by centrifugation at 14 300 x g at 4°C for 15 min. Cell pellets were washed with 50 mM HEPES-KOH, pH 7.0. The supernatant was discarded and the cell pellet (~12.9 g from 6 L culture) was stored at –80°C until ready for purification.

VIII. Purification of CyaZ

VIII.1. ***Preparation of Crude Extract.*** A suspension of cells in 50 mM HEPES-KOH, pH 7.0 (~2 mL of buffer /1 g weight of cell paste) was sonicated for ten bursts of 15 sec each with cooling in an ice/saltwater bath. The temperature was not allowed to rise above 8°C. A spatula tip of DNaseI was added to the mixture before sonication. This was followed by centrifugation at 70 500 x g for 60 min. The supernatant ("crude extract") was decanted and used for further purification.

VIII.2. ***CM-Sepharose Fast Flow Column Chromatography:*** A Fast-Flow CM-Sepharose (GE Healthcare) ion-exchange column (38 x 2.6 cm) was equilibrated with 50 mM HEPES-KOH pH 7.0. The crude extract from the previous step (~30 mL) was loaded onto this column and then washed with 50 mM HEPES-KOH pH 7.0 (~200 mL). Proteins was eluted using a linear gradient (1000 mL) of 0-500 mM NaCl in 50 mM HEPS-KOH pH 7.0 buffer, and absorbance of the fractions (8 mL) at 280 nm was monitored. A prominent peak detected near the middle of the gradient was found to contain an 8.5 kDa protein using

Tris-Tricine gel electrophoresis. These fractions were combined, precipitated using 65% ammonium sulfate, and centrifuged at 15 344 x g at 4°C for 20 min. The pellet was redissolved into 50 mM HEPES-KOH buffer, pH 7.0 to ~3-5 mL, centrifuged at the same speed for 10 min before the supernatant was loaded onto a gel filtration column.

VIII.3. ***Sephacryl S-300HR Gel Filtration Column Chromatography:*** The concentrated sample from the previous step was loaded (1.0 mL/min) onto a Sephacryl S-300HR (GE Healthcare) gel filtration column (78 x 2.6 cm) that was equilibrated with 50 mM HEPES-KOH, pH 7.0. Fractions (10 mL) were collected and monitored for the presence of protein by Tris-Tricine gel electrophoresis, and absorbance at 280 nm. Fractions containing an 8.4 kDa protein were pooled, desalted, and concentrated to a final volume of ~3-5 mL using repeated ultrafiltration over an Amicon YM3 membrane with 50 mM HEPES-KOH pH 7.0. The purified protein was stored in aliquots at -80°C until use.

IX. Biophysical Techniques Used to Characterize CyaY and Fe(II) Binding Property

IX.1. Circular Dichroism Spectroscopy

IX.1.1. ***Far UV:*** The CD spectra of all samples were collected using a Jasco J-710 spectropolarimeter that was purged with nitrogen gas (5 L/min). Spectra were acquired in the region of 180-260 nm with a 0.1 cm path length cell (300 μL), using the following settings: step resolution, 0.2 nm; scan speed, 50 nm/min; accumulation, 1 (buffer) or 5 (samples); response time, 1.0 sec; bandwidth, 1.0 nm; and sensitivity, 50 mdeg. Data obtained when detector voltages were above 700V were disregarded. The CyaY sample concentration was 0.5 mg/mL (40.1 μM) in 5 mM or 50 mM HEPES-KOH pH 7.5 buffer with varying concentrations of guanidine hydrochloride. The pH was adjusted accordingly. Samples were centrifuged briefly before incubating at room temperature for 24 h prior to

taking scans. The guanidine hydrochloride stock solution was diluted with 5 mM or 50 mM HEPES-KOH, pH 7.5. Samples containing $MnSO_4 \cdot 4H_2O$ (1 mM) or TCEP (0.802 mM) were prepared in a similar fashion. Data were analyzed using the Jasco Standard Analysis software or Sigma Plot 8.0.

IX.1.2. ***Thermal Denaturation:*** Thermal denaturation was monitored using circular dichroism spectroscopy. Samples were contained in a water-jacketed circular cell, with a pathlength of 0.1 cm, connected to a variable-temperature water bath. Samples were monitored at 222 nm as the temperature was changed from 10-85° C. The following parameters were used: step resolution, 0.2 nm; wait time, 2 min; temperature slope, 15°C/h; response time, 0.25 sec; bandwidth, 1.0 nm; and sensitivity, 50 mdeg. CyaY sample concentration was 0.5 mg/mL (40.1 μM) in 50 mM HEPES-KOH, pH 7.5. Temperature scans took approximately 5 h. Samples with added iron were prepared in an anaerobic chamber (MBraun Model Unilab 1200/780 with <2 ppm oxygen). CyaY (0.5 mg/mL), $Fe(NH_4)_2(SO_4)_2 \cdot 6H_2O$ (1:1-1:6 CyaY:Fe^{2+}) and buffer were mixed in the anaerobic chamber, loaded into a circular CD cell, stoppered, and removed from the chamber for analysis by CD spectroscopy.

IX.2. Fluorescence Spectroscopy

Fluorescence measurements were carried out on an Aminco Bowman series 2 Fluorimeter. Samples were excited at 280 nm or 295 nm and emission spectra were collected between 300 and 400 nm (Cuvette holds 400 μL of sample with a pathlength of 1 cm). Bandwidths of 2 nm were used for both excitation and emission. For denaturation experiments, protein samples were mixed with guanidine hydrochloride, centrifuged briefly before incubation, and then incubated at room temperature for 24 h before the spectra were taken. Samples

containing 0.045 mg/mL (3.61 μM) CyaY, with an absorbance at 280 nm of 0.066, were prepared in 50 mM or 5 mM HEPES-KOH, pH 7.5, with varying concentrations of guanidine hydrochloride. Samples containing NATA/NAYA standards (concentrations of modeled compounds were measured using UV-vis), $MnSO_4 4H_2O$ (1:1-1:10 CyaY:Mn^{2+}) or TCEP (70.6 μM) were prepared in the same fashion. There were no differences observed in the fluorescence spectra for samples in either 50 mM or 5 mM HEPES-KOH, pH 7.5. For experiments for determining reversibility of CyaY denaturation, guanidine hydrochloride containing samples were diluted 3-fold with 5 mM or 50 mM HEPES-KOH, pH 7.5, and incubated overnight prior to recording fluorescence spectra.

IX.3. Isothermal Titration Calorimetry

Isothermal titration calorimetry data were collected using a VP-ITC MicroCalorimeter. Calorimetric data for exothermic binding of cytidine 2'-monophosphate (2.29 mM 2'-CMP in titrating syringe) to ribonuclease A from bovine pancreas (0.0292 mM) both in 50 mM potassium acetate, pH 5.5, were collected and used as a control. The cytidine 2'-monophosphate has an E_{mM} of 8.9 in 0.1 mM potassium phosphate buffer at pH 7.0 at 270 nm (Sigma Chemical Company). The ITC runs were obtained for 25 automatic injections of 5 μL at 28°C. Experimental data for CyaY (50 μM) titrated with excess $MnSO_4 4H_2O$ (1 mM in the titrating syringe) were collected using the same instrument. CyaY was dialyzed overnight against 50 mM HEPES-KOH, pH 7.5, and the Mn(II) stock solution was prepared in the same buffer. The raw data were collected for 25 automatic injections of 10 μL at 25°C. Anaerobic ITC was performed using CyaY (50 μM) titrated with ferrous ammonium sulfate hexahydrate (1.50 mM in the titrating syringe) in 50 mM HEPES-KOH pH 7.0, containing NaCl (150 mM) and $Na_2S_2O_4$ (2 mM) in both protein and iron solutions.

The raw data were collected for 30 automatic injections of 10 μL at 25°C. The following experimental control settings were used for CyaY titrations with Fe(II): total number of injections, 30; cell temperature, 25°C; reference power, 10 μCal/sec; initial delay, 60 sec; and stirring speed, 300. Injection parameters were: 10 μL/injection; duration, 20 sec; spacing 240 sec; and filter period, 2 sec. The data were analyzed using MicroCal Origin 5.0 software supplied with the instrument.

IX.4. Analytical Ultracentrifugation

CyaY solutions were brought to a concentration of 0.22-1 mg/mL in 50 mM HEPES-KOH, pH 7.5. Samples and buffer blanks were centrifuged at 203 893 x g at 15°C using a 60-Ti rotor in Beckman Optima XL-1 analytical ultracentrifuge. In some experiments, CyaY (35.28 μM) was prepared with TCEP (0.35-1.41 mM), GuHCl (0-2.5 M), $MnSO_4 4H_2O$ (353 μM) or $Fe(NH_4)_2(SO_4)_2 6H_2O$ (1:1-20:1 Fe^{2+}:CyaY). Iron samples were prepared and cells were assembled in the anaerobic chamber at 15°C with <2 ppm oxygen. Scans at 280 nm were used to follow the sedimentation process. Distribution plots were constructed using Sedfit version 8.9 software (http://www.analyticalultracentrifugation.com) by Peter Shuck fitting the raw data to the c(s) and c(M) models (*90*). V-bar, density and viscosity values were calculated using UtraScan 7.1 as follows: varying [CyaY], different stoichiometry of Fe^{2+}:CyaY and CyaY in 50-fold TCEP: 0.717 ml/g, 1.0004 g/ccm, 1.0131 cp; CyaY in 50 mM KCl: 0.717 ml/g, 1.0020 g/ccm, 1.0124 cp; CyaY in 150 mM KCl: 0.717 ml/g, 1.0067 g/ccm, 1.0110 cp. These values were obtained using 50 mM Tris as the buffer because the data were not available for HEPES. All protein samples were run by Peter Ulycznyj from the Centre for Structural and Functional Genomics.

X. Determination of Protein Concentrations

Protein concentrations were determined using the BCA (bicinchoninic acid) Protein Assay kit with BSA (bovine serum albumin) as a standard, according to the manufacturer's instructions for the 60°C protocol (Pierce). When interfering substances such as EDTA, ammonium sulfate or DTT were present, an alternative protocol involving trichloroacetic acid (TCA) was used (*91*). TCA precipitates protein away from these interfering substances.

In some cases protein concentration was determined using a spectrophotometric method. The protein concentration for RNaseA was calculated using an $E_{1\%}$ of 7.1 at 280 nm. A molar extinction coefficient at 280 nm was calculated from the primary amino acid sequence of CyaY using equations 6-11 (*92, 93*). The calculated molar extinction coefficient was determined to be 17 990 M^{-1} cm^{-1} for the denatured protein. The native molar extinction coefficient was determined to be 17 320 M^{-1} cm^{-1}. The following equations used were (*92*):

$$A = \varepsilon \times l \times c \tag{6}$$

$$\varepsilon_M = a\varepsilon_{MTyr} + b\varepsilon_{MTrp} + c\varepsilon_{MCys} \tag{7}$$

$$\varepsilon_{280}\,(M^{-1}cm^{-1}) = a(1490) + b(5500) + c(125) \tag{8}$$

$$Abs_{Gdn\cdot HCl} / \varepsilon_{M\ Gdn\cdot HCl} = C_{denatured} \tag{9}$$

$$Abs_{Native} / \varepsilon_{M\ Native} = C_{native} \tag{10}$$

$$\varepsilon_{M\ Native} = (Abs_{Native})\ (\varepsilon_{M\ Gdn\cdot HCl}) / (Abs_{Gdn\cdot HCl}) \tag{11}$$

XI. Purification of Iron-Complexed CyaY

A stock iron solution of 50 mM ferrous ammonium sulfate hexahydrate was prepared in 0.050 N HCl. CyaY (4.4 mg/mL) was incubated with excess (20-fold) ferrous ammonium sulfate hexahydrate diluted in 20 mM Tris-HCl pH 7.5 (200 μL) for 1 h at 25°C under aerobic or anaerobic conditions (glove box). The protein was purified from the mixture

using a mini-spin column packed with Fast-Flow DEAE-Sepharose resin (500 μL). This column was equilibrated with 20 mM Tris-HCl containing 50 mM NaCl pH 8.0. After loading the column, it was washed with the same buffer to remove unbound iron, and 20 mM Tris-HCl containing 500 mM NaCl pH 8.0 to elute the bound protein. Fractions of 100 μL was collected. The fractions that contained both iron and CyaY were combined (fractions 11 and 12) and passed through a NAP5 desalting column that was equilibrated with 50 mM HEPES-KOH pH 7.5 (Amersham Biosciences). The iron content of the fractions eluted from this column was determined using Ferrozine, see below (*94*).

XII. Iron Quantitation Using a Ferrozine-Based Assay

An aliquot (~100 μL) of desalted sample from the iron-complexation experiment was transferred to a microcentrifuge tube (1.5 mL) and 30% (w/v) trichloroacetic acid was added to obtain a final concentration of 5% TCA (w/v). After centrifugation for 5 min at 16 000 x g, an aliquot of the supernatant (50 μL) was transferred to a clean tube. Saturated ammonium acetate (133 μL), 0.12 M ascorbic acid (166.7 μL), 0.25 M Ferrozine (83.3 μL) and MilliQ water (567 μL) were added to a final volume of 1.0 mL. After 30 min, samples were centrifuged for 1 min at 16 000 x g and the absorbance at 562 nm was measured. A standard curve was constructed using ferrous ammonium sulfate hexahydrate (*94*).

XIII. Chemical Cross-Linking With EDC

An EDC stock solution was made fresh in 50 mM HEPES-KOH pH 7.5. CyaY (17.86 μM) was incubated with EDC (8.93 mM) in the presence or absence of CyaZ (17.86 μM) for various times between 0-30 min in 50 mM HEPES-KOH pH 7.5. EDC was added to the protein solutions to initiate the reaction at room temperature, and the reactions were

quenched with SDS-PAGE sample buffer at the indicated time. The samples were run on SDS-PAGE Tris-Tricine gels, which were subsequently stained with 0.025% (w/v) Coomassie Blue G-250 containing 10% (v/v) acetic acid, and destained with 10% (v/v) acetic acid. Reactions containing BSA (6.45 μM) and CyaY (17.86 μM) were prepared as a control. The effects of including NaCl (0.1 M), KCl (0.15 M) and/or Fe(II) (193.5 μM) were also examined. In addition, cross-linking reactions between apo-catechol 2,3-dioxgyenase (16.29 μM) or holo-catechol 2,3-dioxygenase (16.29 μM) including Fe(II) with and without KCl (0.15 M) were examined.

XIV. α,α'-Bipyridine Assay to Determine the Availability of Fe(II)

This assay has been used to monitor the effects of CyaY on the availability of Fe(II) under aerobic conditions (*63, 64, 66*). CyaY (3 μM), BSA (3 μM, Sigma-Aldrich), holo-ferritin (0.3 μM, Sigma-Aldrich), DmpK (3 μM, microcon to concentrate and buffer exchange to remove DTT from DmpK) or buffer alone were incubated at 30°C with ferrous ammonium sulfate hexahydrate (30 μM) in a total volume of 4 mL. The buffer used was 10 mM HEPES-KOH, pH 7.3, and a 10 mM ferrous ammonium sulfate hexahydrate stock solution in 0.01 N HCl was used as the iron source. Aliquots (500 μL) were withdrawn at the indicated time points and BIPY was added to a final concentration of 2 mM. After 5 min at room temperature, the concentration of $Fe[\alpha,\alpha'\text{-BIPY}]_3^{2+}$ was determined from the absorbance at 520 nm (ε=9, 000 $M^{-1}cm^{-1}$).

XV. Preparation of Apo-Catechol 2,3-Dioxygenase

Holo-catechol 2,3-dioxygenase (3.7 mg/mL) was dialyzed against 50 mM Tris-Acetate containing 1 mM EDTA and 1 mM phenanthroline (pH 7.5). The dialysis solution was

changed daily for a period of three days (1 L). The chelators were removed using 50 mM Tris-Acetate pH 7.5 for two additional days (1 L) (*95, 96*).

XV.1. Reconstitution of Catechol 2,3-Dioxygenase with Fe(II)

Reconstitution of apo-catechol 2,3-dioxygenase (which is inactive in activity assays) involves the incubation of apo-catechol 2,3-dioxygenase (0.4 μM) and ferrous ammonium sulfate hexahydrate with CyaY (0.4 μM), BSA (0.4 μM), KCl (0.15 M) or buffer alone. Buffer used in the reconstitution procedure was 50 mM Tris-HCl pH 7.0. The assay was initiated upon addition of $Fe(NH_4)_2(SO_4)_2 \cdot 6H_2O$ (1 mM), aliquots were removed at various time points, and assayed for activity. The activity assay included 10 μL of the reconstituted sample, 8 μL of catechol (45 mM) and 982 μL 50 mM potassium phosphate buffer pH 7.5, and reaction was monitored at 375 nm for 2 min. One unit is defined as the amount of enzyme that produces 1 μmol of 2-hydroxymuconate semialdehyde per minute under this standard assay (for 2-hydroxymuconic semialdehyde at pH 7.5) ($\varepsilon=4.4x10^4 M^{-1}cm^{-1}$) (*95-97*).

XVI. Electrospray Ionization Mass Spectrometry

The molecular masses of CyaY and CyaZ were determined by direct-injection on a Q-TOF 2 mass spectrometer (Micromass). CyaY was buffer-exchanged into 18 MΩ Milli-Q water using a Microcon YM-10 centrifugal device. In preparation for injection into the mass spectrometer, samples were diluted to 1 μM in 50% acetonitrile: 0.1% formic acid pH 3.01. CyaZ was buffer exchanged into 50 mM Tris-Cl pH 8.0 using a Microcon YM-3 centrifugal device. Final CyaZ concentration (6.73 μM) was achieved by diluting with 0.027% formic acid with 13 mM ammonium formate, pH 3.97. The diluted samples were directly introduced into the spray source at a flow rate of 1.0 μL/min. Alternatively, CyaY was

diluted in 50 mM HEPES-KOH pH 7.5 and to a final concentration of 10 μM, injected onto a Symmetry-300 C18 OPTI-PAK column and then washed with Millipore water, followed by elution with a 10-90% ACN gradient containing 0.1% formic acid. Instrument parameters were: capillary voltage, 3800 V; cone voltage, 45 V; multiplier, 550 V; MCP, 2100 V; and TOF, -9.1 V. Raw spectra were deconvolved using MassLynx software (Micromass). All protein sample analysis was performed by Alain Tessier of the Centre for Biological Applications of Mass Spectrometry.

Results

I. PCR Amplification of *cyaY* and pET3a-Based Expression Plasmid Construction

Since *Pseudomonas sp.* strain CF600 is a strain of *Pseudomonas putida* (V. Shingler, personal communication), the genome sequence of *Pseudomonas putida* KT2440 was used as the starting point for *cyaY* amplification (Fig. 8A). *CyaY* is located at positions 5960296 to 5960628 of the *Pseudomonas putida* KT2440 chromosome, and is predicted to encode a protein of 110 amino acids (*98*). Primers based on the 5' and 3' terminal sequences of *cyaY* from *Pseudomonas putida* KT2440 were used for PCR amplification (see *Materials and Methods*). A 364 bp fragment was amplified from *Pseudomonas sp* strain CF600 genomic DNA using these primers (Fig. 8B) and inserted in the pGEM-T Easy vector at the T-overhangs (Fig. 8C).

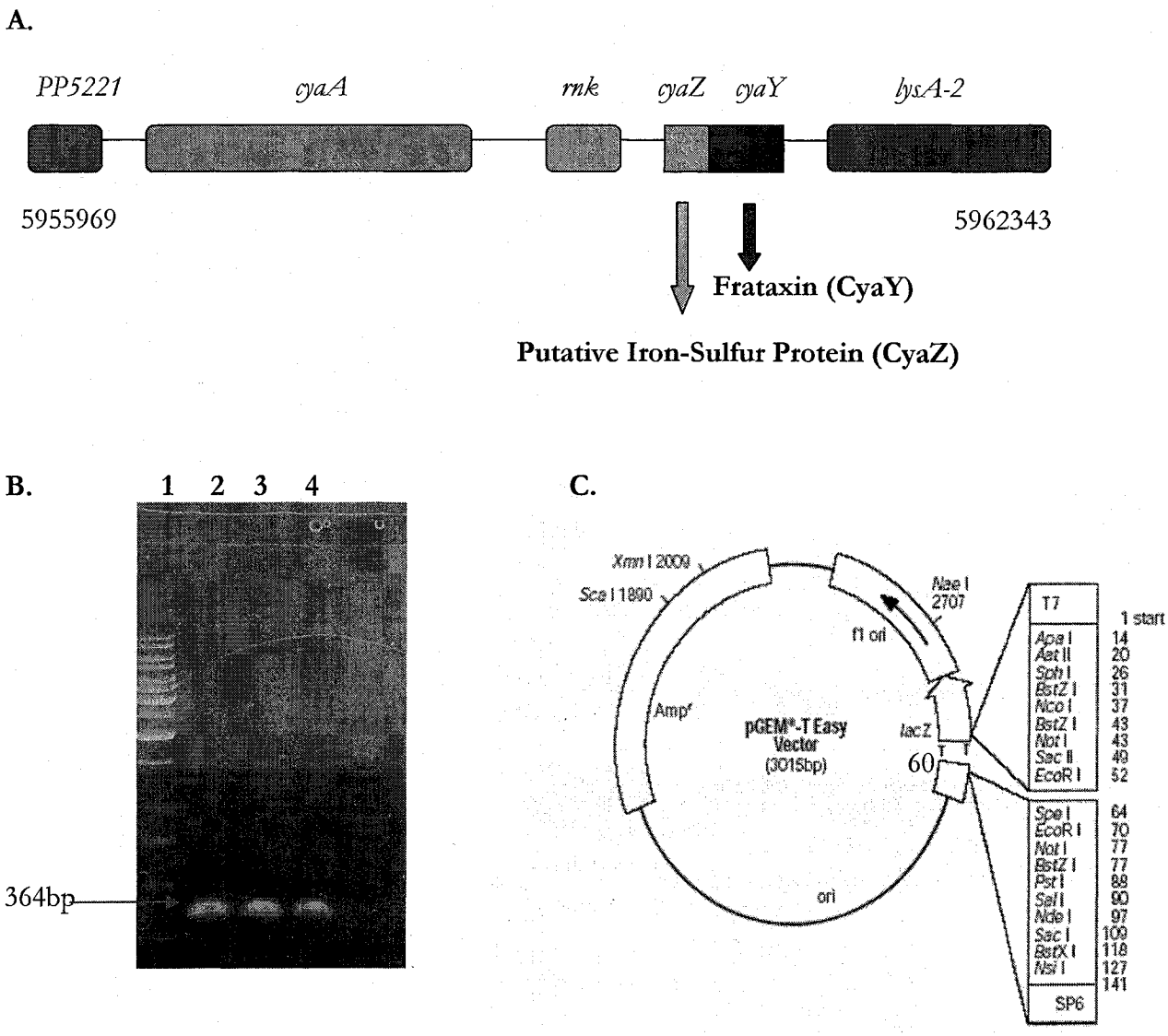

Figure 8: PCR amplification of *cyaY* from the *Pseudomonas sp.* strain CF600 genomic DNA. A. Segment of *Pseudomonas putida* KT2440 genome containing *cyaY* and *cyaZ* genes (*98*). B. Agarose (0.8%) gel electrophoresis of PCR reactions using genomic DNA from three independent cultures of *Pseudomonas sp.* strain CF600. Lane 1: 1 kb ladder (MBI Fermentas); Lane 2: PCR product from genomic DNA from colony 1; Lane 3: PCR product from genomic DNA from colony 2; Lane 4: PCR product from genomic DNA from *Pseudomonas sp.* strain CF600 grown in the presence of phenol. C. Vector diagram of pGEM-T Easy vector map (Promega Corp). The pGEM-T Easy Vector has been linearized with *Eco*RV at base 60. The DNA Ladder contains the following 14 discrete fragments (in base pairs): 10 000, 8000, 6000, 5000, 4000, 3500, 3000, 2500, 2000, 1500, 1000, 750, 500, and 250.

An *Nde*I site was inserted at the 5'-end of the *cyaY* gene and a *Bam*HI site was inserted at the 3'-end of the *cyaY* gene in the PCR primers. A unique *Nde*I site is located at position 97 of the pGEM-T Easy vector (Fig. 8C). Consequently, the digestion of the desired *cyaY* fragment from the pGEM-T Easy construct with *Bam*HI and *Nde*I can yield several different band patterns. Depending on the orientation of the insert, restriction enzyme digestion with *Bam*HI and *Nde*I can generate the following fragment sizes. In the forward orientation (anticlockwise), it can generate fragment sizes of 38 bp, 346 bp and 2983 bp. In the reverse orientation (clockwise), it can generate two possible combinations of 346 bp and 3033 bp or 383 bp and 2996 bp depending on which *Nde*I had digested the recombinant DNA (Fig. 9). A mixture of these band patterns may appear if both *Nde*I site had properly digested the recombinant DNA. There are 2 small bands in lanes 2 and 6 (350 bp and 385 bp), whereas there is only one band in lanes 3 and 5. The band at ~350 bp was cut out from lane 5 (Fig. 9) and the DNA was extracted from the agarose gel and used for further experimentation. This single band was due to a missed *Nde*I cut site in the reverse orientation. In lane 6, it was clear that there was an intense band at ~3000 bp and two other fragments at ~350 bp and ~385 bp which represented incomplete digestion by *Nde*I. This can be explained by the generation of both combinations of *Bam*HI and *Nde*I digested fragments in the reverse orientation in the pGEM-T Easy vector (partial digestion).

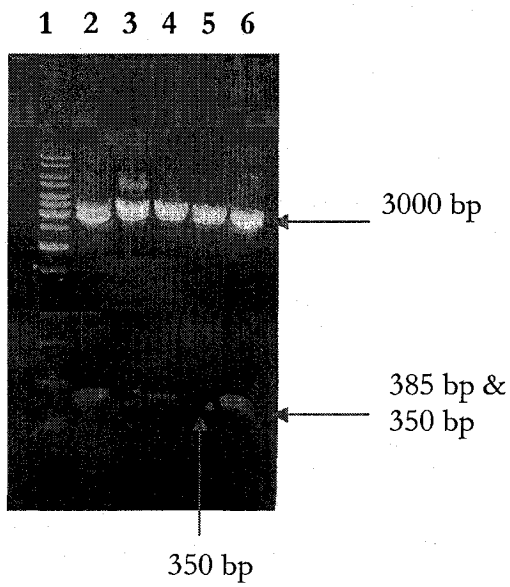

Figure 9: Agarose (0.8%) gel electrophoresis of *Bam*HI and *Nde*I digested pGEM-T(*cyaY)* from 5 different transformants (Col. 1-Col. 5). Lane 1: 1 kB ladder; Lane 2: Col. 1; Lane 3: Col. 2; Lane 4: Col. 3; Lane 5: Col. 4; Lane 6: Col. 5. DNA Ladder contains the following 14 discrete fragments (in base pairs): 10 000, 8000, 6000, 5000, 4000, 3500, 3000, 2500, 2000, 1500, 1000, 750, 500, and 250.

The 350 bp *Bam*HI-*Nde*I fragment was ligated into the *Bam*HI and *Nde*I sites in pET3a (4600 bp, Fig. 10). The resulting pET3a(*cyaY*) plasmid was digested with *Hinc*II (Fig. 11A) to verify that the correct plasmid with insert was obtained. *HincII* cuts at 1237 bp and 4493 bp in the vector, and 822 bp in the *cyaY* fragment: a plasmid map for the correct construct is shown in Fig. 11B. Complete digestion of this plasmid with *Hinc*II would generate 3 fragments of 3256 bp, 1276 bp and 415 bp. If incorrect plasmid had been obtained, fragment sizes of 3256 bp, 1276 bp, 385 bp and 68 bp would have been generated

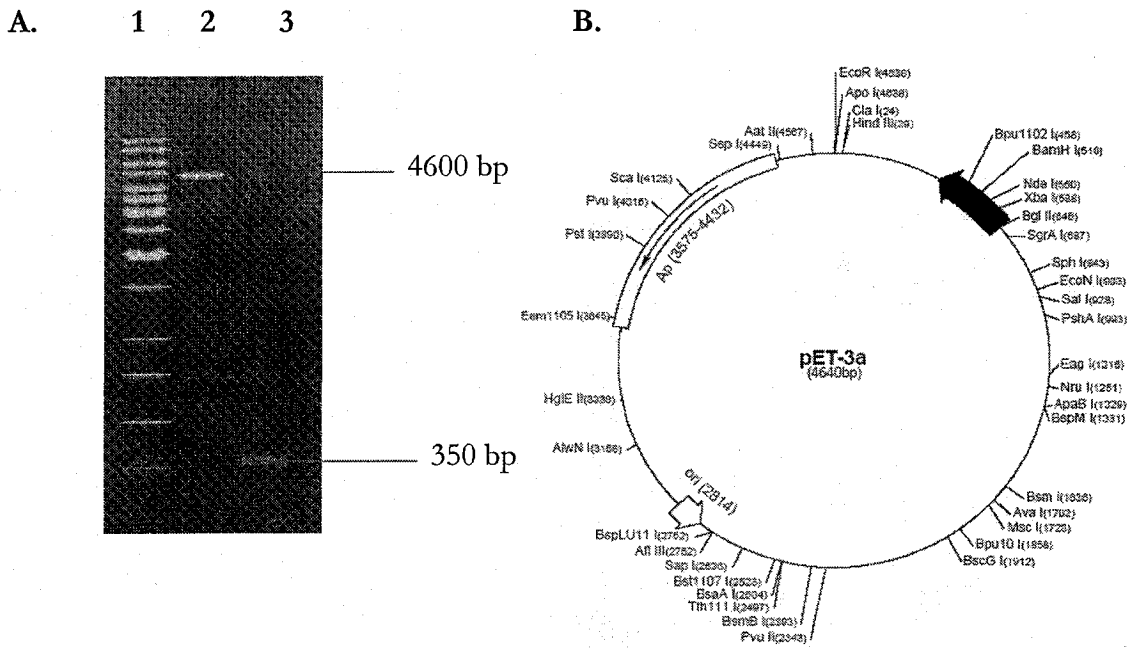

Figure 10: Construction of pET3a(*cyaY*) expression plasmid. A. Agarose (0.8%) gel electrophoresis of pET3a vector and insert fragment for ligation. Lane 1: 1 kb ladder; Lane 2: pET3a vector obtained as described in *Materials and Methods*; Lane 3: *cyaY* fragment. DNA Ladder contains the following 14 discrete fragments (in base pairs): 10 000, 8000, 6000, 5000, 4000, 3500, 3000, 2500, 2000, 1500, 1000, 750, 500, and 250. B. pET3a vector map (Novagen).

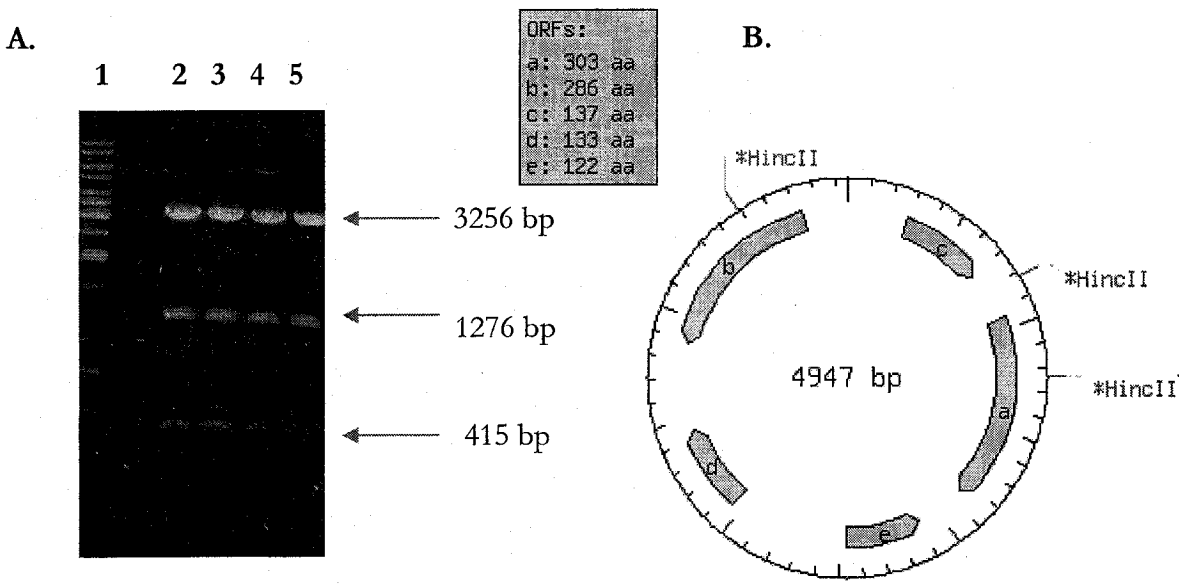

Figure 11: Verification of plasmid construct by digestion with *Hinc*II. A. Agarose (0.8%) gel electrophoresis of pET3a(*cyaY*) plasmids for 4 transformants (Col. 1-Col. 4) digested with *Hinc*II. Lane 1: 1 kb ladder; Lane 2: Col. 1; Lane 3: Col. 2; Lane 4: Col. 3; Lane 5: Col. 4. B. Recombinant plasmid with *Hinc*II sites are shown. Diagram generated using Nebcutter (*99*). DNA Ladder contains the following 14 discrete fragments (in base pairs): 10 000, 8000, 6000, 5000, 4000, 3500, 3000, 2500, 2000, 1500, 1000, 750, 500, and 250. ORF box provides a table of the genes shown on the display with their coordinates, polypeptide lengths, protein IDs at GenBank and flanking, single-cutter restriction enzymes (*99*).

That the correct plasmid with insert had been obtained was confirmed by DNA sequence analysis (Fig. 12). Nucleotide sequencing of the insert revealed 97% sequence identity at the nucleotide level with *Pseudomonas putida* KT2440: however, the amino acid sequence is identical with that of CyaY from *Pseudomonas putida* KT2440 genome (Fig. 12).

DNA Sequence of CyaY

[redacted]***ATG***AGTTTGAGTGAAGCGCGTTTCCATGACCTGGTCGACGCGACCCAACAG
GCCCTGGAAGATCTGTTCGACGAGAGCGGTCTGGACCTGGACATGGAGAACTCCGCTGGTGTCCTGACCGT
CAAGTTCGAGGGCGGCGCCCAGCTGATCTTCAGCCGTCAGGAGCCACTGCGCCAGTTGTGGCTTGCCGACC
GCTCCGGTGGTTTCCACTTCGATTACGACGAAGACAGCGGCAAGTGGGTGTGCGAAAAGAGCGAAGAGTTA
CTGGGTGAAATGCTTGAGCGTATCGTCTGGGAGCGGGCCGGCGAGAAGCTGGACTTCGACGAAATC***TGA***[redacted]
[redacted]

Protein Sequence of CyaY (110 amino acids)

M	S	L	S	E	A	R	F	H	D	L	V	D	A	T	Q	Q	A	L	E	D	L	F	D
E	S	G	L	D	L	D	M	E	N	S	A	G	V	L	T	V	K	F	E	G	G	A	Q
L	I	F	S	R	Q	E	P	L	R	Q	L	W	L	A	D	R	S	G	G	F	H	F	D
Y	D	E	D	S	G	K	W	V	C	E	K	S	E	E	L	L	G	E	M	L	E	R	I
V	W	E	R	A	G	E	K	L	D	F	D	E	I	**Stop**									

Figure 12: DNA sequence of CyaY from *Pseudomonas sp.* strain CF600 (top). Primary amino acid sequence of CyaY from *Pseudomonas sp.* strain CF600 (bottom). Start and stop codons are italicized and bolded. The nucleotide sequence upstream and downstream (part of the pET3a vector sequence) of the start and stop codons are italicized and shaded.

I.1. Purification of CyaY from *Pseudomonas sp.* Strain CF600 Expressed in *E. coli*

First, the plasmid pET3a(*cyaY*) was transformed into *E. coli* BL21(DE3). Purification of CyaY from crude extracts of these transformants was achieved using Fast-Flow-DEAE Sepharose, Sephacryl S-300HR Gel Filtration and High Performance Phenyl Sepharose column chromatographies. Proteins present at each stage of the purification process may be seen on the SDS-PAGE gel shown in Fig. 13. Approximately 150 mg of pure CyaY (Fig. 13 lane 7) was obtained from 4 L of bacterial culture. The apparent molecular weight of the purified CyaY was estimated to be ~13 kDa from SDS-PAGE gels. A minor band at ~25 kDa was also present in several CyaY preparations (e.g. Fig. 13, lane 8), which may represent a dimer form or a contaminant.

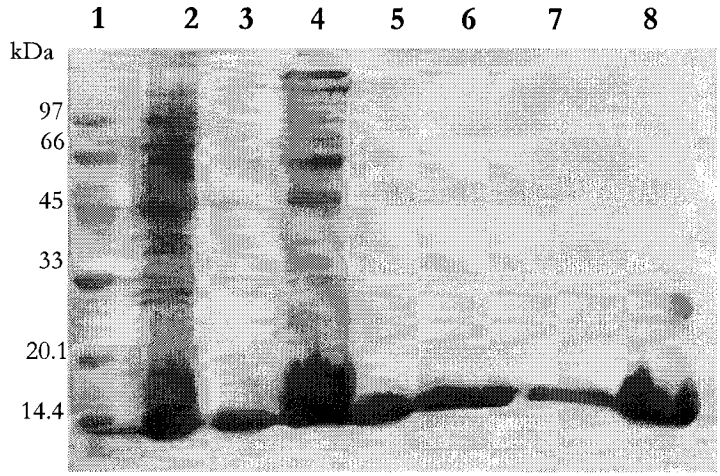

Figure 13: SDS-PAGE (12%) gel electrophoresis showing samples at various steps of the purification of CyaY from *E. coli.* Lane 1: LMW molecular marker (phosphorylase b: 97 kDa, albumin: 66 kDa, ovalbumin: 45 kDa, carbonic anhydrase: 33 kDa, trypsin inhibitor: 20.1 kDa and α-lactalbumin: 14.4 kDa); Lane 2: Crude extract of CyaY; Lane 3: Pooled DEAE fractions; Lane 4: Concentrated DEAE fractions; Lane 5: Pooled Sephacryl S-300HR gel filtration fractions; Lane 6: Concentrated S-300HR gel filtration fractions; Lane 7: Pooled Phenyl Sepharose fractions; Lane 8: Concentrated Phenyl Sepharose fractions. Samples were diluted 1:1 with sample buffer except crude extract which was diluted 1:4.

I.2. Sequence and Structural Analysis of CyaY

Genes encoding yeast (*61*) (NP_010163, Yfh1), human (*23*) (Q16595, Hfra) and *E. coli (40)* (S30697, CyaY) frataxins have been sequenced and exhibit between 28-39% identity with the protein sequence of CyaY from *Pseudomonas putida* (Fig. 14). A model of the three-dimensional structure of CyaY from *Pseudomonas sp.* strain CF600 was generated using Swiss-PDB with CyaY from *E. coli* (1EW4) as the template (Fig. 15). The model consists of six-antiparallel beta-sheets flanked by two parallel alpha-helices, with a negatively charged surface that could be involved in Fe(II) binding. Comparison of the primary amino acid sequences of CyaY from *Pseudomonas sp.* strain CF600 to the three frataxin orthologues (Hfra, Yfh1 and CyaY) shows that there are 13 invariant residues between the CyaY from *Pseudomonas sp.* strain CF600 and CyaY from *E. coli* (Asp31, Gly37, Val38, Thr40, Gln54,

Pro56, Gln59, Trp61, Leu62, Gly67, Asp72, Trp78, and Leu91 using the numbering of the CyaY sequence). All the conserved residues of CyaY are located on the β-sheet side of the protein. The sole cysteine residue Cys83, is exposed on the surface of the protein which could allow it to form a disulfide bond between two CyaY monomers.

```
CYAY_ECOLI      ------------------------------------------------------------
CYAY_PSEPK      ------------------------------------------------------------
FRDA_HUMAN      MWTLGRRAVAGLLASPSPAQAQTLTRVPRPAELAPLCGRRGLRTDIDATCTPRRASSNQR
FRDA_YEAST      ---------------------MIKRSLASLVRVSSVMGRRYMIAAAGGER-ARFCPAVTN


CYAY_ECOLI      ----------------------------MNDSEFHRLADQLWLTIEERLDDW----DGD
CYAY_PSEPK      ---------------------------MSLSEARFHDLVDATQQALEDLFD------ESG
FRDA_HUMAN      GLNQIWNVKKQSVYLMNLRKSGTLGHPGSLDETTYERLAEETLDSLAEFFEDLADKPYTF
FRDA_YEAST      KKNHTVNTFQKRFVESSTDGQVVPQEVLNLPLEKYHEEADDYLDHLLDSLEELS-EAHPD
                                           :    :.  .:     : : ::


CYAY_ECOLI      SDIDCEINGGVLTITFENGS-KIIINRQEPLHQVWLATKQGG-YHFDLKGD--EWICDRS
CYAY_PSEPK      LDLDMENSAGVLTVKFEGGA-QLIFSRQEPLRQLWLADRSGG-FHFDYDEDSGKWVCEKS
FRDA_HUMAN      EDYDVSFGSGVLTVKLGGDLGTYVINKQTPNKQIWLSSPSSGPKRYDWTGK--NWVYSHD
FRDA_YEAST      CIPDVELSHGVMTLEIPAFG-TYVINKQPPNKQIWLASPLSGPNRFDLLNG--EWVSLRN
                   * . . **:*: :       ::.:* * :*:**:   .*  ::*      :*:  :.


CYAY_ECOLI      GETFWDLLEQAATQQAGETVSFR---------
CYAY_PSEPK      EELLGEMLERIVWERAGEKLDFDEI-------
FRDA_HUMAN      GVSLHELLAAELTKALKTKLDLSSLAYSGKDA
FRDA_YEAST      GTKLTDILTEEVEKAISKSQ------------
                   : ::*     :    .
```

Figure 14: Primary amino acid sequence of frataxin orthologues using CLUSTALX (*69*). * indicate identity of amino acids at these positions; : indicate strongly similar amino acids; . indicate weakly similar amino acids, and – indicate gaps to better align the amino acid sequences.

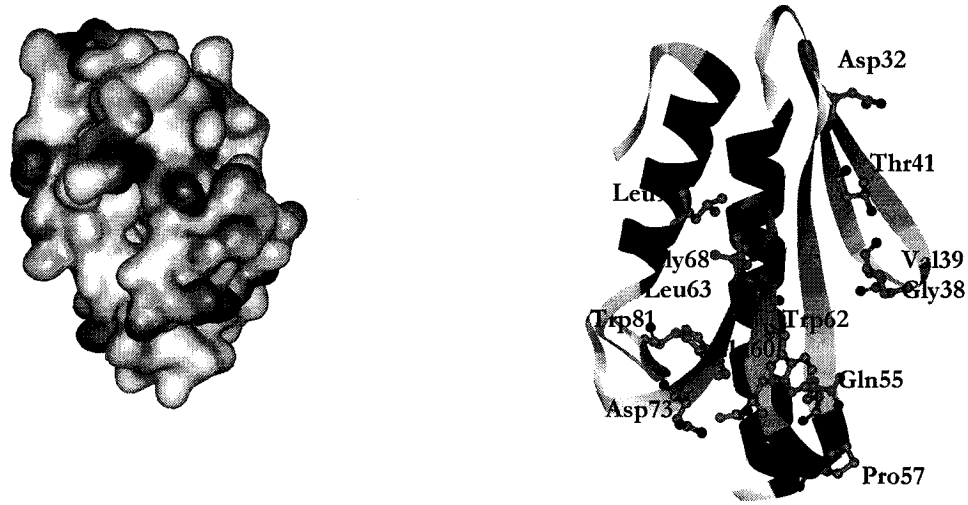

Figure 15: Structure of CyaY from *Pseudomonas sp.* strain CF600 modeled using Swiss-Model. The representation on the right shows the elements of secondary structure (helix red and strand blue) and positions of conserved residues between CyaY from *E. coli* and CyaY from *Pseudomonas sp.* strain CF600. The electrostatic potential surface of CyaY is shown on the left. Acidic residues are red and basic residues are colored in blue. Structures were created using Swiss-PDB (*55*) and WebLab Viewers (*56*).

II. PCR Amplification of a Gene Encoding a Conserved Hypothetical Protein and Expression Plasmid Construction

In the genome of *Pseudomonas putida* KT2440, *cyaY* is clustered together with a gene located at positions 5960070 to 5960294 that potentially encodes a 74-residue protein predicted to contain an iron-sulfur cluster (*98*) (Fig. 8A). This gene will be referred to as *cyaZ*. A similar arrangement of genes is found in the genome of *Pseudomonas syringae (100)* and *Pseudomonas fluorescencs PfO-1(101)* but in *E. coli (102)* and in *Pseudomonas aeruginosa* PAO-1 (*103*), *cyaY* is not clustered with such a gene. Since iron-sulfur cluster proteins could participate in iron-trafficking, it was of interest to isolate and characterize the protein encoded by *cyaZ*.

Primers were designed to amplify *cyaZ* from the *Pseudomonas sp.* strain CF600 genomic DNA and to insert *Bam*HI and *Nde*I restriction sites on the 5' and 3' ends of this

gene. PCR reactions were carried out as described in *Materials and Methods*. The 244 bp PCR product was ligated into the pGEM-T Easy vector (Fig. 16A). Digestion with *Bam*HI and *Nde*I of pGEM-T(*cyaZ*) yielded three fragments with sizes of 3009 bp, 296 bp and 240 bp (Fig. 16A). The fragment at 3015 bp is the pGEM-T Easy vector while that at 240 bp is *cyaZ*. When the *cyaZ* gene was inserted into the pGEM-T Easy vector in the reverse orientation (anticlockwise), and digested with *Nde*I site in the pGEM-T Easy vector cloning site, it can generate an additional fragment at 296 bp (Fig. 8C). The pGEM-T(*cyaZ*) construct was then digested with *Bam*HI and *Nde*I and the 240 bp fragment was ligated into *Bam*HI and *Nde*I digested pET3a expression vector. The pET3a(*cyaZ*) construct was then digested with *Bgl*II to ensure that the correct plasmid was obtained. *Bgl*II digests at position 646 in pET3a and 176 in the insert. The pET3a(*cyaZ*) construct was digested with *Bgl*II and generated two fragments at 4562 bp and 272 bp (Fig. 16B). Subsequent sequencing of the DNA from this construct for two separate transformants revealed silent mutations at some positions in the *Pseudomonas sp.* strain CF600 *cyaZ* sequence as compared to the *Pseudomonas putida* KT2440 *cyaZ* sequence. CyaZ from *Pseudomonas sp.* strain CF600 showed 98% sequence identity at the nucleotide level and 100% sequence identity at the protein level compared to CyaZ from *Pseudomonas putida* KT2440 (Fig. 17).

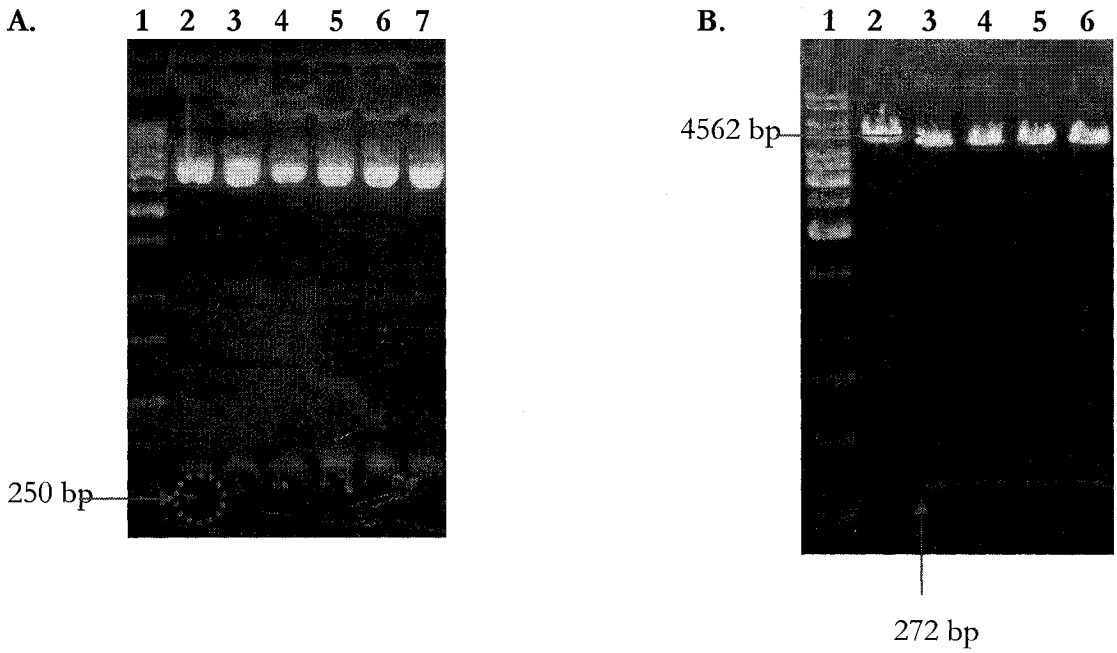

Figure 16: PCR amplification of *cyaZ* and expression plasmid construction. A. Agarose (1.4%) gel electrophoresis of pGEM-T(*cyaZ*) digested with *Bam*HI and *Nde*I. The band circled represents the fragment (~250 bp) that was cut out. Plasmid DNA from two different single colonies (2 or 5) were used. Lane 1: 1 kB ladder; Lane 2-4: Col. 2; Lane 5-7: Col. 5. The 250 bp from all Col. 2 (Col. 5) digests were pooled together and concentrated before ligation. B. Agarose (0.8%) gel electrophoresis of pET3a(*cyaZ*) plasmid DNA from different colonies (Col. 1-Col. 4) digested with *Bgl*II. Lane 1: 1 kB ladder; Lane 2: Col. 1 digested with *Nru*I (One *Nru*I cut site at position 3389 in pET3a); Lane 3: Col. 1; Lane 4: Col. 2; Lane 5: Col. 3; Lane 6: Col. 4. The DNA Ladder contains the following 14 discrete fragments (in base pairs): 10 000, 8000, 6000, 5000, 4000, 3500, 3000, 2500, 2000, 1500, 1000, 750, 500, and 250.

DNA Sequence of CyaZ

ATGAGTAGCGCCCAGGCCCGGCCGCCCAAGCCGCTTTACAGCAACGTCAGCCC
GGCAGTGCCGTCACCGTGCATCAGCGTATGCCGGCTGGACGAACAGCGGGTGTGCACCGGTTGCCATCGGC
ATGTCGAGCACATCCGCGAATGGCGCTCGGCCGATGACGAACGGCGCCGGCAGATCTGCCGCGAGGCCCAG
GTCTTGCGCGAGCAGGCTAAGGCACAC***TGA***

Protein Sequence of CyaZ (74 amino acids)

M S S A Q A R P P K P L Y S N V S P A V P S P C I S V C R L D E Q R V C
T G C H R H V E H I R E W R S A D D E R R R Q I C R E A Q V L R E Q A K
A H ***Stop***

Figure 17: DNA sequence of CyaZ from *Pseudomonas sp.* strain CF600 (top). Amino acid sequence of the translated product (bottom). The start and stop codons are bolded and italicized. The nucleotide sequence upstream of the start codon is italicized and shaded. The downstream nucleotide sequence is not available.

II.1. Purification of CyaZ from *Pseudomonas sp.* Strain CF600 Expressed in *E. coli*

The pET3a(*cyaZ*) construct was transformed into *E. coli* BL21(DE3) and crude extracts of this strain were used for purification of CyaZ. Purification of CyaZ was achieved by CM-Sepharose column chromatography followed by gel filtration chromatography on Sephacryl S-300HR. Proteins obtained at various steps of the purification procedure are shown in Fig. 18. A major band with an estimated molecular weight of 8 kDa was present together with a minor band at ~16 kDa (Fig. 18). The minor species was observed in several different preparations of CyaZ. Approximately 1.5 mg of pure protein was obtained from 6 L bacterial culture.

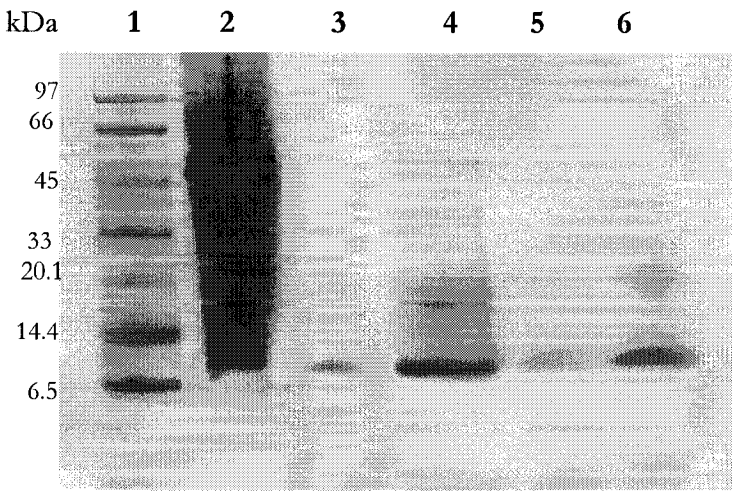

Figure 18: Tris-Tricine gel electrophoresis of fractions from CyaZ. Lane 1: LMW molecular marker; Lane 2: Crude extract of CyaZ; Lane 3: Pooled CM-Sepharose fractions; Lane 4: 65% Ammonium sulfate precipitated CM-Sepharose fractions; Lane 5: Pooled Sephacryl S-300HR gel filtration fractions; Lane 6: Concentrated Sephacryl S-300HR gel filtration fractions. All samples were diluted 1:1 with sample buffer, except crude extract which was diluted 1:4.

III. Electrospray Ionization Mass Spectrometry

Purified CyaY and CyaZ were subjected to electrospray ionization mass spectrometry to verify the molecular masses and compositions of the purified proteins. The molecular

masses of the major species in the CyaY and CyaZ preparations were found to be 12 472 Da (Fig. 19A) and 8 397 Da (Fig. 20A), respectively. The expected molecular masses of CyaY and CyaZ minus their N-terminal methionines are 12 472 Da and 8 402 Da, so this confirms the identities of the purified proteins. An additional minor peak at 24 943 Da represents the dimer form of CyaY (Fig. 19A), while the peak at 12 509 Da represents the potassium adduct of CyaY. The peak at 12 710 Da represents a HEPES adduct of CyaY (Fig. 19B). The peaks at 12 738 Da and 12 922 Da have not been identified. Similarly, a dimer peak of CyaZ was observed at 16 794 Da (Fig. 20A). The additional peak at 8 429 Da represents a possible sulfur adduct of CyaZ (Fig. 20B). Other peaks on the mass spectrum were not identifiable.

A.

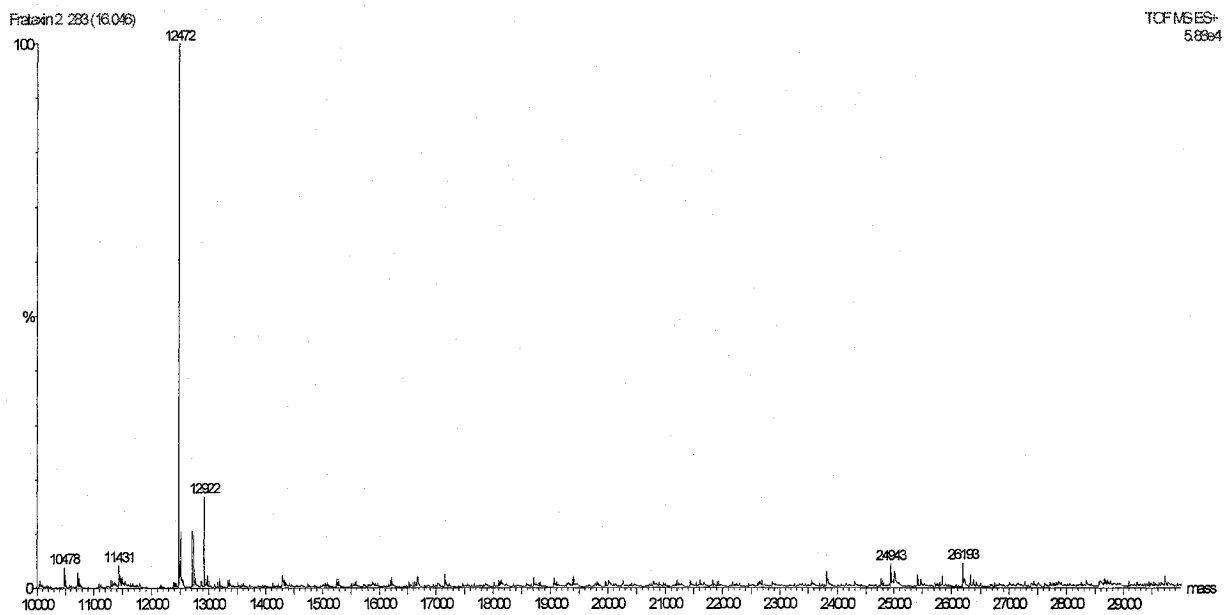

B.

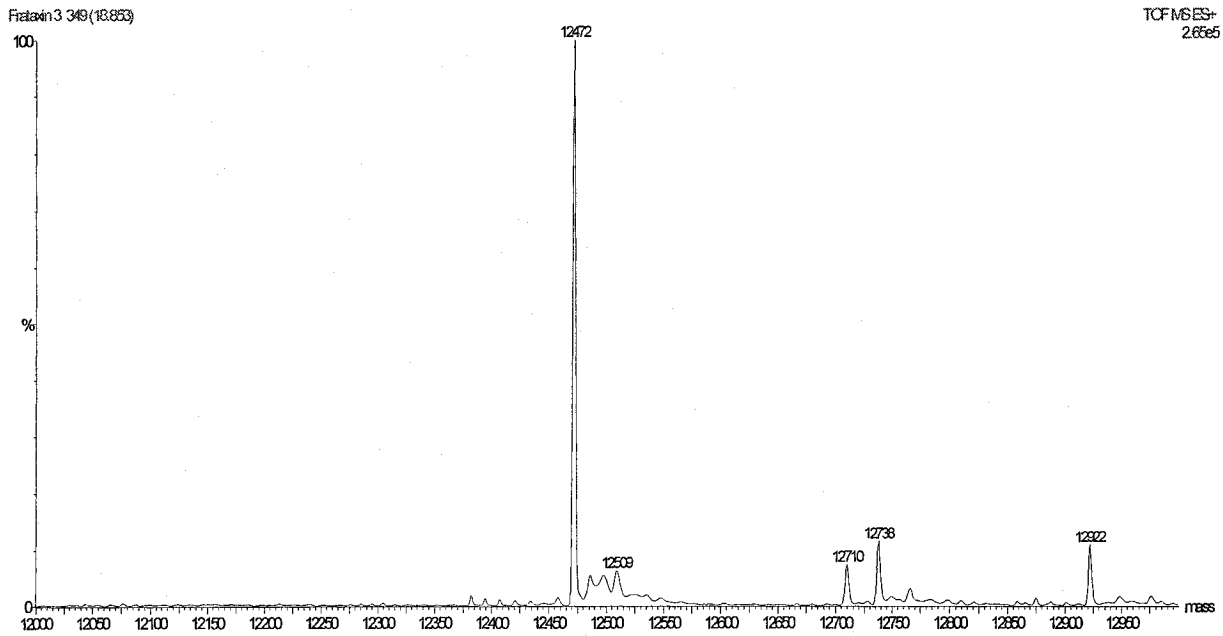

Figure 19: Mass spectra of CyaY. A. The top spectrum shows the main peak at 12 472 Da and a minor peak at 24 943Da (dimer). The bottom spectrum shows more detail around the main peak at 12 472 Da.

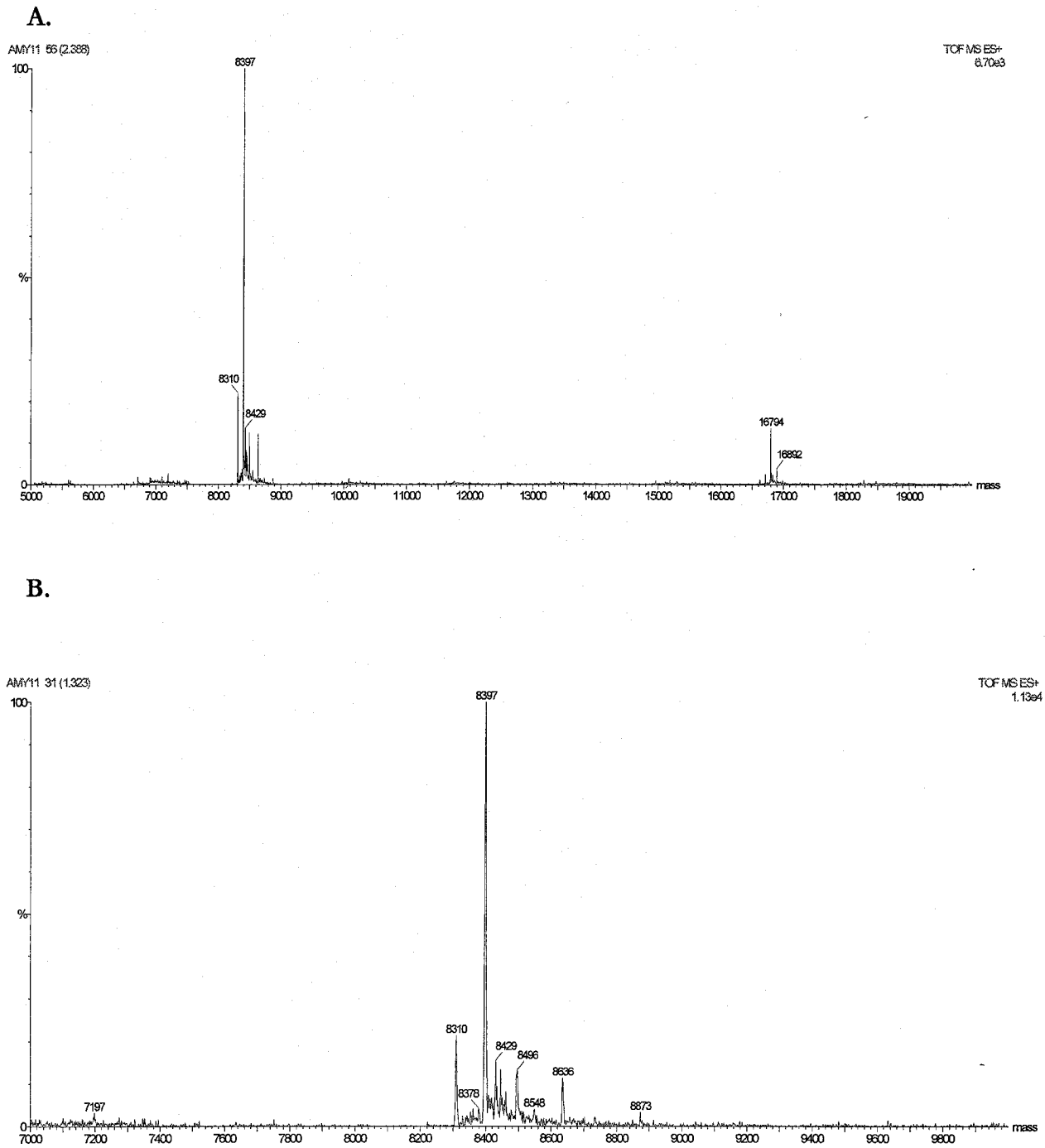

Figure 20: Mass spectra of CyaZ. The top spectrum shows the main peak at 8 397 Da and a minor peak at 16 794 Da (dimer). The bottom spectrum shows the region around the main peak at 8 397 Da. Sample was exchanged into 50 mM Tris-HCl pH 8.0 and directly injected into the MS Q-ToF (see *Materials and Methods*).

IV. Effects of Reductant on CyaY Indicate a Tendency to Dimerize

Both SDS-PAGE and mass spectrometry results indicated the presence of a dimer form of CyaY. Dimers should be dissociated in SDS sample buffer and any disulfide-linked dimers should be reduced by β-mercaptoethanol present in the sample buffer. However, disulfide linked dimers are sometimes observed when gels are overloaded with proteins in the presence of insufficient reductant (J. Powlowski, personal communication). To test this possibility, CyaY was incubated with a 10-fold excess of reductant TCEP (0.353 mM). After 1 h incubation with TCEP at room temperature (lane 4) or on ice (lanes 3 and 5) the upper band was only faintly visible (Fig. 21). After 24 h, both CyaY that was at room temperature (lane 7) and incubated on ice (lane 8) were solely in the low molecular weight monomer form.

The upper band thus appears to be a disulfide-bonded dimer. The stability of the monomer form was examined after TCEP was removed using a NAP5 desalting column. The presence of the monomer and dimer forms in samples kept on ice (Fig. 21, lane 10) or at room temperature (Fig. 21, lane 11) was monitored using SDS-PAGE. The intensity of the upper band increased significantly in samples kept at 4°C or room temperature after 4.5 h (Fig. 21, lanes 13 and 14) and 24 h (Fig. 21, lanes 16 and 17). The disulfide-bonded monomer re-formed to some extent with more dimer formation at room temperature versus 4°C. Thus, it appears that CyaY can form disulfide-bonded dimers in the absence of excess reductant. The dimer band of CyaZ also disappeared with excess TCEP (data not shown).

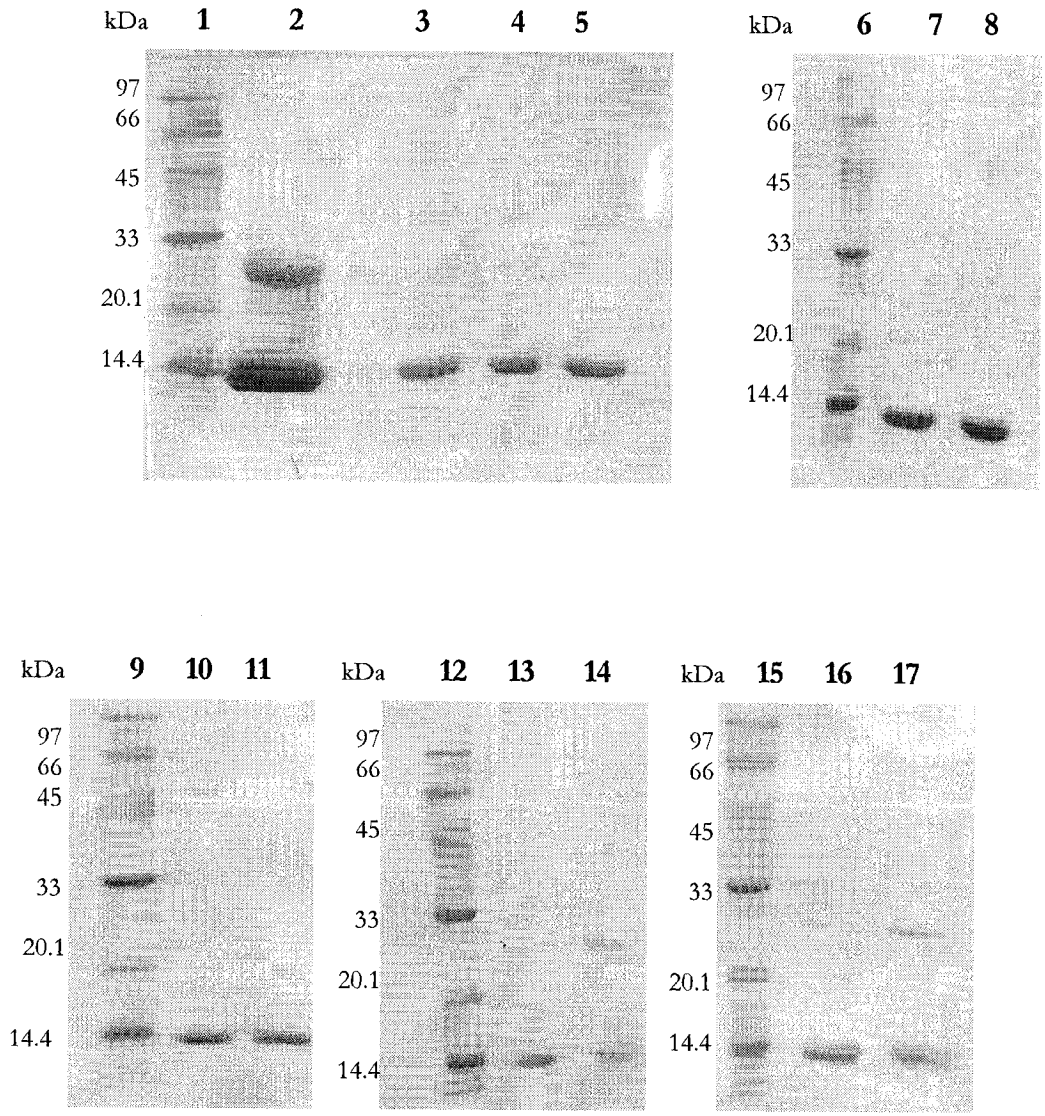

Figure 21: SDS-PAGE (12%) gel electrophoresis for TCEP-CyaY treated samples. Lane 1, 6, 9, 12 and 15 are LMW molecular markers. Lane 2: CyaY; Lane 3: CyaY-TCEP incubated on ice; Lane 4: CyaY-TCEP incubated at room temperature (samples not boiled); Lane 5: CyaY-TCEP incubated on ice (samples not boiled); Lane 7: CyaY-TCEP after 24 h at room temperature; Lane 8: CyaY-TCEP after 24 h on ice. Samples were then run though NAP5 column to remove excess TCEP. Lane 10: CyaY on ice at time 0; Lane 11: CyaY at room temperature at time 0; Lane 13: CyaY on ice at 4 h 30 min; Lane 14: CyaY at room temperature at 4 h 30 min; Lane 16: CyaY on ice at 24 h; Lane 17: CyaY at room temperature at 24 h. All samples were diluted 1:1 with sample buffer, except lane 2 which was diluted 1:4. Protein concentrations for TCEP incubated samples were 17.64 μM and 441 μM for CyaY alone with no TCEP.

V. Biophysical Techniques to Characterize CyaY

V.1. Circular Dichroism Spectroscopy of CyaY and Unfolding by Guanidine-HCl

Secondary structure and thermal stability of CyaY were examined using circular dichroism spectroscopy. The far-UV CD spectrum displayed features of α-helical and β-sheet secondary structures (Fig. 22A). The model based on primary sequence (Fig. 15) reveals a protein fold consisting of a six-stranded antiparallel β-sheet flanked by two parallel α-helices. The CD spectrum shown in Fig. 22A suggests the presence of α-helix (peak of 208 nm & 222 nm), however, the double minimum indicates a mixture of both α-helical and β-sheet structure (*104*).

The stability of CyaY from *Pseudomonas sp* strain CF600 was monitored using far-UV CD in the presence of varying concentrations of guanidine hydrochloride. As the concentration of guanidine hydrochloride denaturant increased, the secondary structure was lost (Fig. 23A). There was a dramatic change in the secondary structure of CyaY that occurred in the region of 1.5-2.0 M guanidine hydrochloride, and unfolding appeared to be complete with 3.0 M GuHCl. The presence of excess TCEP (0.802 mM) appeared to have a slight stabilizing effect since CyaY starts unfolding at 1.5 M GuHCl, but both CyaY samples were completely unfolded at 3.0 M GuHCl (Fig. 23B). In a separate experiment in which the CD spectrum was monitored as a function of temperature, the melting point of CyaY was estimated to be ~42°C (Fig. 22B).

A.

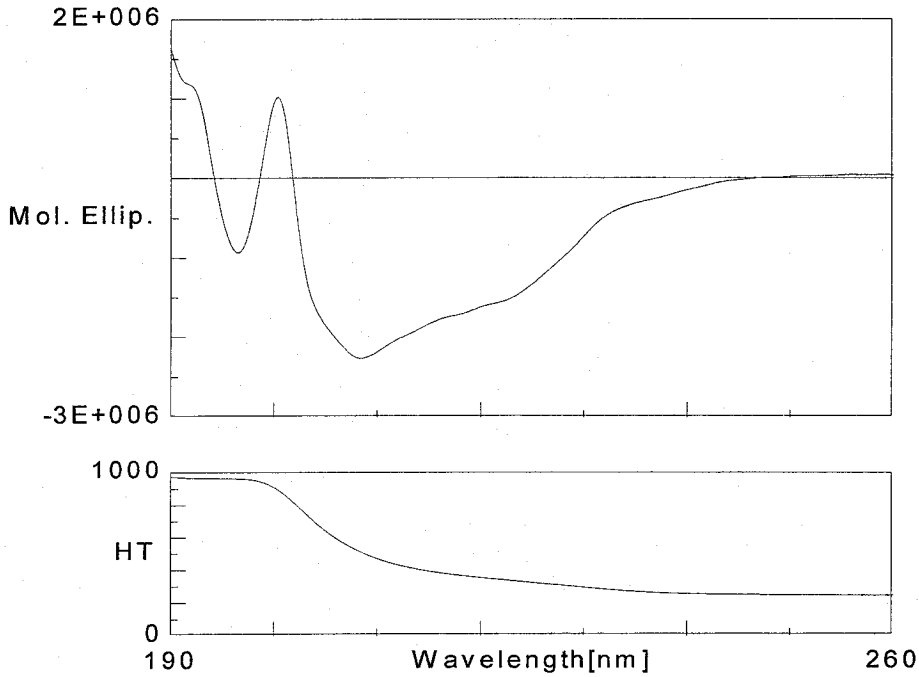

B.

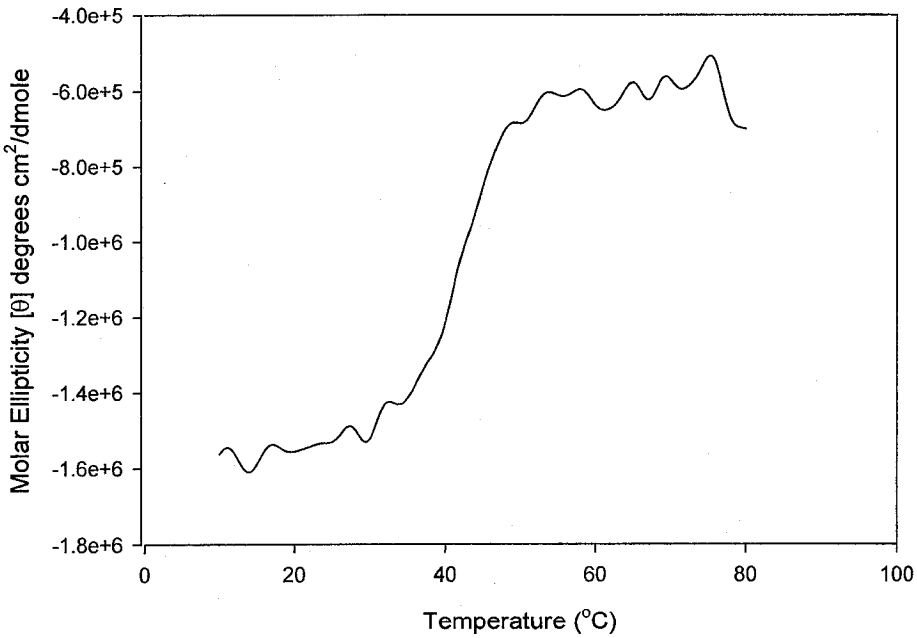

Figure 22: A. Far-UV CD spectrum of CyaY from *Pseudomonas sp.* strain CF600 showing secondary structure. The spectrum is shown at the top, while the bottom graph shows the voltage (HT) during the CD scan. The sample contained 0.5 mg/mL (40.1 μM) CyaY in 50 mM HEPES-KOH pH 7.5 buffer. B. Thermal denaturation of CyaY from *Pseudomonas sp.* strain CF600 monitored at 222 nm. The sample contained 40.1 μM in 50 mM HEPES-KOH pH 7.5 in a circular cell (0.1 cm).

A.

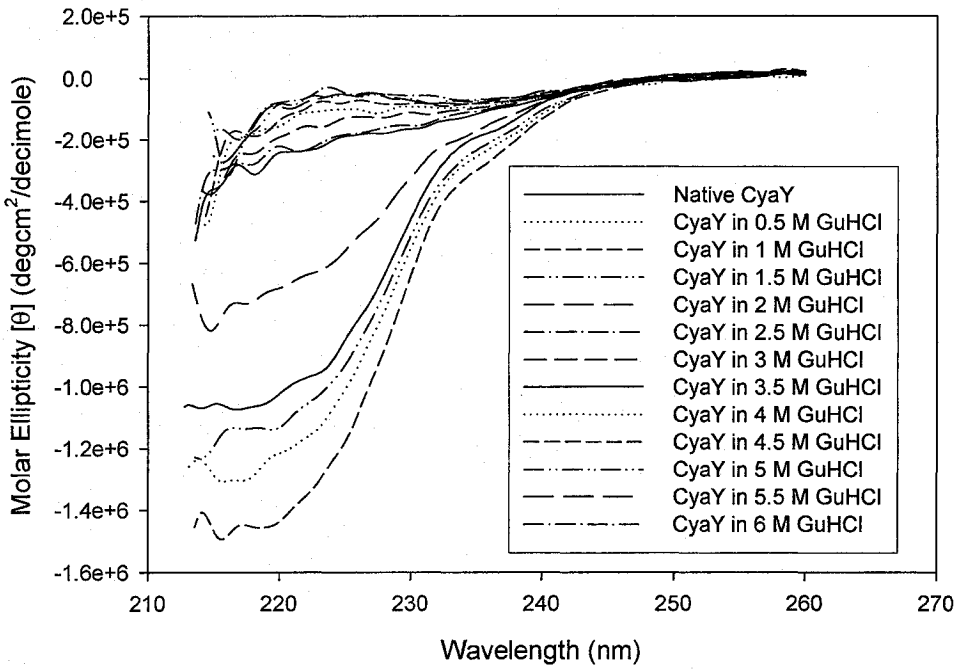

B.

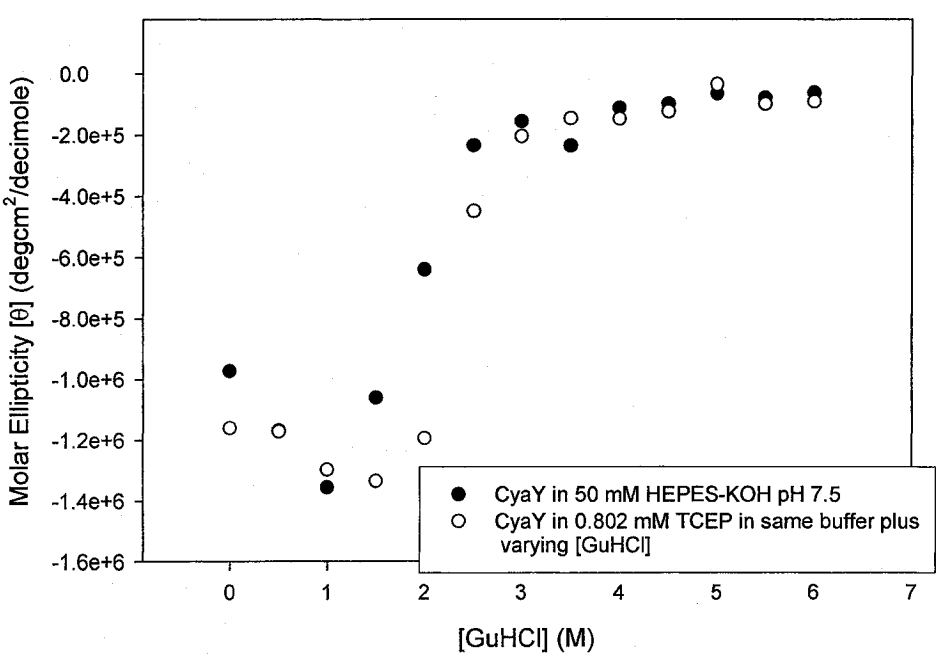

Figure 23: Denaturation of CyaY monitored using CD spectroscopy. A. Far-UV CD spectra of CyaY from *Pseudomonas sp.* strain CF600 with varying concentrations of GuHCl. CyaY (40.1 μM) in 50 mM HEPES-KOH pH 7.5 with guanidine hydrochloride concentrations of 0-6 M in 0.5 M increments. B. Unfolding of CyaY and CyaY + 20-fold TCEP (0.802 mM) monitored at 222 nm.

V.2. Fluorescence Spectroscopy of CyaY and Unfolding by Guanidine-HCl

CyaY has 3 tryptophan, 1 tyrosine and 6 phenylalanine residues which can contribute to fluorescence. Fluorescence spectroscopy with varying concentrations of guanidine hydrochloride was used to monitor CyaY unfolding. Fluorescence changes occurring in the presence of 0-6 M GuHCl using excitation wavelengths of either 280 nm, or 295 nm are shown in Fig. 24 A & B. The spectral changes were reversible, as indicated by the intensity at any given wavelength. A sample of denatured CyaY (e.g. 6 M GuHCl) was diluted back to 2 M GuHCl, and the signal was the same as for the sample at 2 M GuHCl (data not shown). Smaller increments of guanidine hydrochloride were used to more closely examine changes occurring in the range of 0.5-2.0 M GuHCl, where the largest spectral changes were observed (Fig. 25 A & B). Denaturation appeared to be complete at 3.0 M GuHCl. A similar experiment done in the presence of 10-fold excess of TCEP gave very similar results (data not shown). The results of the GuHCl-induced unfolding of CyaY monitored by fluorescence spectroscopy showed good agreement with results obtained using CD spectroscopy (Fig. 26).

A.

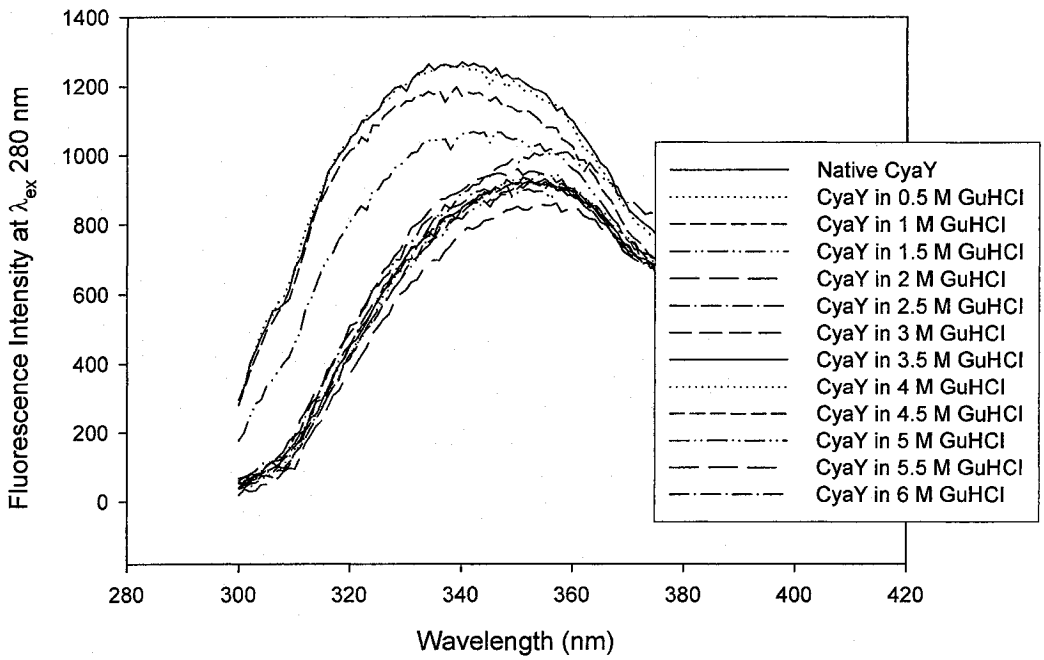

B.

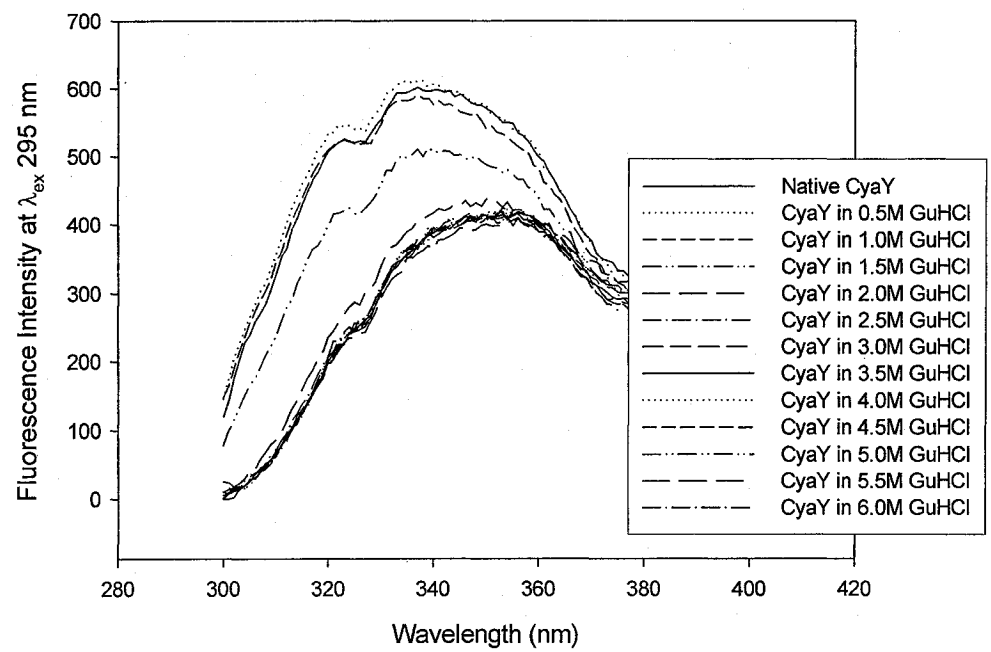

Figure 24: Fluorescence spectra of CyaY in the presence of varying concentrations of guanidine hydrochloride in 0.5 M increments. A. λ_{ex}: 280 nm. B. λ_{ex}: 295 nm. Samples contained CyaY (0.45 mg/mL) in buffer 50 mM HEPES-KOH pH 7.5 with varying [GuHCl].

A.

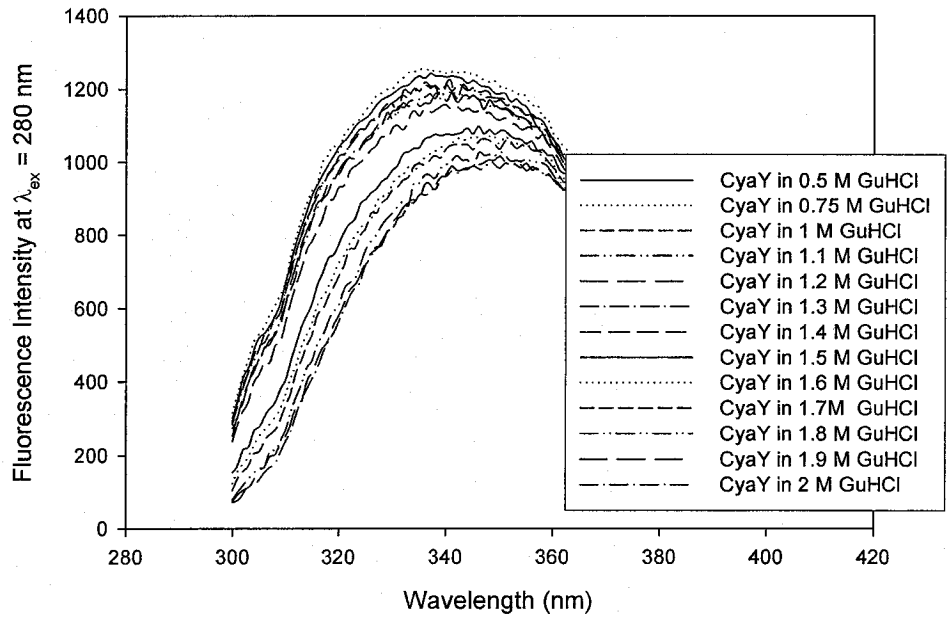

B.

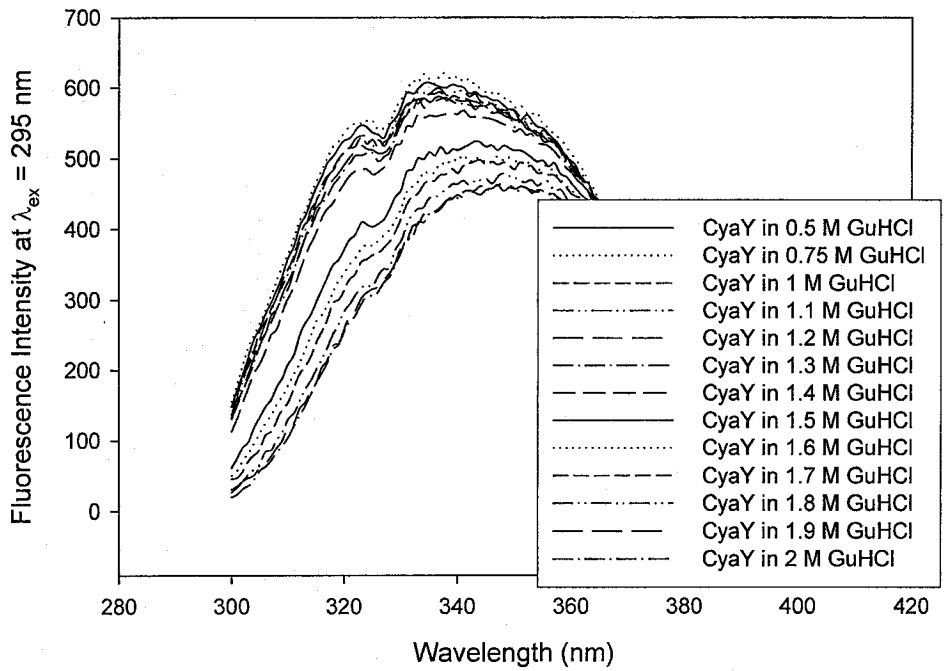

Figure 25: Fluorescence spectra of CyaY in the presence of varying concentrations of guanidine hydrochloride in 0.1 M increments. A. λ_{ex}: 280 nm. B. λ_{ex}: 295 nm. Samples contained CyaY (0.45 mg/mL) in buffer 50 mM HEPES-KOH pH 7.5 with varying [GuHCl].

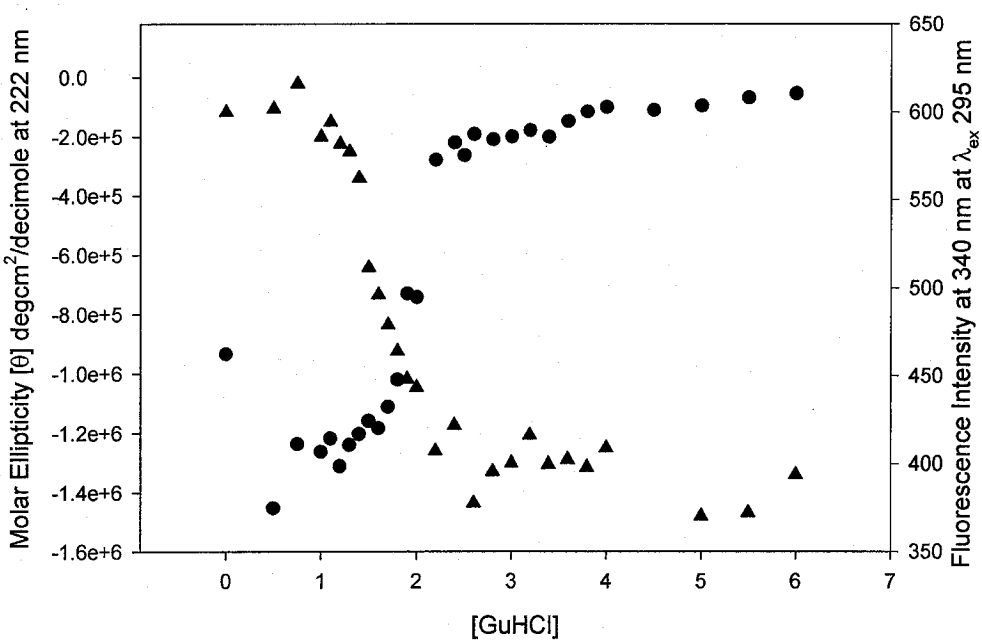

Figure 26: Overlap of denaturation results of CyaY with GuHCl for CD and fluorescence. Circles represent CD data for CyaY in varying [GuHCl] at 222 nm. Triangles represent data for CyaY in varying [GuHCl] at 340 nm with λ_{ex} 295 nm.

The fluorescence spectra of CyaY were compared with those of model compounds to obtain information about the environments of aromatic residues in the protein. Fig. 27 shows fluorescence spectra of a mixture of the tryptophan model compound, NATA (10.83 μM), and the tyrosine model compound, NAYA (3.61 μM), in 5 mM HEPES-KOH pH 7.5 buffer (Fig. 27A) and in 6 M GuHCl (Fig. 27B). In comparison to the spectra of the model compounds, it is evident that the CyaY spectra are blue shifted and decreased in fluorescence intensity. This suggests that the aromatic residues are buried in native CyaY, and are in a relatively nonpolar environment as well as being quenched. When spectra of denatured CyaY in 6 M GuHCl were compared to those of the model compounds in 6 M GuHCl, the difference was in fluorescence intensities (Fig. 27B). Although CyaY was completely denatured in 6 M GuHCl, the aromatic residues were still not completely exposed or freely accessible to the environment in comparison to the standards and were still quenched.

A.

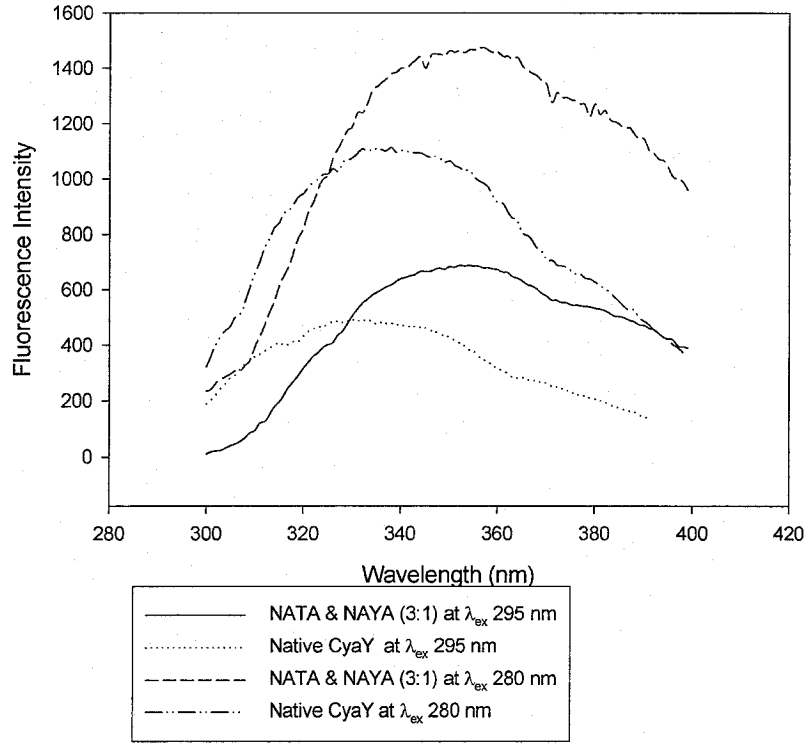

B.

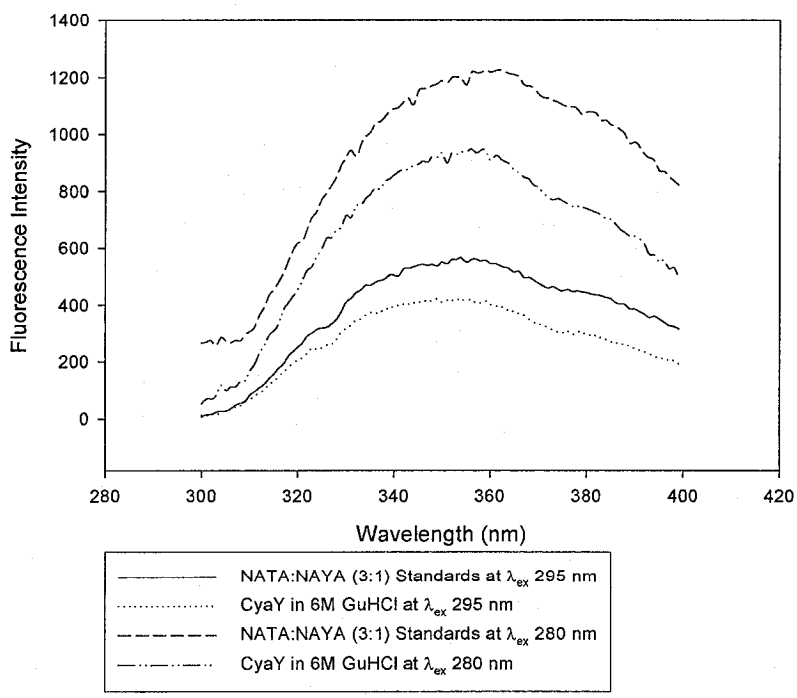

Figure 27: Comparison of fluorescence spectra of CyaY with spectra of NATA/NAYA mixtures. A. NATA (10.83 μM) & NAYA (3.61 μM) in 5 mM HEPES-KOH pH 7.5 compared to native CyaY. B. NATA (10.83 μM) & NAYA (3.61 μM) in 6 M GuHCl in the same buffer compared to 6 M GuHCl denatured CyaY.

V.3. Analytical Ultracentrifugation to Determine Native Molecular Weight of CyaY in the Presence and Absence of Fe(II)

As the oligomeric state of frataxins vary depending on the source and the presence or absence of iron, it is important to determine the molecular weight of this newly-purified CyaY and whether it changes in the presence of iron. Gel-filtration chromatography (data not shown) and SDS-PAGE suggested purified CyaY was a mixture of both monomer and dimer. Analytical ultracentrifugation can be used to determine the sedimentation coefficient and native molecular weight of a protein (*90*). Sedimentation velocity measurements show preparations contained mainly monomer (average molecular weight: 12 040 Da, compared to 12 472 predicted from the sequence), as well as small amounts of dimer (average molecular weight: 27 540 Da) and tetramer (average molecular weight: 43 920 Da) which correspond to sedimentation coefficients of ~1.44 s, ~2.48 s and ~3.46 s, respectively (Table 2). Changing the concentrations of CyaY did not seem to influence the distribution of monomer and dimer species indicating that these species did not equilibrate during the time of the experiment (Fig. 28 & Table 2). The addition of excess TCEP or KCl up to 150 mM did not appear to change the distribution of the species either (Fig. 29 & Table 3), nor did addition of Fe(II) in ratios of 1:1-20:1 (Fe^{2+}:CyaY) (Fig. 30 & Table 4). Sample runs containing CyaY incubated with Fe(III) were also performed, but Fe(III) absorbed strongly at 280 nm and interfered with the data analysis (data not shown).

Samples	8.82 μM CyaY	17.6 μM CyaY	35.3 μM CyaY	52.9 μM CyaY	70.6 μM CyaY
[Loading] Signal	0.20 0.010 0.024	0.48 0.057 0.045	0.86 0.13 0.073	1.1 0.13 0.10	1.7 0.23
% Total	77 3.9 9.3	76 9.0 7.1	75 11 6.3	79 9.3 7.2	80 11
Weight (Signal) Average Svedbergs	1.5 2.7 3.5	1.5 2.5 3.5	1.4 2.4 3.4	1.4 2.4 3.4	1.4 2.5
Molecular Weight (Da)	13310 32300 46940	11900 26650 42790	11980 26410 44620	11190 24730 41350	11800 26910

Table 2: Summary of sedimentation velocity AUC data for varying [CyaY] for Fig. 28. Values were obtained with Sedfit v. 8.9 (*90*).

Samples	CyaY + 50-fold TCEP	CyaY + 50 mM KCl	CyaY + 150 mM KCl
[Loading] Signal	0.67 0.17 0.12	0.73 0.16 0.11	0.70 0.13 0.090
% Total	68 17 12	69 16 11	70 13 9.0
Weight (Signal) Average (Svedbergs)	1.5 2.3 3.4	1.5 2.2 3.5	1.4 2.3 3.3
Molecular Weight (Da)	13310 26130 48670	12980 24800 47270	12290 24850 43670

Table 3: Summary of sedimentation velocity AUC data for CyaY with 50-fold TCEP and varying [KCl] for Fig. 29. Values were obtained with Sedfit v. 8.9 (*90*).

Samples	1:1 Fe^{2+}: CyaY	6:1 Fe^{2+}: CyaY	20:1 Fe^{2+}: CyaY
[Loading] Signal	0.60 0.080 0.096	0.60 0.11 0.097	0.51 0.15 0.088
% Total	72 9.6 12	71 13 12	62 18 11
Weight (Signal) Average (Svedbergs)	1.4 2.3 3.3	1.5 2.4 3.4	1.5 2.4 3.5
Molecular Weight (Da)	11930 25430 42770	12990 28180 47690	13010 26570 48050

Table 4: Summary of sedimentation velocity AUC data for CyaY with different ratios of Fe(II) for Fig. 30. Values were obtained with Sedfit v. 8.9 (*90*).

A.

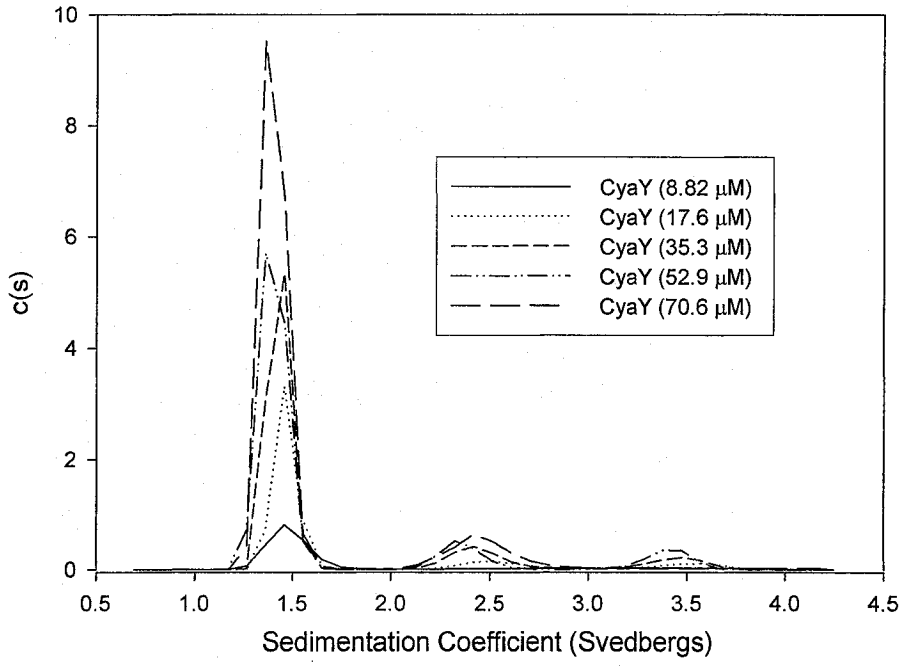

B.

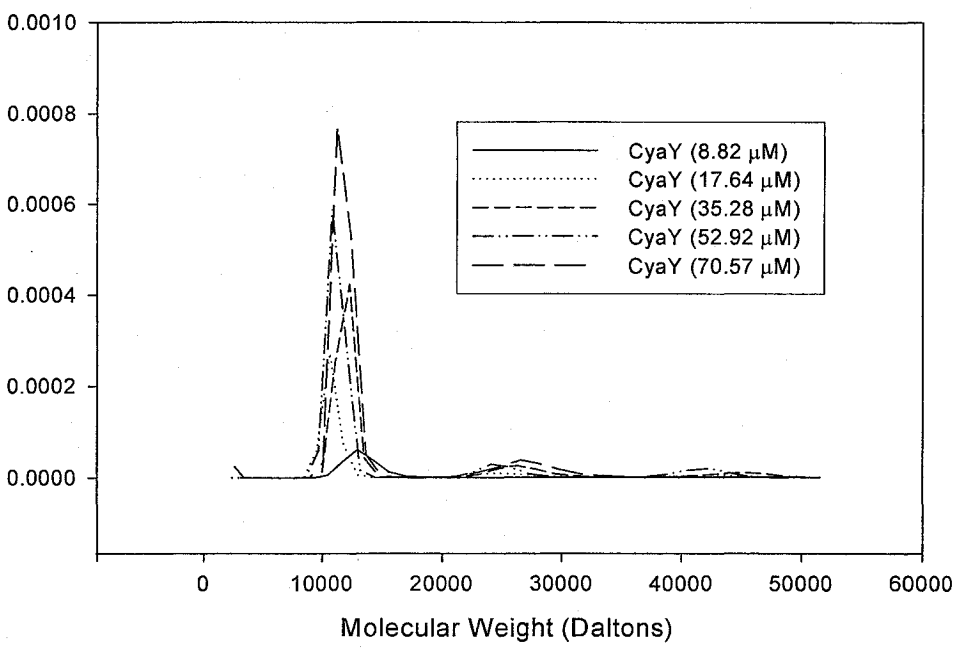

Figure 28: Sedimentation velocity AUC data for varying concentrations of CyaY of 8.82 μM, 17.6 μM, 35.3 μM, 52.9 μM and 70.6 μM in 50 mM HEPES-KOH pH 7.5. Blanks contained the appropriate buffer minus the CyaY. Graph A represents the c(s) model and graph B represents the c(M) model. All AUC runs were monitored at A_{280} at 203 893 x g at 15°C.

A.

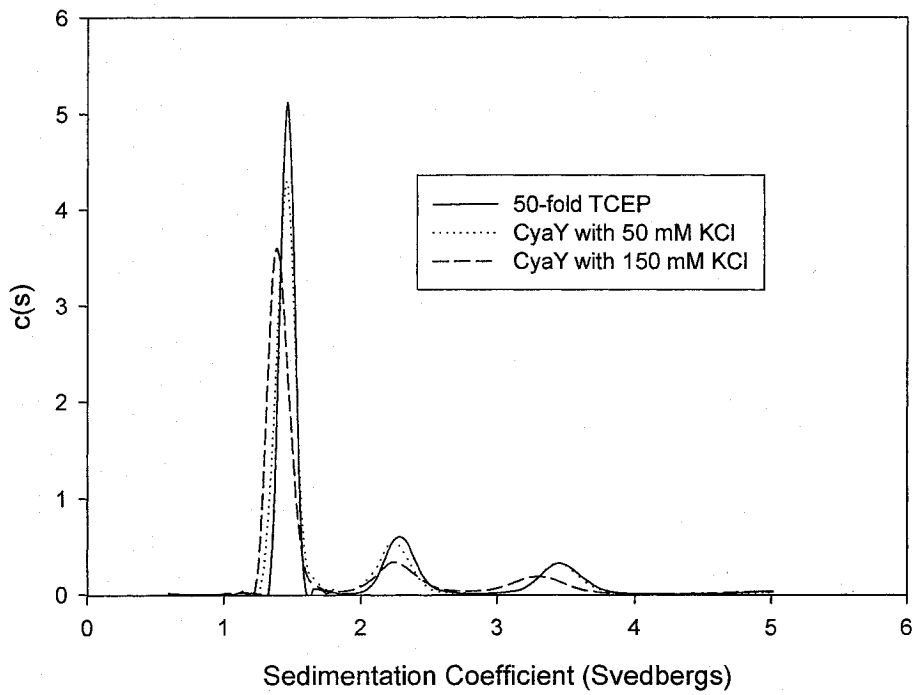

B.

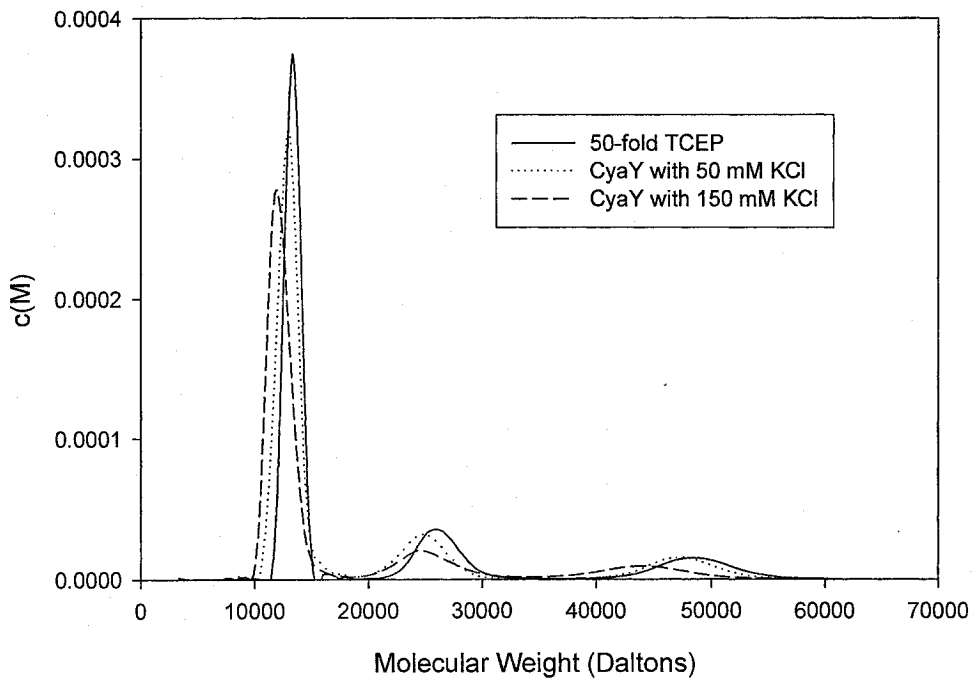

Figure 29: Sedimentation velocity AUC data for CyaY (35.3 μM) in TCEP (1.76 mM), CyaY (35.3 μM) with KCl (50 mM), CyaY (35.28 μM) with KCl (150 mM) in 50 mM HEPES-KOH pH 7.5. Blanks contained the appropriate buffer minus the CyaY. Graph A represents the c(s) model and graph B represents the c(M) model.

A.

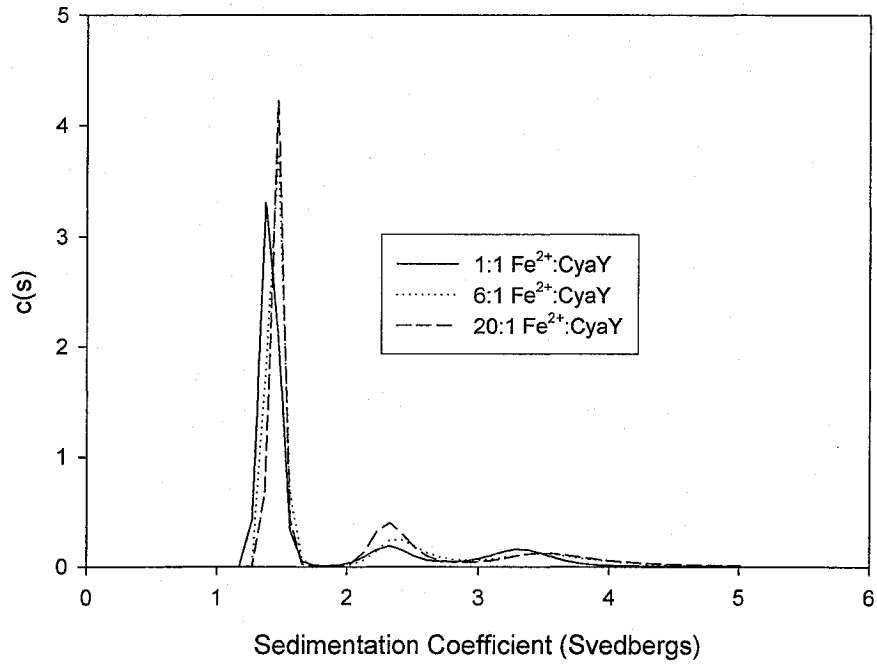

B.

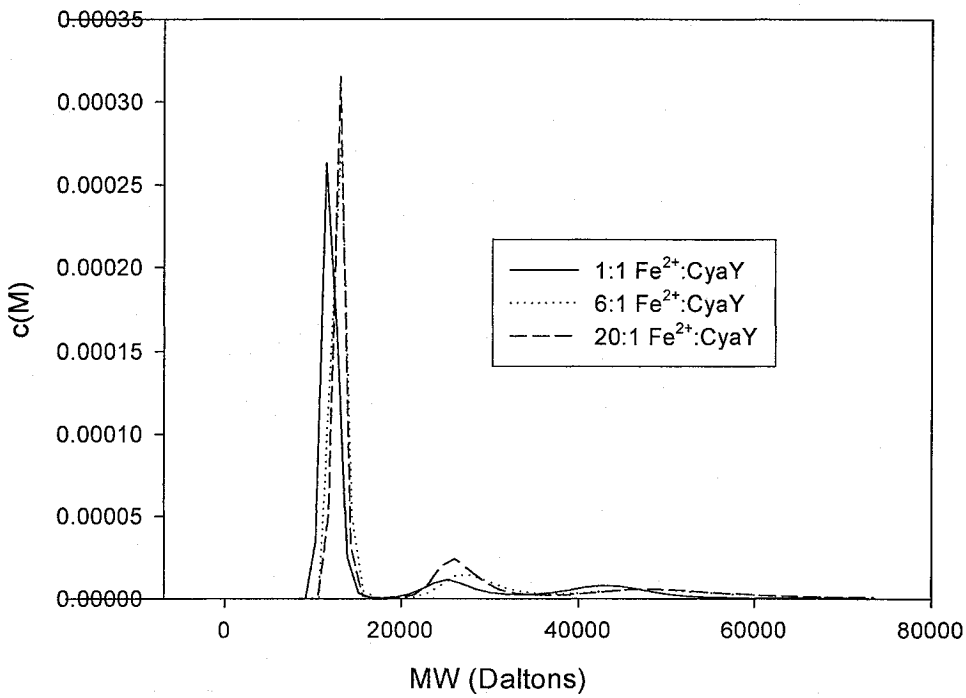

Figure 30: Sedimentation velocity AUC data for CyaY (35.3 μM) with varying [Fe^{2+}] of 35.3 μM, 211 μM and 706 μM in 50 mM HEPES-KOH pH 7.5. Blanks contained the appropriate buffer minus the CyaY. Graph A represents the c(s) model and graph B represents the c(M) model.

V.3.1. Native Gel Electrophoresis of CyaY in the Presence and Absence of Fe(II)

As it was not possible to determine the molecular weight of CyaY in the presence of Fe(III) by AUC, non-denaturing gel electrophoresis was used to examine this question. Similar experiments were done previously using Yfh1p, the yeast frataxin orthologue (*61*). Non-denaturing gel electrophoresis indicates three bands for purified CyaY (Fig. 31A), assigned to monomer, dimer and tetramer by comparison with AUC results. Addition of different ratios of Fe(II) to aerobic samples of CyaY did not alter the distribution of species (Fig. 31B). Since Fe(II) oxidizes to Fe(III) during incubation for 30 min at room temperature in native sample buffer, the sample probably consists of a mixture of both Fe(II) and Fe(III) with CyaY. Native gels were also stained with an iron staining solution containing potassium ferricyanide (data not shown) (*60*). No iron-containing aggregates were detected by this method, in contrast to the yeast homologue Yfh1, where aggregation was detected in the presence of excess iron atoms (*61*) .

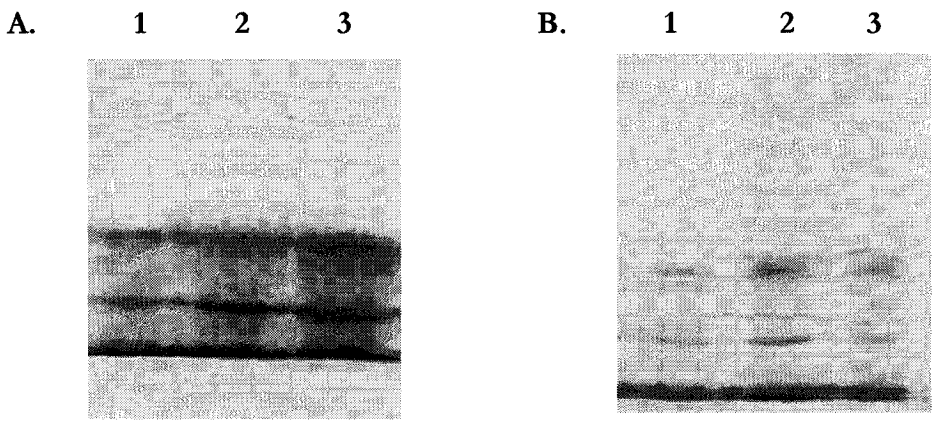

Figure 31: Non-denaturing gel electrophoresis of CyaY. A. Lane 1: CyaY (176 μM); Lane 2: CyaY (441 μM); Lane 3: CyaY (882 μM). B. Lane 1: 1 CyaY:6 Fe^{2+} (176 μM:1.06 mM); Lane 2: 1 CyaY : 12 Fe^{2+} (176 μM:2.12 mM); Lane 3: 1 CyaY:24 Fe^{2+} (176 μM:4.23 mM).

V.4. Isothermal Titration Calorimetry of Metal Ion-Binding to CyaY

Frataxin from various sources has been shown to bind or associate with iron and other metals. The objective of these experiments was to determine whether Fe(II) or Mn(II) bind to CyaY and if so, with what stoichiometry. First, a control ITC run was performed by monitoring binding of cytidine 2'-monophosphate to ribonuclease A (bovine pancreas), a reaction that has previously been well-characterized by ITC (*105*). The raw data were integrated and the total cumulative heat was plotted against the total ligand concentration (Fig. 32). The one binding site binding model was used to fit the calorimetric data to yield the number of binding sites and thermodynamic parameters for this interaction. The control run gave an n value of 0.73 ± 0.016, K_d value 2.1 μM, and ΔH = -12 ± 0.39 kcal/mol (Fig. 32B). These results were relatively close to the literature value of n = 0.95 ± 0.001, K_d value 4.0 μM and a ΔH = -13 ± 0.02 kcal/mol (*105*). The explanation for the deviations in n values could be error in the concentrations determined.

The difficulty of doing an ITC experiment with Fe(II) is that it oxidizes rapidly unless precautions are taken to prevent it. Consequently, a similar-sized divalent cation, Mn (II), was used as a substitute in these ITC experiments. Mn(II) is known to substitute for Fe(II)-binding sites in iron-binding proteins such as ribonucleotide reductase from *E. coli (106)*. Titration of CyaY (50 μM) with Mn(II) revealed an endothermic reaction (Fig. 33): thermodynamic parameters obtained by fitting to the one site binding model were: n = 1.1 ± 0.073, K_d = 14 μM, and a ΔH = 0.99 ± 0.091 kcal/mol. Thus, it appears that 1 Mn(II) binds per monomer of CyaY. This experiment was repeated with more than one preparation of CyaY, and the results were identical to those of Fig. 33.

The titration of CyaY (50 μM) with ferrous ammonium sulfate hexahydrate was done in the presence of sodium dithionite (2 mM) to maintain Fe(II) in the reduced state (Fig. 34).

Fitting to a one site binding model yielded thermodynamic parameters of: n = 0.79 ± 0.0032, K_d = 0.60 μM and a ΔH = -140 ± 0.90 kcal/mol. Thus, CyaY appears to bind Fe(II) with a 1:1 stoichiometry and much more tightly than Mn(II) binding.

A.

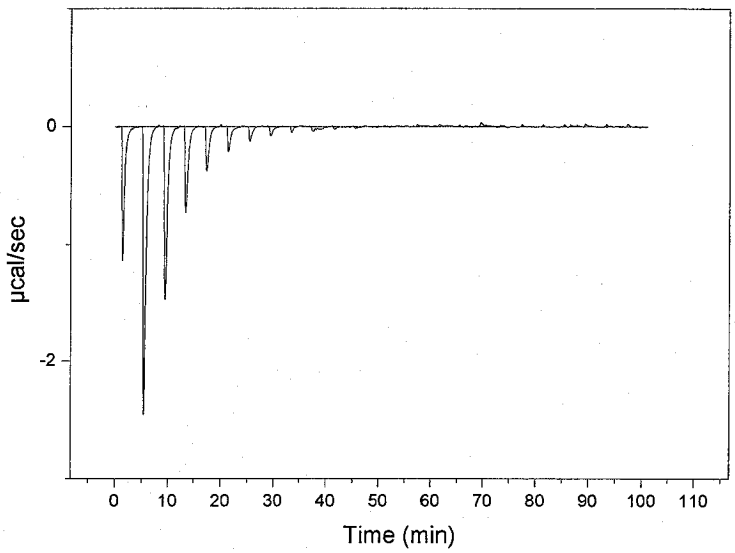

B.

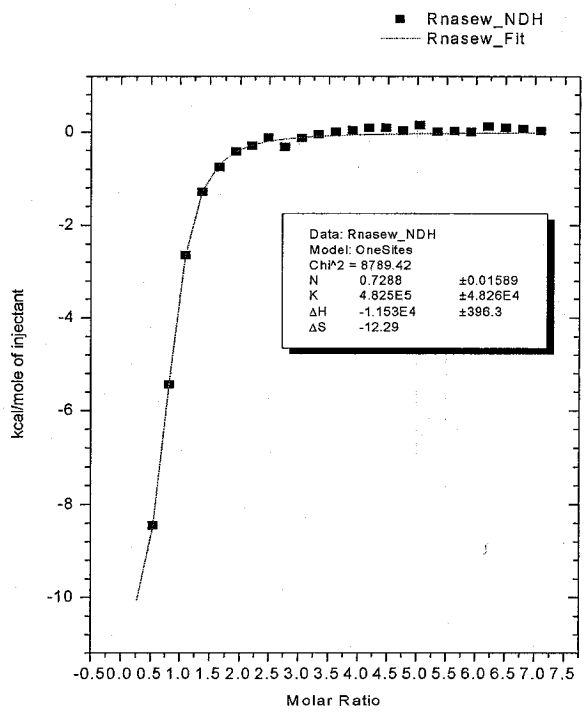

Figure 32: Binding of 2'-CMP to RNaseA monitored with ITC. A. ITC data of RnaseA (0.0292 mM) titrated with 2'CMP (2.29 mM) in buffer containing 0.2 M K-acetate pH 5.5. The raw data were obtained for 25 automatic injections of 5 µL at 28°C. B. Titration plot derived from integrated heats of binding for RNaseA (0.0292 mM) titrated with 2'CMP (2.29 mM). The line represents the nonlinear best fit data using the single-site binding model.

A.

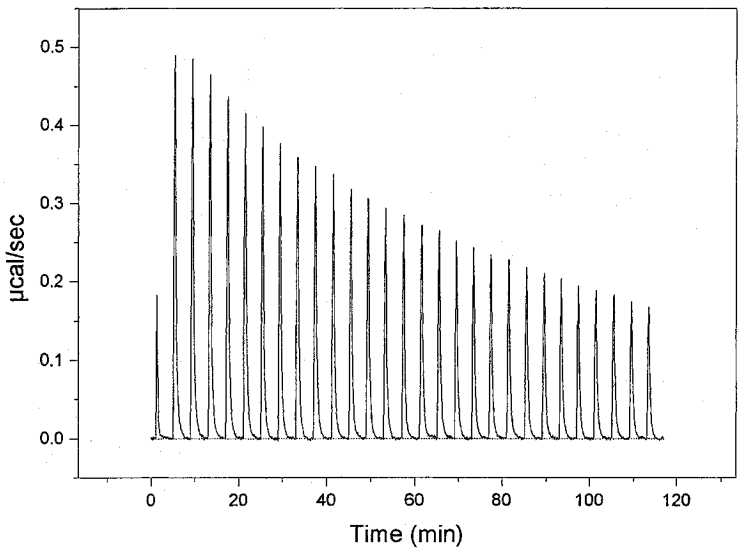

B.

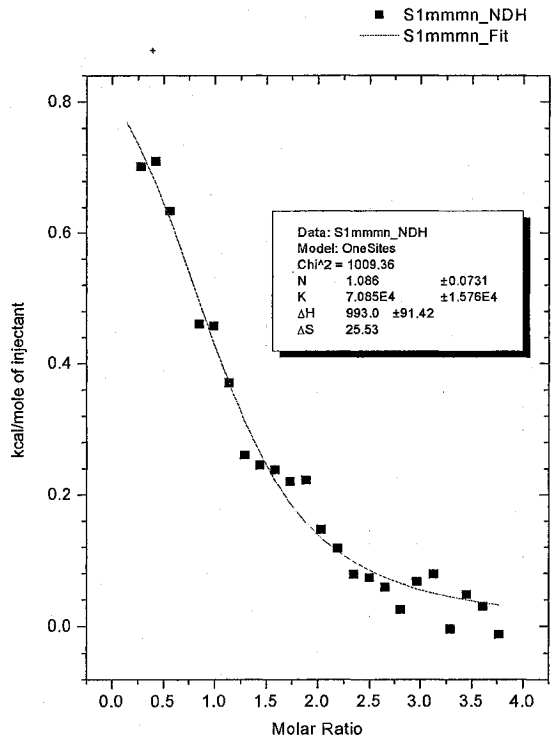

Figure 33: Binding of Mn(II) to CyaY. A. ITC data of CyaY (50 µM) titrated with $MnSO_4 \cdot 4H_2O$ (1 mM) in 50 mM HEPES-KOH pH 7.5. The raw data were collected for 25 automatic injections of 10 µL at 25°C. CyaY was also dialyzed against 50 mM HEPES-KOH pH 7.5 overnight before loading onto the ITC apparatus. B. Titration plot derived from integrated heats of binding for CyaY (50 µM) titrated with $MnSO_4 \cdot 4H_2O$ (1 mM) in 50 mM HEPES-KOH pH 7.5.

A.

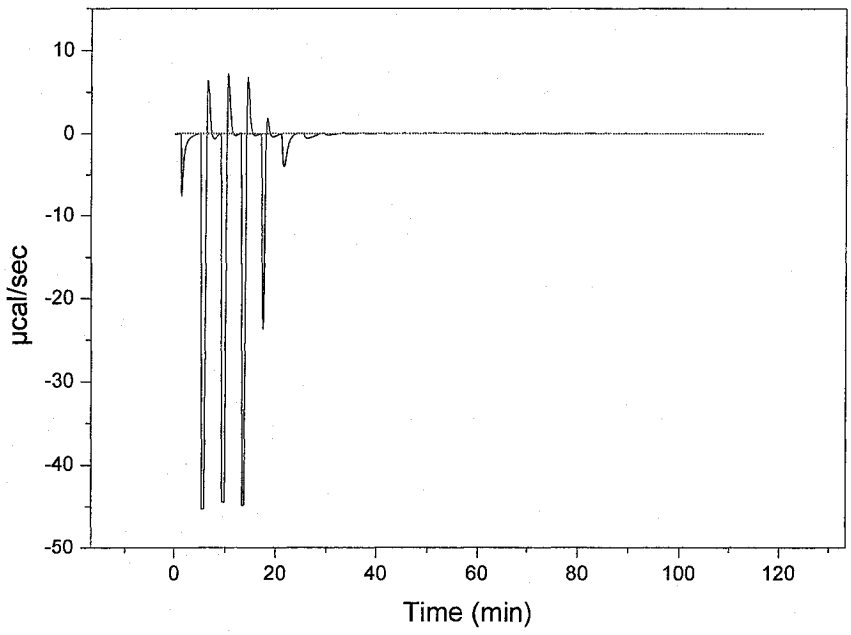

B.

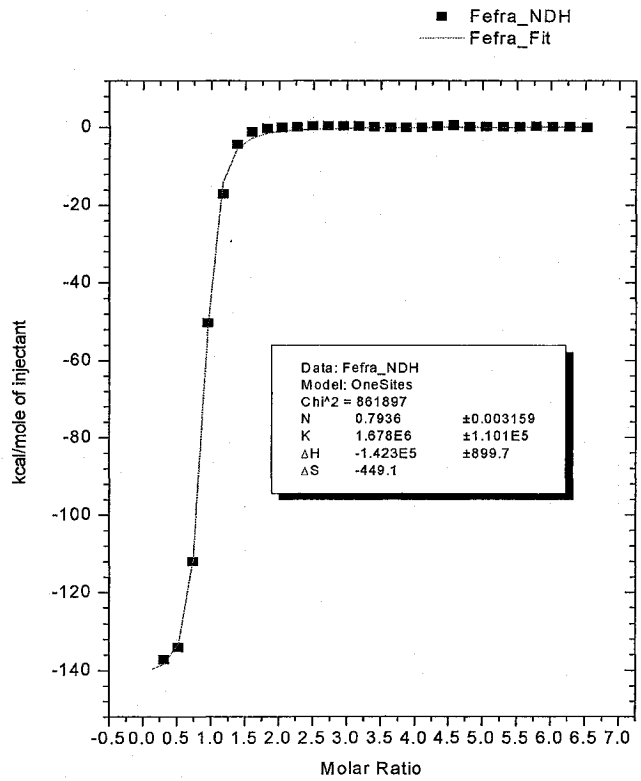

Figure 34: Binding of Fe(II) to CyaY. A. ITC data of CyaY (50 µM) titrated with $Fe(NH_4)_2(SO_4)_2{\cdot}6H_2O$(1.5 mM) in 50 mM HEPES-KOH pH 7.0 containing NaCl (150 mM) and $Na_2S_2O_4$ (2 mM) in both the protein and iron solution. The raw data were collected for 30 automatic injections of 10 µL at 25°C. B. Titration plot derived from integrated heats of binding for CyaY (50 µM) titrated with $Fe(NH_4)_2(SO_4)_2{\cdot}6H_2O$ (1.5 mM) in 50 mM HEPES-KOH pH 7.0 containing NaCl (150 mM) and $Na_2S_2O_4$ (2 mM) in both protein and iron solutions.

V.5. Mn(II) Binding to CyaY Monitored Using CD Spectroscopy

Binding of Mn(II) to CyaY was also studied using CD spectroscopy. Upon addition of 1 Mn^{2+}/CyaY, there appeared to be a change in secondary structure (Fig. 35). After the addition of 1 Mn(II), increasing the Mn(II) concentration further did not appear to have an effect on the secondary structure of CyaY. These results correlate with the findings of ITC (Fig. 33). However, under the conditions of this experiment, and given the K_d calculated in Fig. 33, 100% complex formation is not expected with 1 Mn(II)/CyaY.

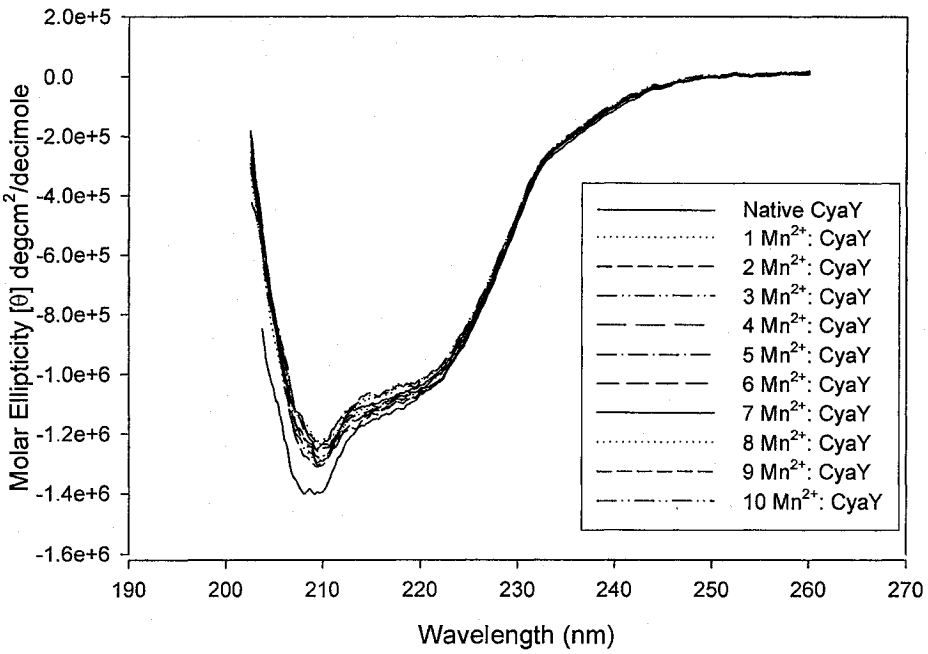

Figure 35: Far-UV CD spectra of CyaY (0.5 mg/mL) with varying [$MnSO_4{\cdot}4H_2O$] in 5 mM HEPES-KOH pH 7.5.

VI. Attempted Isolation of CyaY-Iron Complexes

In these experiments isolation of iron-containing complexes of CyaY were attempted. CyaY (561 μM) was incubated with iron (11.22 mM) under either aerobic or anaerobic conditions as described in *Materials and Methods.* The reaction mixtures were then run through a mini-spin column (incubated for 1 h at 25°C) packed with Fast-Flow DEAE Sepharose resin (aerobic or anaerobic) using NaCl (0.5 M) to elute CyaY from the column after washing through excess free iron. Fractions that contained protein were then passed through a NAP5 column equilibrated with 50 mM HEPES-KOH pH 7.5 to remove excess salt. All fractions were then examined for protein concentration and for iron. Under anaerobic conditions, the free iron and protein eluted near the same fractions and there were no stable bound Fe^{2+}:CyaY complexes under these conditions (Fig. 36A). Conversely, a Fe^{3+}:CyaY complex with a stoichiometry 1-3:1 eluted from the column under aerobic conditions (Fig. 36B).

A.

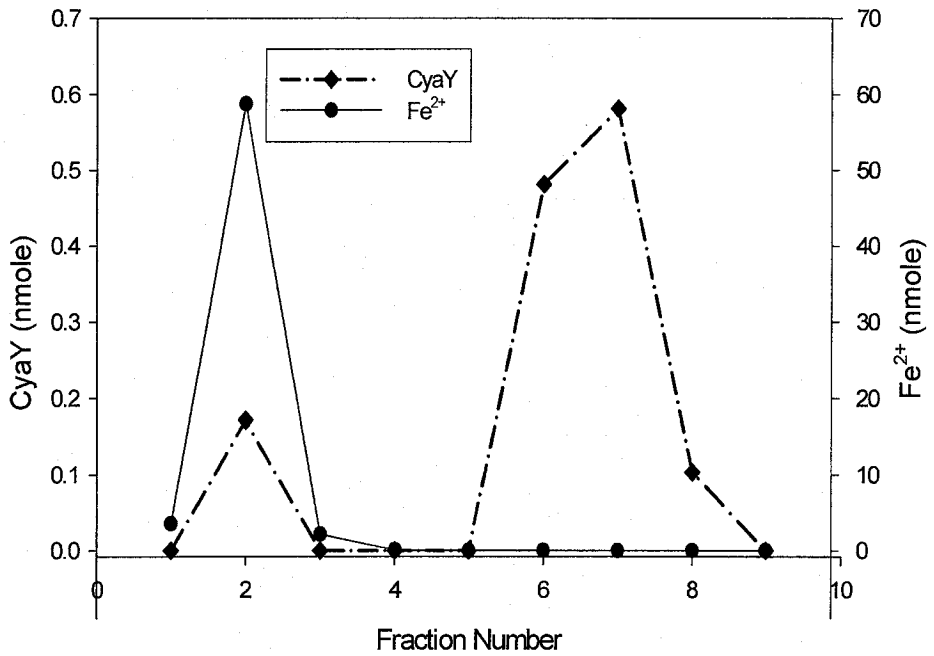

B.

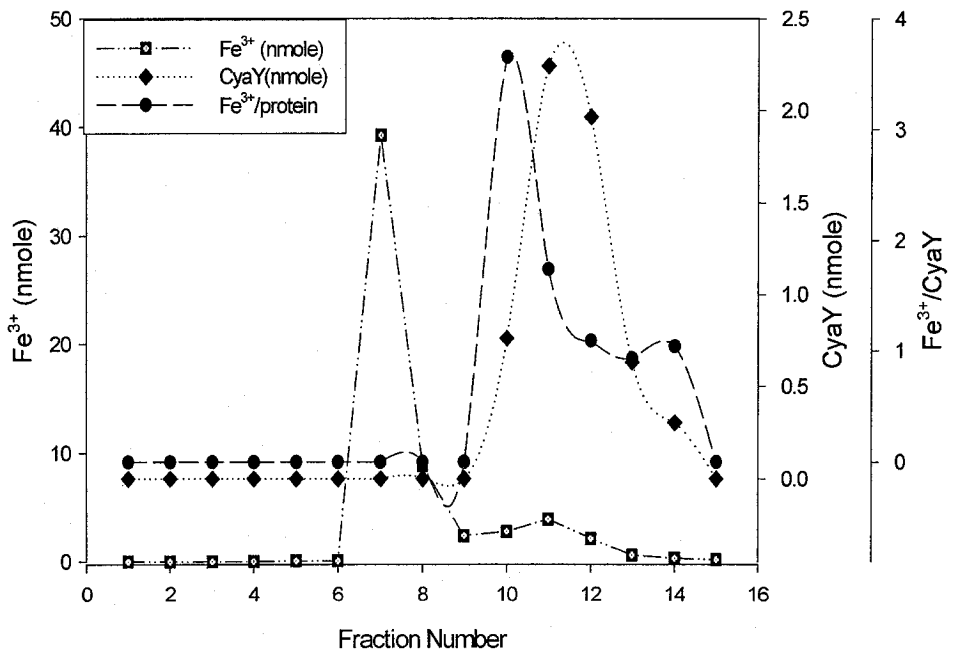

Figure 36: Chromatograms for the elution of iron-complexed CyaY from DEAE-Sepharose columns. A. CyaY (352.8 μM) was incubated with Fe^{2+} (7.05 mM). B: CyaY (561 μM) was incubated with Fe^{3+} (11.22 mM). Fractions were separated using a DEAE-Sepharose column with 20 mM Tris-HCl containing 500 mM NaCl. Fractions were desalted using a NAP5 column and then analyzed for protein and iron content. Fraction numbers are different between A and B because a small-prep (500 μL resin) was used for A and a large-prep (5.0 mL of resin) for B.

VII. Roles of CyaY in Iron Bioavailability and Iron Solubility

VII.1. CyaY Promotes Fe(II) Availability as Measured Using α,α'-Bipyridine Assays

An iron(II) chelator, α,α'-bipyridine, was used to study the ability of CyaY to maintain Fe(II) in a reduced and bioavailable form as has been done previously for other frataxin orthologues (*63, 64, 66*). CyaY (3 μM), DmpK (3 μM), holo-ferritin (0.3 μM), CyaZ protein (3 μM) or buffer was incubated with a 10-fold excess of Fe(II) (30 μM) in 10 mM HEPES-KOH, pH 7.3. Aliquots of each sample were withdrawn at specific time points and the concentration of $Fe[\alpha,\alpha'\text{-BIPY}]_3^{2+}$ was determined at 520 nm. Fe(II) in buffer alone oxidized rapidly to Fe(III), holo-ferritin did not slow oxidation of Fe(II) to Fe(III) (Fig. 37A), as expected from results reported in the literature (*64, 66*). CyaY significantly retarded oxidation of Fe(II) to Fe(III) (Fig. 37A). Similar experiments with yeast frataxin indicated that ionic strength affects this phenomenon (*64*). Therefore, the effects of increasing salt concentrations on iron oxidation were examined in the absence and presence of CyaY (Fig. 37B). Although increasing [KCl] alone retarded Fe(II) oxidation, the effect was more pronounced in the presence of CyaY.

The effects of two other proteins, CyaZ and DmpK were also examined. CyaZ is the protein encoded adjacent to CyaY on the *Pseudomonas* chromosome, and thus could be involved in CyaY function, while DmpK is important for iron center assembly in phenol hydroxylase (*81*). The combination of the CyaY and CyaZ slowed the oxidation almost completely (Fig. 37C). Thus, CyaZ appeared to have a pronounced effect on the retardation of oxidation of Fe(II) to Fe(III). DmpK had a similar effect to that of CyaY (Fig. 37C).

A.

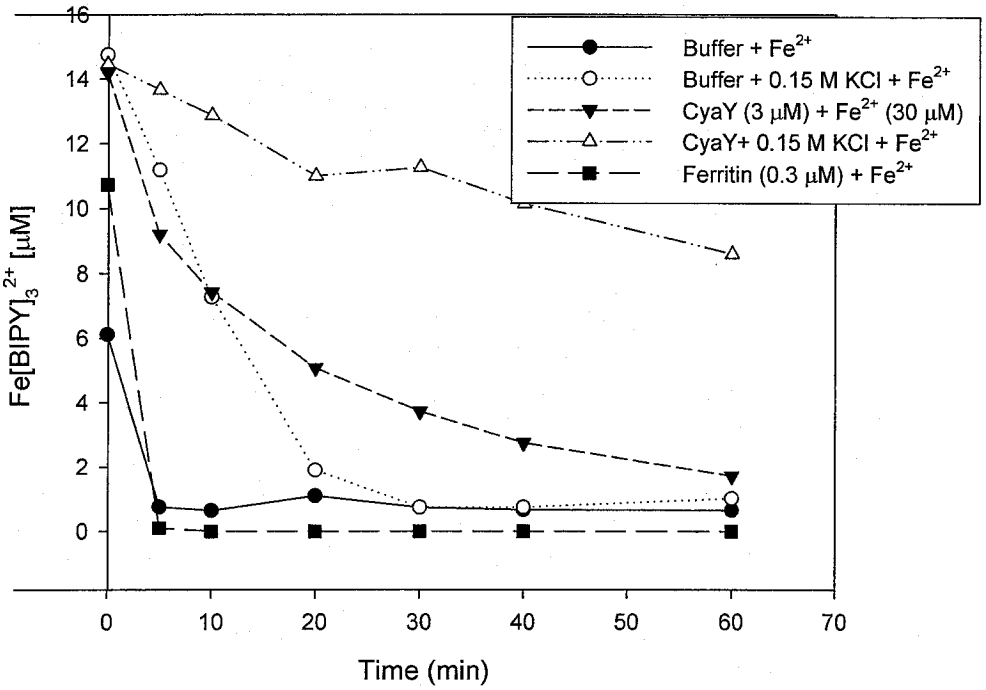
Buffer + Fe2+
Buffer + 0.15 M KCl + Fe2+
CyaY (3 μM) + Fe2+ (30 μM)
CyaY+ 0.15 M KCl + Fe2+
Ferritin (0.3 μM) + Fe2+
Fe[BIPY]3 2+ [μM]
Time (min)
0
2
4
6
8
10
12
14
16
0
10
20
30
40
50
60
70

B.

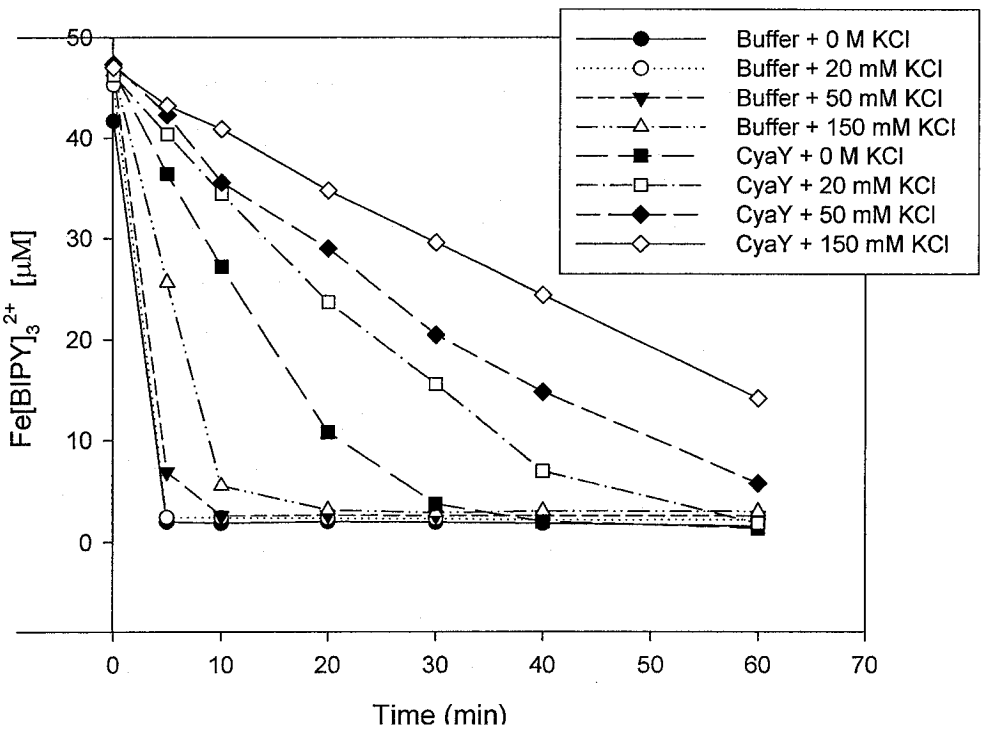
Buffer + 0 M KCl
Buffer + 20 mM KCl
Buffer + 50 mM KCl
Buffer + 150 mM KCl
CyaY + 0 M KCl
CyaY + 20 mM KCl
CyaY + 50 mM KCl
CyaY + 150 mM KCl
Fe[BIPY]3 2+ [μM]
Time (min)
0
10
20
30
40
50
0
10
20
30
40
50
60
70

C.

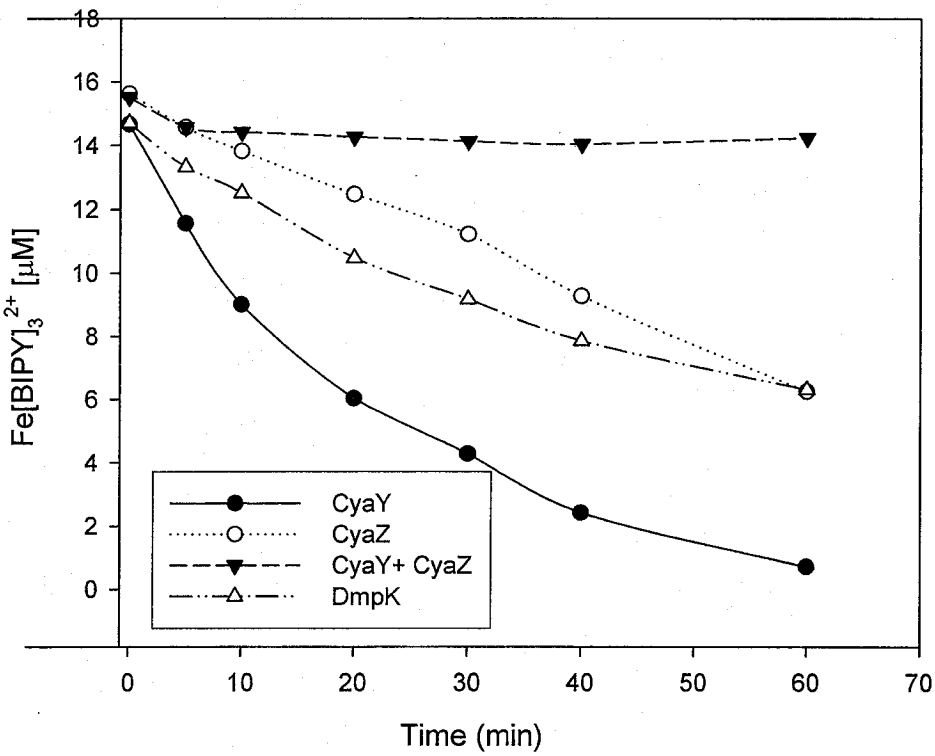

Figure 37: Fe(II) availability as determined by using α, α'-bipyridine assay. A. CyaY (3 μM), holo-ferritin (0.3 μM), or buffer alone was incubated with ferrous ammonium sulfate hexahydrate (30 μM). B. CyaY (2 μM) and $Fe(NH_4)_2(SO_4)_2{\cdot}6H_2O$ (100 μM) with varying concentrations of KCl. C. CyaY (3 μM), CyaZ (3 μM), DmpK (3 μM) were incubated with Fe^{2+} (30 μM). Each sample (4 mL) was incubated at 30°C. Aliquots (500 μL) were withdrawn at the indicated time points. BIPY was added to the aliquot to a final concentration of 2 mM. After 5 min at room temperature, the concentration of $Fe[\alpha,\alpha'\text{-BIPY}]_3^{2+}$ was monitored at 520 nm. Buffer used was 10 mM HEPES-KOH pH 7.3.

VII.2. CyaY from *Pseudomonas sp.* Strain CF600 Promotes Fe(II) Solubility

One of the potential roles of CyaY and other frataxin orthologues is to maintain iron in a soluble form (*61*). A simple experiment examining this is to incubate Fe(II) in the presence and absence of CyaY to see its effect. Under aerobic conditions, both samples turned yellow, which was an indication of iron oxidation. However, the oxidation of iron in the presence of CyaY was slower as indicated by the light yellow coloration (Fig. 38A). A visible pellet of ferric oxyhydroxide precipitate was formed in the sample that did not contain CyaY, but there was no iron precipitation in the sample that contained CyaY (Fig. 38B). Thus, CyaY does appear to have an ability to keep the Fe(II) in a soluble form.

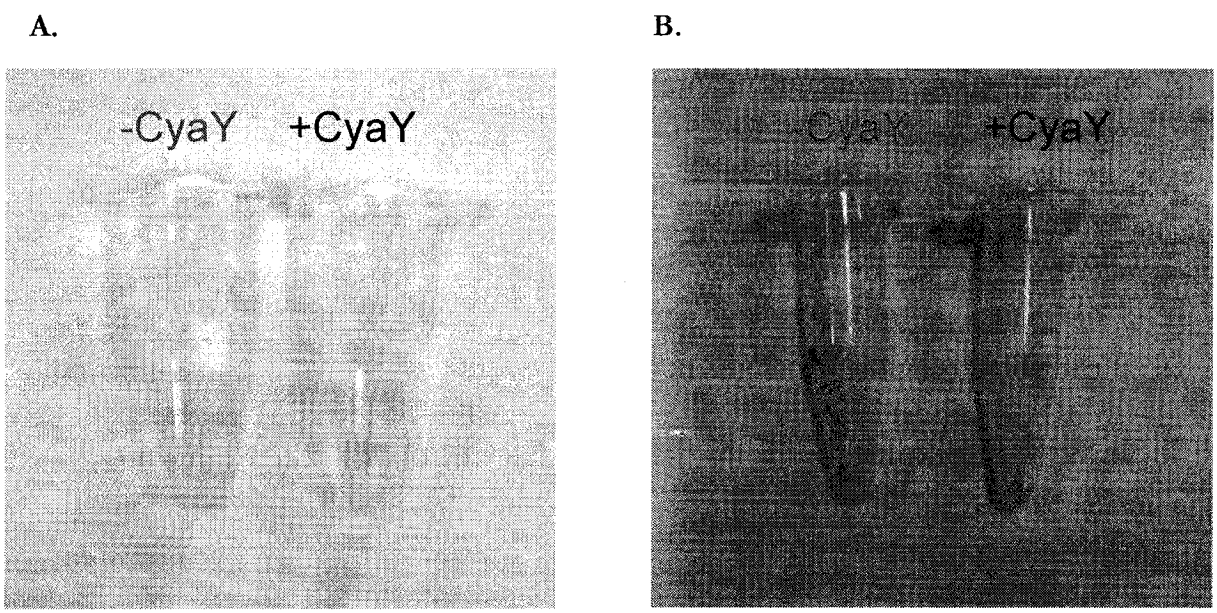

Figure 38: CyaY promotes Fe(II) solubility. $Fe(NH_4)_2(SO_4)_2{\cdot}6H_2O$ (320 μM) incubated in the presence or absence of CyaY (8 μM). The samples were incubated at room temperature for 1 h (left). Samples were centrifuged at 16 000 x g for 5 min to sediment the precipitate (visible in tubes on right).

VII.3. Reconstitution of Apo-Catechol 2,3-Dioxygenase by Fe(II) in the Presence of CyaY

Catechol 2,3-dioxygenase (C2,3-D) is an Fe(II) dependent enzyme that catalyzes the conversion of catechol to α-hydroxymuconic ε-semialdehyde (*95-97*). Active site Fe(II) can be readily removed, and the resulting apoenzyme can be reconstituted with Fe(II) (*95, 96*). Given the effect that CyaY appears to have on maintaining Fe(II) in a soluble form, the effect of CyaY on this apo-C23-D reconstitution by Fe(II) was monitored. Conversion of apo-C2,3-D to holo-C2,3-D was achieved upon addition of Fe(II), and there was a significant increase in the kinetics for rate of reactivation and extent of reactivation of C2,3-D in the presence of CyaY (Fig. 39). These observations are consistent with CyaY playing a role in maintaining iron in a bioavailable form during the reactivation reaction (Fig. 39). Addition of KCl to a reconstitution mixture containing CyaY and C2,3-D almost completely inhibited reactivation (data not shown).

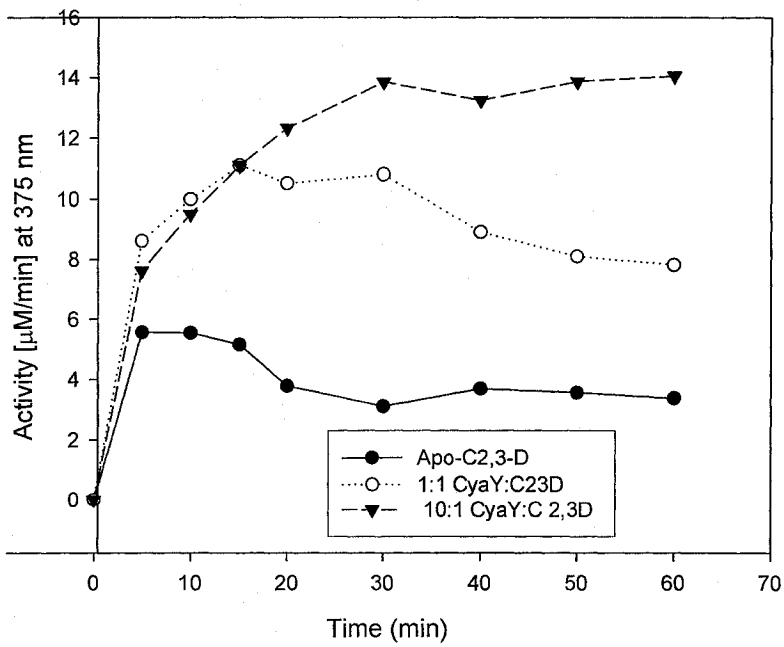

Figure 39: Reconstitution of catechol 2,3-dioxygenase with Fe(II) in the presence and absence of CyaY. Apo-catechol 2,3-dioxygenase (0.4 μM), CyaY (0.4 μM and 4 μM) were mixed with $Fe(NH_4)_2(SO_4)_2{\cdot}6H_2O$ (1 mM) in 50 mM Tris-HCl pH 7.0 and samples were assayed for activity at the indicated times.

VIII. CyaZ is an Iron-Sulfur Protein

The function of CyaZ is not known: when the protein sequence was compared to the database at NCBI using BLAST, results such as "hypothetical protein", "protein of unknown function", or "predicted [Fe-S] protein" emerged. CyaZ was expressed and purified as described earlier, and was found to enhance the ability of CyaY to keep Fe(II) in a bioavailable form (page 85). The UV-visible spectrum of the protein indicates the presence of an [Fe-S] cluster (Fig. 40). Biological $[2Fe\text{-}2S]^{2+}$ centers have characteristic visible absorption bands centered around 330 nm (ε = between 11 000-16 000 M^{-1} cm^{-1}), 375 nm (literature value not found) and 460 nm (ε = between 6 000-10 000 $M^{-1}cm^{-1}$) (*107*). The peaks at ~330 nm, 375 nm and 460 nm observed in Figure 40 are characteristic of [2Fe-2S] cluster *(108)*. Extinction coefficients for CyaZ were estimated to be 11 900 $M^{-1}cm^{-1}$ (330 nm), 7 249 $M^{-1}cm^{-1}$ (375 nm) and 6 097 $M^{-1}cm^{-1}$ (460 nm) which are within the ranges observed in other [2Fe-2S] centers. The iron stoichiometry was found to be 1.8 per CyaZ, using the ferrozine assay as described in *Materials and Methods*. Thus, CyaZ is in fact an iron-sulfur protein (*109*).

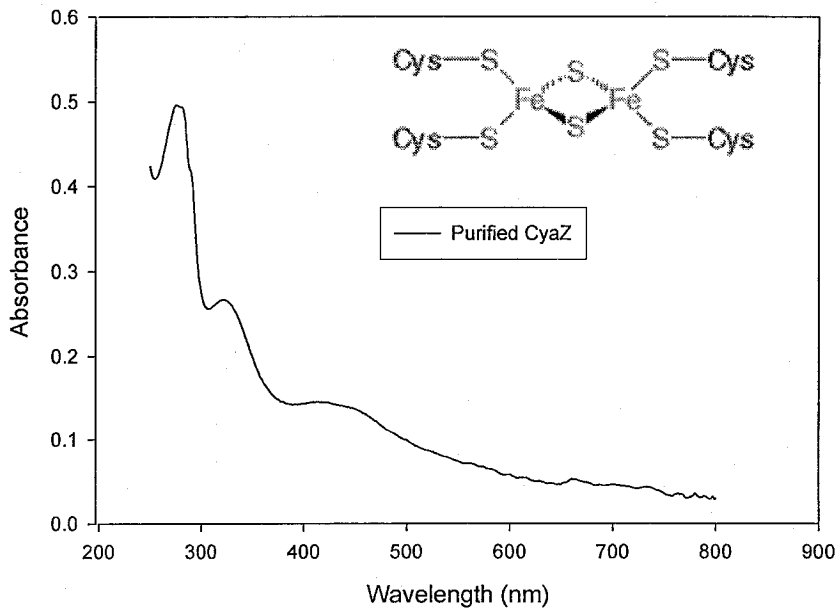

Figure 40: UV-visible spectrum of CyaZ. The samples contained CyaZ (0.35 mg/mL) in 50 mM HEPES-KOH 7.0.

IX. Chemical Cross-Linking of CyaY with CyaZ

Chemical cross-linking is a technique commonly used to detect protein-protein interactions. 1-Ethyl-3-(3-dimethylaminopropyl)carbodiimide hydrochloride (EDC) is a carbodiimide that couples carboxyl groups to primary amines via an amide bond (*110*). It is a zero-length cross-linker (no spacer between molecules being coupled) in which both proteins must be in close proximity for a bond to form. EDC was used to probe for an interaction between CyaY and CyaZ. No cross-linked product was observed in samples containing CyaY alone plus EDC, or CyaZ alone plus EDC (Fig. 41A, lanes 5-8). A band at ~20.1 kDa was observed in EDC cross-linking reaction mixtures containing both CyaZ (~8.4 kDa) and CyaY (12.5 kDa) (Fig. 41A, lanes 9-10) consistent with formation of a 1:1 CyaY-CyaZ complex. In order to help rule out collision-induced cross-linking, these reactions were repeated with 10-fold lower concentrations of CyaY and CyaZ. A 20 kDa cross-linked product was still observed using these lower concentrations (Fig. 41B). The addition of Fe(II) (194 μM) to cross-linking reactions gave similar results to these shown in Fig. 41A (data not shown). In the CyaY-CyaZ cross-linking experiment, bands were visible at 33 kDa which could represent the combination of a dimer of CyaY with a monomer of CyaZ (25 kDa + 8.4 kDa), or a dimer of CyaZ protein with a monomer of CyaY (16.8 kDa + 12.5 kDa). A minor band at ~40 kDa also appeared and could represent an interaction between a dimer of CyaY and a dimer of CyaZ (16.8 kDa + 25 kDa). A faint band at ~60 kDa could represent an interaction between a trimer of CyaY and a trimer of CyaZ (25.2 kDa + 37.5 kDa). The high molecular bands become more pronounced as the incubation time increases (Fig. 42B). The plot of log MW versus R_f generates molecular weight similar to those described above.

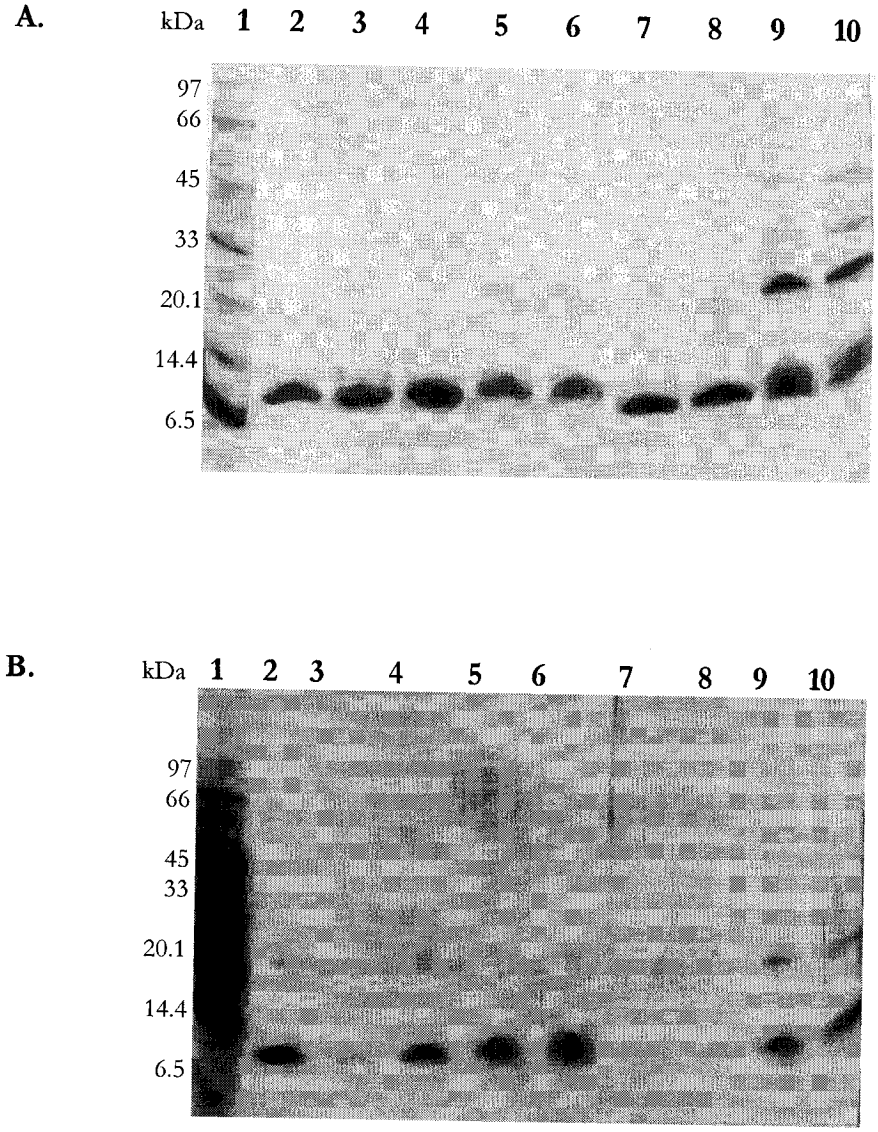

Figure 41: Cross-linking by EDC between CyaY and CyaZ. Tris-Tricine Gel A and B. Lane 1: LMW + aprotinin; Lane 2: CyaY alone; Lane 3: CyaZ alone; Lane 4: CyaY+CyaZ; Lane 5: CyaY+EDC (15 min); Lane 6: CyaY+EDC (30 min); Lane 7: CyaZ+EDC (15 min); Lane 8: CyaZ+EDC (30 min); Lane 9: CyaY+CyaZ+EDC (15 min); Lane 10: CyaY+CyaZ+EDC (30 min). Protein and EDC concentrations used were 19.35 μM and 9.68 mM in 50 mM HEPES-KOH pH 7.5 at room temperature for Gel A. Protein concentrations were diluted 10-fold for Gel B. Gel A. was stained with Coomassie blue, and Gel B was stained with silver staining solution (see *Materials and Methods*). Molecular weight marker contains phosphorylase b: 97 kDa, albumin: 66 kDa, ovalbumin: 45 kDa, carbonic anhydrase: 33 kDa, trypsin inhibitor: 20.1 kDa, α-lactalbumin: 14.4 kDa and aprotinin: 6.5 kDa.

Cross-linking reactions were carried out with BSA and CyaY as an additional control. A band appears at ~78 kDa indicating an interaction between CyaY and BSA (Fig. 42A). The time courses shown in Fig. 42 A and B indicate that while the interaction between CyaY and CyaZ is almost immediate (Fig. 42B, lane 2), that between BSA and CyaY was much slower (Fig. 42A, lane 2).

The effects of high salt concentrations on the cross-linking interactions were also examined. The addition of sodium chloride to the CyaY + CyaZ cross-linking reactions did not disrupt the protein-protein interactions between these proteins (Fig. 43A). However, the presence of salt did abolish the appearance of the band at ~78 kDa in the BSA + CyaY mixtures (Fig. 43B). This suggests that the interaction between CyaZ and CyaY was not electrostatic in nature, and that of BSA and CyaY interaction may be due to non-specific electrostatic interactions.

The chemical cross-linking reaction between catechol 2,3-dioxygenase and CyaY was also examined. These gels suggests that there were no interactions between them (Fig. 44, gel A & B). Thus, the improvement in reconstitution of catechol 2,3-dioxygenase in the presence of CyaY, shown in Fig. 39, may not involve a physical interaction between the two proteins.

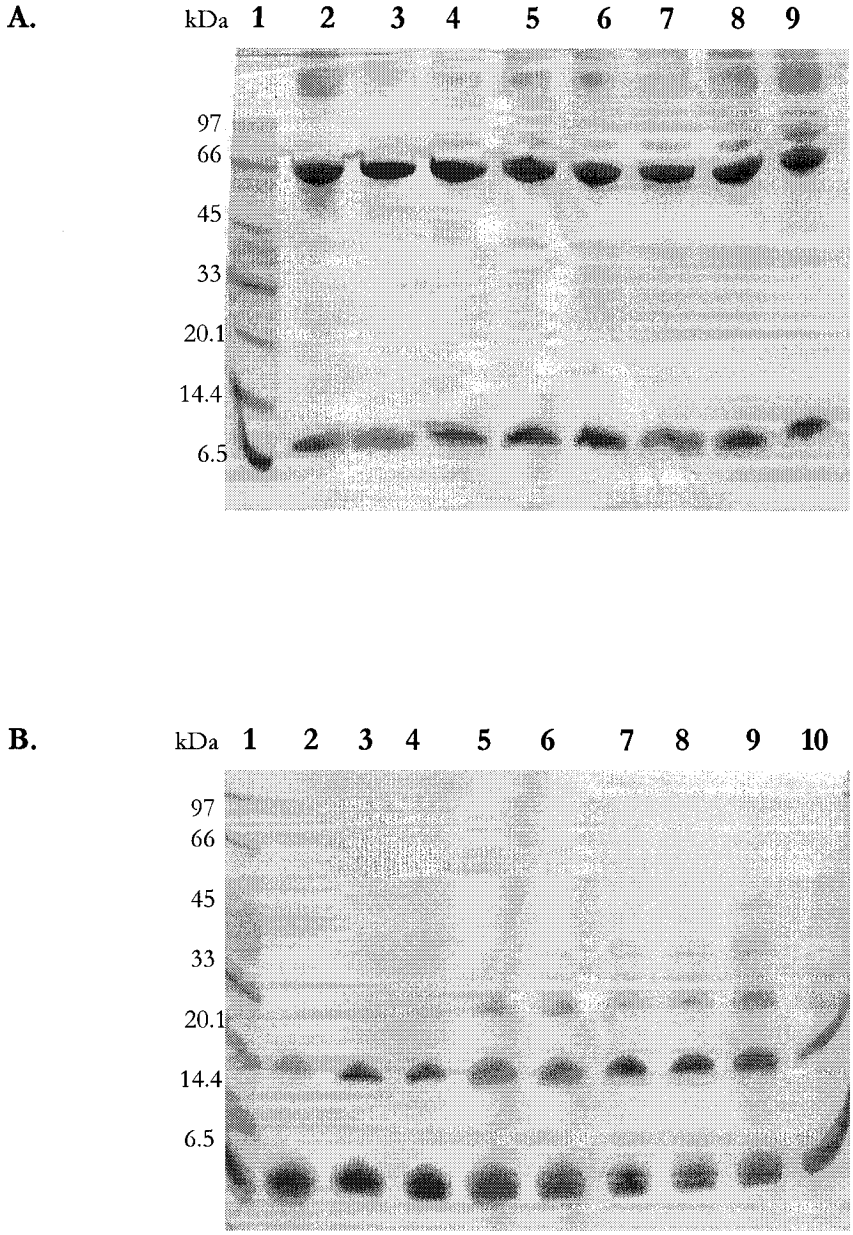

Figure 42: Time course of EDC-dependent cross-linking between CyaY and BSA (A) or CyaY and CyaZ (B). Tris-Tricine Gel A. Lane 1: LMW+aprotinin; Lane 2: 0 min; Lane 3: 2 min; Lane 4: 4 min; Lane 5: 6 min; Lane 6: 8 min; Lane 7: 10 min; Lane 8: 15 min; Lane 9: 30 min. Samples contained BSA (5.95 μM) with EDC (8.93 mM) in 50 mM HEPES-KOH pH 7.5. Gel B. Lane 1: LMW+aprotinin: Lane 2: 0 min; Lane 3: 2 min; Lane 4: 4 min; Lane 5: 6 min; Lane 6: 8 min; Lane 7: 10 min; Lane 8: 12 min; Lane 9: 15 min; Lane 10: 15 min at 4°C. Samples contained CyaY and CyaZ at 17.86 μM and EDC at 8.93 mM.

A.

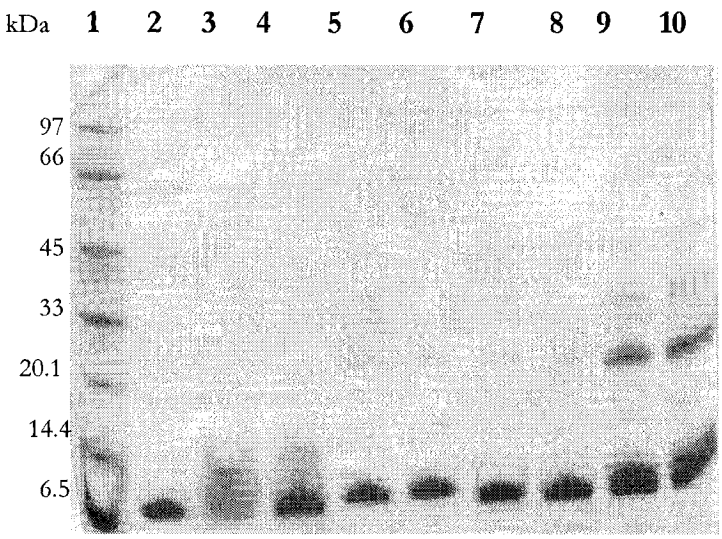

B.

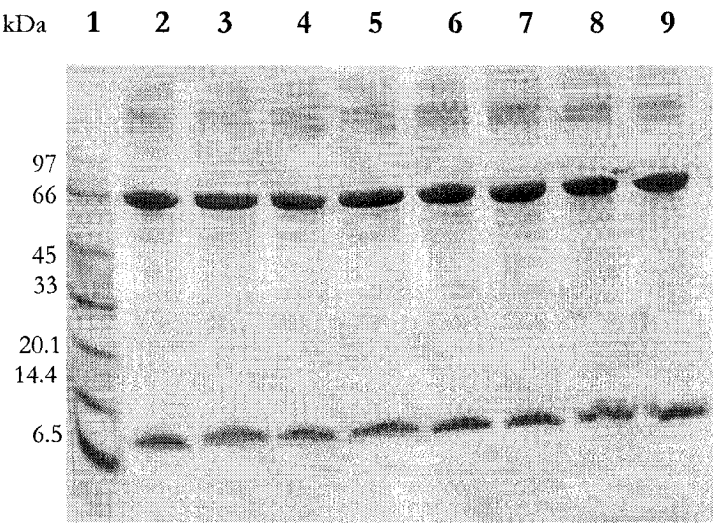

Figure 43: Cross-linking by EDC between CyaY and CyaZ in the presence of salt. Tris-Tricine Gel A. Lane 1: LMW + aprotinin; Lane 2: CyaY alone; Lane 3: CyaZ alone; Lane 4: CyaY+CyaZ; Lane 5: CyaY+EDC (15 min); Lane 6: CyaY+EDC (30 min); Lane 7: CyaZ+EDC (15 min); Lane 8: CyaZ+EDC (30 min); Lane 9: CyaY+CyaZ+EDC (15 min); Lane 10: CyaY+CyaZ+EDC (30 min). Protein and EDC concentrations used were 19.35 μM and 9.68 mM. All samples contained 0.1 M NaCl. Time course cross-linking between CyaY, BSA and 0.15 M NaCl. Tris-Tricine Gel B. Lane 1: LMW+aprotinin; Lane 2: 0 min; Lane 3: 2 min; Lane 4: 4 min; Lane 5: 6 min; Lane 6: 8 min; Lane 7: 10 min; Lane 8: 15 min; Lane 9: 30 min. Samples contained BSA (5.95 μM) with EDC (8.93 mM).

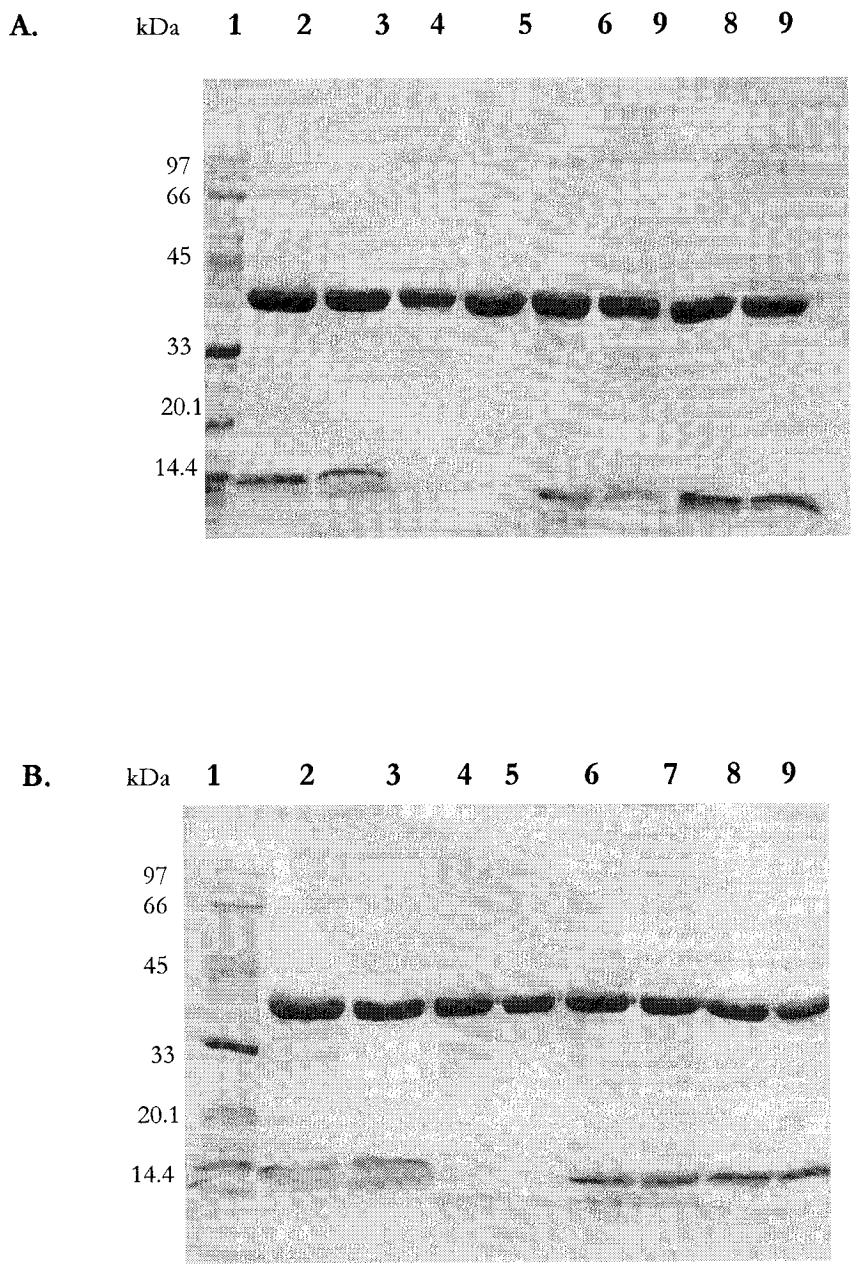

Figure 44: Cross-linking by EDC between catechol 2,3-dioxygenase and CyaY. SDS-PAGE (12%) Gel A. Lane 1: LMW; Lane 2: CyaY + Apo-C23D + Fe^{2+}; Lane 3: CyaY + Holo-C23D; Lane 4: Apo-C23D + Fe^{2+} + EDC (30 min); Lane 5: Holo-C23D + EDC (30 min); Lane 6: CyaY + Apo-C23D + Fe^{2+} + EDC (15 min); Lane 7: CyaY + Apo-C23D + Fe^{2+} + EDC (30 min); Lane 8: CyaY + Holo-C23D + EDC (15 min); Lane 9: CyaY + Holo-C23D + EDC (30 min). Gel B contains the same contents as Gel A with the addition of KCl in each sample. Concentrations used were: CyaY (16.29 μM), apo-catechol 2,3-dioxygnease (16.29 μM), holo-catechol 2,3-dioxygenase (16.29 μM), Fe^{2+} (1 mM), EDC (8.145 mM) and KCl (0.150 M).

Discussion

Frataxins are proteins expressed in organisms from bacteria to humans that have recently been implicated in important iron-trafficking reactions. The objective of this thesis was to overexpress and characterize the *Pseudomonas sp.* strain CF600 frataxin orthologue, CyaY, focusing on its iron-binding properties and potential roles in donation of iron to enzymes of the *dmp* operon encoded phenol degradative pathway. It was also of interest to identify a possible accessory role for a putative iron-sulfur protein (CyaZ) that is encoded upstream of *cyaY* in the *Pseudomonas sp.* strain CF600 genome.

Both the *cyaY* and *cyaZ* genes from *Pseudomonas sp.* strain CF600 were PCR-amplified successfully from genomic DNA and cloned into the T7-polymerase dependent pET3a expression vector. BLAST results for the *Pseudomonas sp.* strain CF600 CyaY sequence showed identity of 39% to *E. coli* CyaY (CAA47281), 29% to yeast Yfh1 (1XAQA), and 28% to human Hfra (Q16595) at the protein level. Conservation between CyaY from *E. coli* and *Pseudomonas sp.* strain CF600 is mostly with the Glu and Asp residues and in the negative patch between residues 20-23 of *E. coli* CyaY. The protein sequence alignment did not exhibit any sequence identity towards other known iron binding proteins outside this family.

Molecular weight measurements using mass spectrometry confirmed that the correct proteins had been purified. The molecular weight of the CyaY from *Pseudomonas sp.* strain CF600 was estimated to be 12 472 Da using Q-ToF mass spectrometry corresponding to the exact mass deduced from the gene sequence of CyaY, but with the N-terminal methionine group cleaved off (MW: 12471.75 Da). A small peak at 24 943 Da observed in the mass spectrum indicated the presence of dimer (Fig. 19A): a similar conclusion was made on the basis of SDS-PAGE experiments which also suggested that the dimer is disulfide-bonded.

The band at ~25 kDa disappeared upon addition of the reductant, TCEP, and the removal of the reductant resulted in its reappearance (Fig. 21). The modeled three-dimensional structure of CyaY from *Pseudomonas sp.* strain CF600 indicted that the sole cysteine residue, Cys83, was relatively exposed to the surface, allowing the possibility of disulfide bond formation (Fig. 45). A peak at 12 509 Da in the mass spectrum (Fig. 19B) represented a potassium adduct of the CyaY protein and a few other very minor peaks were not assigned.

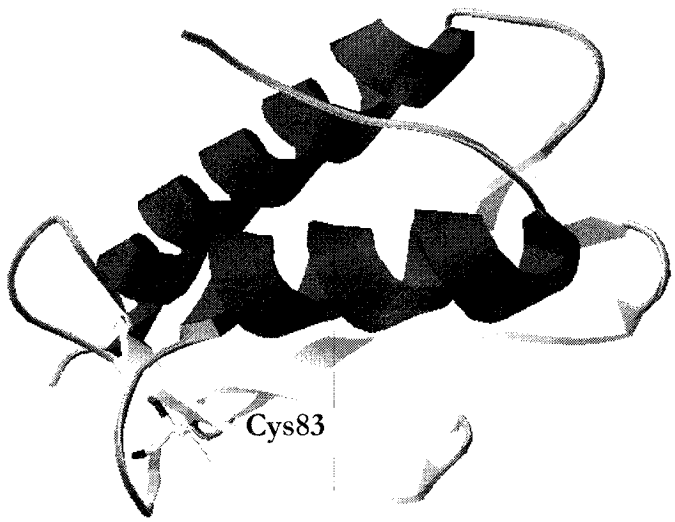

Figure 45: Modeled 3-D structure of CyaY from *Pseudomonas sp.* strain CF600 showing the surface-exposed Cys83 (structure generated with Swiss-PDB) (*55*).

In the genome of *Pseudomonas putida* KT2440, *cyaY* is clustered together with a gene that we have called *cyaZ*, which potentially encodes a 74 amino acid protein predicted to contain an iron-sulfur cluster. According to the literature, *cyaY* and *cyaZ* possesses their own transcription and translation control factors (*46*). Iron-sulfur clusters are cofactors of proteins found in all organisms, and they are important in redox reactions, catalysis, and they also carry out some regulatory functions (for a recent review, see (*111*)). Since CyaY was predicted to be an iron-binding protein, it is possible that an associated redox protein may

influence its iron-trafficking properties. Results from sequence comparisons of the *cyaZ*-encoded protein revealed the highest sequence identities with a MutT/nudix family protein from *Pseudomonas syringae* (74%, AAZ35858), a protein of unknown function DUF1289 (72%, YP233290), followed by sequences of many hypothetical and conserved protein of unknown function. An interesting aspect of the DUF1289 family is that it consists of a number of hypothetical bacterial proteins, in which the aligned region includes approximately 56 residues, and contains 4 highly conserved cysteine residues towards the N-terminus. *CyaZ* homologues were clustered with *cyaY* homologues in *Pseudomonas syringae (100)* and *Pseudomonas fluorescens* PfO-1 *(101),* but not in *E. coli* (*102*) and in *Pseudomonas aeruginosa* PAO-1(*103*). It is very possible that the cluster of *cyaY* and *cyaZ* gene may help explain how metal ions are distributed to their final destination in bacterial systems.

As no CyaZ orthologues has been purified and shown to contain an iron-sulfur cluster, it was important to purify and characterize it. The theoretical molecular weight of CyaZ is 8402.50 Da and the molecular weight of the purified protein was determined to be 8 397 using electrospray ionization mass spectrometry (Fig. 20A). The discrepancy in molecular weight may be explained by the formation of disulfide bonds between 4 cysteine residues, resulting in loss of 4 hydrogens, a mass loss of 4 Da. A minor peak at 16 794 Da suggested the presence of a dimeric form of this protein, which is consistent with the observation of a band at ~17 kDa SDS-PAGE (Fig. 20B). An additional peak in the electrospray ionization mass spectrum at 8 429 Da could represent an adduct with sulfur that was part of the iron-sulfur cluster.

The presence of peaks at ~330 nm, 425 nm and 460 nm on the UV-visible spectrum of CyaZ indicates the presence of a [2Fe-2S] cluster. Similar UV-visible spectra have been reported for ferrochelatase from *S. pombe, C. crescentus,* and *M. tuberculosis* as well as other

proteins that contain a [2Fe-2S] cluster *(108, 109)*. The presence of $2Fe^{2+}$/CyaZ was confirmed using a colourimetric assay for iron. These data show that, as predicted by the presence of conserved cysteine residues in the amino acid sequence, CyaZ does in fact contain an iron-sulfur cluster.

CD spectroscopy was used to probe the secondary structure and stability of CyaY. The CD spectrum was consistent with a structure with an α,β fold. This is consistent with the known 3-D structure of CyaY from *E. coli* which comprises a six-stranded antiparallel β-sheet flanked by two parallel α-helix. The CD spectrum was also used to probe the stability of CyaY to denaturation by heat or guanidine hydrochloride. The thermal denaturation curves of CyaY (*Pseudomonas. sp.* strain CF600), CyaY (*E. coli*), Hfra, and Yfh1 indicated melting temperatures of 42°C, 50.1±0.7°C, 69.4±0.04°C and 35.8±1.2°C, respectively (*16*). The length of the C-terminus was one of the variables that affected the stability of the frataxins. Yeast frataxin lacks additional hydrophobic residues Leu198, Leu200, Leu203, and Tyr205 that are present in Hfra. This renders this structure less stable than human frataxin since the function of these hydrophobic residues is to anchor the C-terminus to the groove by pointing precisely into the hydrophobic core for additional stability in structure. Although Tyr205 is absent in CyaY from *Pseudomonas sp.* strain CF600, Leu198 is conserved in CyaY. Residues Leu200 and Leu203 of Hfra is replaced by Phe200 and Ile203 in CyaY from *Pseudomonas sp.* strain CF600. Although Phe200 and Ile203 are both hydrophobic residues, the larger size of these two amino acids could have a destabilizing effect on the overall structure.

Upon addition of the reductant TCEP, there was only a small shift in the CD GuHCl induced denaturation curve. This is consistent with the fact that a disulfide-bonded dimer is a minor species in the CyaY sample. The addition of Fe(II) to CyaY from *E. coli*,

Hfra, or Yfh1 has been reported to increase the relative stabilities of these frataxin orthologues (*16*). However, the addition of Fe(II) to CyaY from *Pseudomonas sp.* strain CF600 quenched the CD signal, so it was impossible to conclude if stability was affected.

Fluorescence spectroscopy was also used to monitor the unfolding of CyaY from *Pseudomonas sp.* strain CF600 by guanidine hydrochloride. The 3 tryptophan, 1 tyrosine and 6 phenylalanine residues are the fluorophores (Fig. 46). As the concentration of GuHCl increased, there was a small increase in fluorescence intensity at 1.0 M GuHCl followed by a progressive decrease until, at 3 M GuHCl, CyaY was completely denatured (Fig. 26). Similar results were obtained using the integrated area under the fluorescence emission spectrum which takes into account both the red shift and a decrease in fluorescence intensity (data not shown). These results were essentially identical to those observed when denaturation was monitored by CD spectroscopy (Fig. 26). The addition of the reductant TCEP to samples did not affect the denaturation results (data not shown). The main transition from 1-3 M follows the shape of a curve expected for a single transition without intermediates.

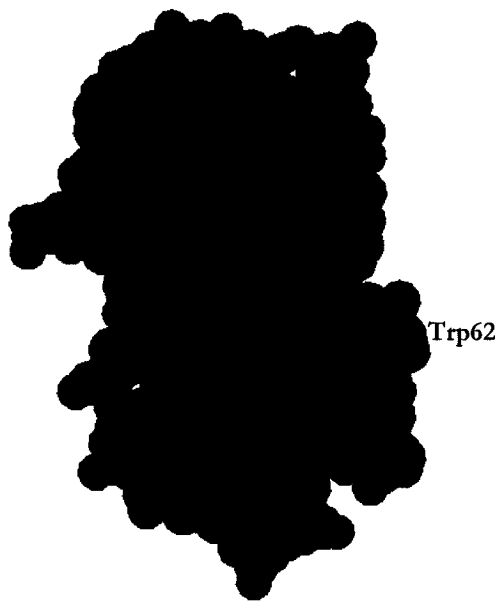

Figure 46: Spacefill model of the 3-D structure of CyaY from *Pseudomonas sp.* strain CF600 with Cys83, Tyr74, Trp62, Trp81 and Trp99 (Swiss-PDB) (*55*).

The emission spectrum of CyaY was significantly blue-shifted and decreased in fluorescence intensity compared to tryptophan and tyrosine model compounds. This indicates that the Trp and Tyr are in a more nonpolar environment compared to the model compounds or to the unfolded state, strongly suggesting that they are buried. Unfolding relieved most of the quenching, but comparisons with model compounds suggest that there is still some structure even at 6 M GuHCl. Alternatively, it is possible that the differences in fluorescence intensity between completely unfolded CyaY and the equivalent concentration of model compounds is caused by errors in the determination of concentration of protein, model compounds, or both. The predicted three-dimensional structure of CyaY suggests that the fluorophores are exposed to the environment in the native structure (Fig. 46). This is not consistent with the unfolding data and the simplest explanation is that the model generated for CyaY from *Pseudomonas sp.* strain CF600 is incorrect in the placement of these residues at the surface. The alternative explanation that they are buried at a dimer interface is not an alternative as the major form of CyaY is the monomer (see below).

The quaternary structure of CyaY was examined carefully, using analytical ultracentrifugation. The major species observed was always the monomer. Small amounts of dimer and tetramer were observed under all conditions and with all preparations of protein. Varying the concentration of CyaY over a range of 8.82-70.6 μM did not shift the equilibrium significantly. This indicates that the different species did not equilibrate significantly during the time course of the run (*90*). These results were similar to those reported for CyaY from *E. coli* (*40*), although there were small differences in molecular weight and sedimentation coefficient. Small quantities of dimer and tetramer species were observed under all conditions: for CyaY from *E. coli*, tetramer species were also reported. In addition, only the monomer appeared to be present in the *E. coli* CyaY preparations (*40*).

A sedimentation velocity run was done in the presence of reductant, TCEP, to see if the multimeric species disappeared (Fig. 29); this would indicate that the multimer was disulfide bonded. A similar distribution curve was observed for CyaY in the absence of TCEP. The CyaY preparation from *E. coli* contains two cysteine residues and experiments indicated that multimers of this protein were not disulfide-bonded either (*40*). Thus, the dimeric and tetrameric forms observed for CyaY from *Pseudomonas sp.* strain CF600 appear to be non-covalent complexes. Small amounts of multimeric species were observed for CyaY from *E. coli* in the presence of Fe(II) and an oxidant (*40*). The amounts formed were dependent on salt concentrations. These conditions were not used for the experiments reported here, but the effects of Fe(II) under anaerobic conditions, and of salt alone, were examined separately. The addition of Fe(II) under anaerobic conditions did not affect the distribution of species, nor did the addition of salt in the absence of iron. Addition of Fe(III) gave uninterpretable data since the absorbances in the cell were too high. These results indicate that CyaY from *Pseudomonas sp.* strain CF600 does not form a multimer in response to the presence of Fe(II). The effects of Fe(II) on aggregation under aerobic conditions were examined using gel electrophoresis.

Native gel electrophoresis has been used to demonstrate aggregation of the yeast frataxin homologue, Yfh1, in the presence of iron under aerobic conditions (*61*). Native gel electrophoresis showed three distinct bands consistent with monomer, dimer and tetramer forms of CyaY from *Pseudomonas sp.* strain CF600 (Fig. 31). The addition of Fe(II) under aerobic conditions where Fe(II) can oxidize to Fe(III) did not result in any aggregation. These findings indicate that *Pseudomonas sp.* strain CF600 CyaY does not behave like the yeast orthologue which assembles into large complexes around an iron core.

Iron-binding stoichiometry for CyaY was examined by a variety of methods. ITC binding experiments were performed to examine binding of Fe(II) and Mn(II) to CyaY. Mn(II) was used as substrate for Fe(II) since it does not oxidize readily and it can often substitute into binding sites for iron, as in ribonucleotide reductase (*106*). One binding site binding models yielded acceptable values for all the calorimetric data. Mn(II) bound with a stoichiometry of 1.1 ± 0.073, while Fe(II) bound with a stoichiometry of 0.79 ± 0.0032 (Fig. 33 and 34), consistent with 1:1 binding. The dissociation constant for Fe(II) was estimated to be 0.6 μM, while that for Mn(II) was much weaker with a K_d of 14 μM. A similar experiment with CyaY of *E. coli* showed a binding stoichiometry of two ferrous ions/monomer with a dissociation constant of K_d=3.8 μM (*40*). Thus, the *Pseudomonas* homologue binds one fewer iron, but more tightly. As the sequence identities of *Pseudomonas* and *E. coli* CyaY are only 39%, this is perhaps not unexpected. However, since the iron binding site for *E. coli* CyaY is only relatively broadly defined (see Introduction for a review), it is difficult to pinpoint specific substitutions that might be responsible for Fe(II) binding.

Attempts were also made to examine Mn(II) binding using fluorescence and CD spectroscopies. During titration with Mn(II), a small change was observed in the CD spectrum upon the addition of 1 Mn^{2+}/CyaY, but no significant changes were observed after a ratio of 10 Mn^{2+}/CyaY (Fig. 35). This is qualitatively consistent with what was observed during the ITC titration. Changes in the fluorescence properties of CyaY upon titration with Mn(II) were very small so it was difficult to conclude anything from these experiments.

Attempts were made to isolate iron-CyaY complexes for use in metalloproteins reconstitution assays. Using DEAE column chromatography, it was possible to isolate an Fe(III)-CyaY complex, but not an Fe(II)-CyaY complex (Fig. 36). It was perhaps not surprising that a stable Fe(II)-CyaY complex could not be obtained since Fe(II) must be

loosely bound if CyaY acts as an iron-chaperone, binding iron loosely so that it can readily adsorb or release iron depending on availability. The ability to isolate an Fe(III)-CyaY complex was initially of less interest since the apo proteins we are interested in reconstituting require Fe(II). However, given the observation that CyaY interacts with the iron-sulfur protein, CyaZ, the Fe(III)-CyaY complex may be useful in further studies of the interaction with CyaZ; for example, reduced CyaZ might be able to reduce Fe(III)-CyaY to Fe(II)-CyaY.

Chelators specific for Fe(II) have been used to monitor the ability of yeast and human frataxin orthologues to prevent iron oxidation and improve its availability (*64, 66*). Similar experiments were done using CyaY from *Pseudomonas sp.* strain CF600, with appropriate controls (Fig. 37). As was shown previously (*64, 66*), the buffer alone and holo-ferritin had no effect on the retardation of oxidation of Fe(II). As has been reported for the yeast and human frataxin orthologues, CyaY and CyaZ significantly hindered the oxidation of Fe(II) to Fe(III) allowing iron to become more bioavailable to BIPY. Interestingly, the combination of both CyaY and CyaZ had an enhanced effect on keeping the iron in a bioavailable form (Fig. 37C). This is the first indication that CyaZ might play a role in promoting iron bioavailability. The rate of spontaneous Fe(II) oxidation is also influenced by the ionic strength of certain anions (*112, 113*), explaining why addition of increasing KCl concentrations retarded oxidation of Fe(II) to Fe(III) in the experiments reported here (Fig. 37B). The effects of CyaY and KCl were cumulative, indicating that the interaction of CyaY with Fe(II) is not simply a nonspecific electrostatic interaction. Interestingly, DmpK, which has been reported to be involved in assembly of the binuclear iron center of phenol hydroxylase (*81*), also had the ability to retard Fe(II) oxidation.

Retarded Fe(II) oxidation kinetics were also observed for *E. coli* CyaY (*40*). A difference of approximately 2-fold in retardation of Fe(II) oxidation was observed, which is

a considerably smaller difference that that seen in Fig. 37A. Thus, it appears that the *Pseudomonas* CyaY might be a more effective protein in this regard, especially when it is accompanied by CyaZ.

One of the expected roles of frataxin is to maintain iron in a soluble form (*61*). A graphical demonstration of this ability was obtained by incubating Fe(II) in the presence or absence of CyaY, and observing the appearance of ferric oxyhydroxide precipitate in the samples (Fig. 38). Oxidation of iron in the presence of CyaY was slower, as shown by the lighter yellow coloration and the absence of precipitate (Fig. 38). This is a convincing demonstration that CyaY from *Pseudomonas sp.* strain CF600 can help maintain Fe(II) in a soluble form.

There are several iron-containing proteins that are part of the *dmp*-operon encoded phenol degradative pathway (*114-117*). It is possible that CyaY could play a role in assembling the iron centers of these proteins. DmpP and DmpQ both contain iron-sulfur clusters which, in other organisms, have been shown to involve the participation of frataxin orthologues in their assembly (*118, 119*). Catechol 2,3-dioxygenase (DmpB) is an Fe(II)-containing enzyme that catalyzes the conversion of catechol to α-hydroxymuconic ε-semialdehyde (*95-97*). The apo form of this enzyme can be generated easily by dialysis against chelators, and the holo form can be regenerated using ferrous iron salts, albeit slowly (*95-97*). The reconstitution of catechol 2,3-dioxygenase was therefore a simple system that could be used to monitor the effects of CyaY on iron insertion.

There was a significant influence on the rate and extent of reconstitution of apo catechol 2,3-dioxygenase by Fe(II) in the presence of CyaY (Fig. 39). This result is consistent with the results obtained for BIPY assays, which indicated that CyaY kept Fe(II) in a reduced form for a much longer period. No interaction between the proteins was detected

using EDC cross-linking (Fig. 44), but this does not rule out the possibility of complex formation, which has been observed in other frataxin mediated reactions (*66*).

Given the combined effects of CyaY and CyaZ on retarding Fe(II) oxidation, it was of interest to examine whether these two proteins interact. Cross-linking using EDC results in the appearance of a species with a molecular weight of ~20.1 kDa, which likely represents the bond formation between CyaZ (~8.4 kDa) and CyaY (12.5 kDa) (Fig. 41). This species was observed even using dilute solutions, suggesting that it is not the result of collision-induced cross-linking. Furthermore, the kinetics of the appearance of the cross-linked product were faster in comparison with a control reaction between BSA and CyaY (Fig. 42). Although the BSA-CyaY interaction was disrupted upon addition of NaCl (Fig. 43B), the addition of sodium chloride to the CyaY plus CyaZ mixture did not disrupt the protein-protein interaction. This result indicates that the interaction is not due to non-specific electrostatic interactions, and that it is not primarily electrostatic in nature.

Future Work

More studies must be done on CyaZ to determine its possible involvement in iron-trafficking in bacterial systems. Additional characterization of CyaZ using biophysical techniques is necessary. Furthermore, it would be of interest to examine whether CyaZ can participate in redox reactions with CyaY or CyaY-Fe(III). Finally, a CyaZ knockout may be helpful in trying to establish a physiological role for this protein

We have been interested for a number of years in the assembly of iron into the apo form of phenol hydroxylase from *Pseudomonas sp.* strain CF600 (*81*). The assembly of the oxo-bridged binuclear iron center appeared to be aided by a small protein, DmpK. *In vitro* studies of this process have been carried out using $Fe(NH_4)_2SO_4 \cdot 6H_2O$ but it would be preferable to use a biological iron donor. One potential donor is CyaY, possibly in combination with CyaZ. It would be of interest to observe the effect of CyaY on the reconstitution of apo-phenol hydroxylase.

Site-directed mutagenesis would be useful in studying the Fe(II) binding properties of CyaY. If the crystal structure of CyaY from *Pseudomonas sp.* strain CF600 was available, the selection of mutants would be simpler. On the basis of previous work done with *E. coli* homologue, the following 13 residues could be targets: Asp31, Gly37, Val38, Thr40, Gln54, Pro56, Gln59, Trp61, Leu62, Gly67, Asp72, Trp78, and Leu91 (*43*). Site-directed mutagenesis of these residues may assist in finding potential binding sites for Fe(II) or Fe(III). Random mutagenesis could be useful in finding residues that mediate the interaction between CyaY and CyaZ.

References

(1) James, S. C. (1998) Iron storage in bacteria. *Adv. Microb. Physiol. 40*, 281-351.

(2) Andrews, S. C., Robinson, A. K., and Rodriguez-Quinone, F. (2003) Bacterial iron homeostasis. *FEMS Microbiol. Rev. 27*, 215-237.

(3) Chiancone, E., Ceci, P., Ilari, A., Ribacchi, F., and Stefanini, S. (2004) Iron and proteins for iron storage and detoxification. *BioMetals 17*, 197-202.

(4) Hudson, S. J., Andrews, S. C., Hawkins, C., Williams, J. M., Izuhara, M., Meldrum, F. C., Mann, S., Harrison, P. M., and Guest, J. R. (1993) Overproduction, purification and characterization of the *Escherichia coli* ferritin. *Eur. J. Biochem. 218*, 985-995.

(5) Yariv, J., Kalb, A. J., Sperling, R., Bauminger, E. R., Cohen, S. G., and Ofer, S. (1981) The composition and the structure of bacterioferritin of *Escherichia coli*. *Biochem. J. 197*, 171-175.

(6) Zhao, G., Ceci, P., Ilari, A., Giangiacomo, L., Laue, T. M., Chiancone, E., and Chasteen, N. D. (2002) Iron and Hydrogen Peroxide Detoxification Properties of DNA-binding Protein from Starved Cells. *J. Biol. Chem. 277*, 27689-27696.

(7) Carrondo, M. A. (2003) Ferritins, iron uptake and storage from the bacterioferritin viewpoint. *EMBO J. 22*, 1959-1968.

(8) Harrison, P. M., and Arosio, P. (1996) The ferritins: molecular properties, iron storage function and cellular regulation. *Biochim. Biophys. Acta. 1275*, 161-203.

(9) Smith, J. (2004) The Physiological Role of Ferritin-Like Compounds in Bacteria *Crit. Rev. Microbiol. 30*, 173-185.

(10) Abdul-Tehrani, H., Hudson, A. J., Chang, Y. S., Timms, A. R., Hawkins, C., Williams, J. M., Harrison, P. M., Guest, J. R., and Andrews, S. C. (1999) Ferritin mutants of *Escherichia coli* are iron deficient and growth impaired, and *fur* mutants are iron deficient. *J. Bacteriol. 181*, 1415-1428.

(11) Altuvia, S., Almiron, M., Huisman, G., Kolter, R., and G., S. (1997) The *dps* promoter is activated by OxyR during growth and by IHF and sigma S in stationary phase. *Mol. Microbiol. 13*, 265-272.

(12) Martinez, A., and Kolter, R. (1997) Protection of DNA during oxidative stress by the nonspecific DNA-binding protein Dps. *J. Bacteriol. 179*, 5188-5194.

(13) Delatycki, M. B., Williamson, R., and Forrest, S. M. (2000) Friedreich ataxia: an overview. *J. Med. Genet. 37*, 1-8.

(14) Pandolfo, M. (2002) The Molecular Basis of Friedreich Ataxia-Frataxin Structure and Function. *Adv. Exp. Med. Biol. 516*, 108.

(15) Fujita, R., Agid, Y., Trouillas, P., Seck, A., Thommasi-Davenas, C., Driesel, A. J., Olek, K., Grzeschik, K.-H., Nakamura, Y., Mandel, J. L., and Hanauer, A. (1989) Confirmation of Linkage of Friedreich Ataxia to Chromosome 9 and Identification of a New Closely Linked Marker. *Genomics 4*, 110-111.

(16) Adinolfi, S., Nair, M., Politou, A., Bayer, E., Martin, S., Temussi, P., and Pastore, A. (2004) The Factors Governing the Thermal Stability of Frataxin Orthologues: How To Increase a Protein's Stability. *Biochem. 43*, 6511-6518.

(17) Bradley, J. L., Blake, J. C., Chamberlain, S., Thomas, P. K., Cooper, J. M., and A.H.V., S. (2000) Clinical, biochemical and molecular genetic correlations in Friedreich's ataxia. *Hum. Mol. Genet. 9*, 275-282.

(18) Pandolfo, M. (2002) Frataxin deficiency and mitochondrial dysfunction. *Mitochondrion 2*, 87-93.

(19) Gibson, T. J., Koonin, E. V., Musco, G., Pastore, A., and Bork, P. (1996) Friedreich's ataxia protein: phylogenetic evidence for mitochondrial dysfunction. *Trends. Neurosci. 19*, 465-468.

(20) Musco, G., Stier, G., Kolmerer, B., Adinolfi, S., Martin, S., Frenkiel, T., Gibson, T., and Pastore, A. (2000) Towards a structural understanding of Friedreich's ataxia: the solution structure of frataxin. *Struct. 8*, 695-707.

(21) Puccio, H., and Koenig, M. (2002) Friedreich ataxia: a paradigm for mitochondrial diseases. *Curr. Opin. Genet. Dev. 12*, 272-277.

(22) Wilson, R. B. (2003) Frataxin and frataxin deficiency in Friedreich's ataxia. *J. Neurol. Sci. 207*, 103-105.

(23) Yoon, T., and Cowan, J. A. (2003) Iron-Sulfur Cluster Biosynthesis. Characterization of Frataxin as an Iron Donor for Assembly of [2Fe-2S] Clusters in ISU-Type Proteins *J. Am. Chem. Soc. 125*, 6078-6084.

(24) Jiralerspong, S., Liu, Y., Montermini, L., Stifani, S., and Pandolfo, M. (1997) Frataxin Shows Developmentally Regulated Tissue-Specific Expression in the Mouse Embryo. *Neurobiol. Dis. 4*, 103-113.

(25) Lodi, R., Cooper, J. M., Bradley, J. L., Manners, D., Styles, P., Taylor, D. J., and Schapira, A. H. V. (1999) Deficit in i*n vivo* mitochondrial ATP production in patients with Friedreich ataxia. *Proc. Natl. Acad. Sci. USA 96*, 11492-11495.

(26) Tan, G., Chen, L.-S., Lonnerdal, B., Gellera, C., Taroni, F. A., and Cortopassi, G. A. (2001) Frataxin expression rescues mitochondrial dysfunctions in FRDA cells. *Hum. Mol. Genet. 10*, 2099-2107.

(27) Koutnikova, H., Campuzano, V., Foury, F., Dollé, P., Ornella, C., and Koenig, M. (1997) Studies of human, mouse and yeast homologues indicate a mitochondrial function for frataxin. *Nat. Genet. 16*, 345-351.

(28) Puccio, H., Simon, D., Cossée, M., Criqui-Filipe, P., Tiziano, F., Melki, J., Hindelang, C., Matyas, R., Rustin, P., and Koenig, M. (2001) Mouse models for Friedreich ataxia exhibit cardiomyopathy, sensory nerve defect and Fe-S enzyme deficiency followed by intramitochondrial iron deposits. *Nat. Genet. 27*, 181-185.

(29) Cossée, M., Puccio, H., Gansmuller, A., Koutnikova, H., Dierich, A., LeMeur, M., Fischbeck, K., Dollé, P., and Koenig, M. (2000) Inactivation of the Friedreich ataxia mouse gene leads to early embryonic lethality without iron accumulation. *Hum. Mol. Genet. 9*, 1219-1226.

(30) Babcock, M., de Silva, D., Oaks, R., Davis-Kaplan, S., Jiralerspong, S., Montermini, L., Pandolfo, M., and Kaplan, J. (1997) Regulation of Mitochondrial Iron Accumulation by Yfh1p, a Putative Homolog of Frataxin. *Science 276*, 1709-1712.

(31) Cavadini, P., Gellera, C., Patel, P. I., and Isaya, G. (2000) Human frataxin maintains mitochondrial iron homeostasis in *Saccharomyces cerevisiae*. *Hum. Mol. Genet. 9*, 2523-2530.

(32) Branda, S. S., Yang, Z.-Y., Chew, A., and Isaya, G. (1999) Mitochondrial intermediate peptidase and the yeast frataxin homolog together maintain mitochondrial iron homeostasis in *Saccharomyces cerevisiae*. *Hum. Mol. Genet. 8*, 1099-1110.

(33) Foury, F., and Talibi, D. (2001) Mitochondrial Control of Iron Homeostasis. *J. Biol. Chem. 276*, 7762-7768.

(34) Lesuisse, E., Santos, R., Matzanke, B. F., Knight, S. A. B., Camadro, J.-M., and Dancis, A. (2003) Iron use for haeme synthesis is under control of the yeast frataxin homologue (Yfh1). *Hum. Mol. Genet. 12*, 879-889.

(35) Sheng, L. D., Ohshima, K., Jiralerspong, S., Bojanowski, M. W., and Pandolfo, M. (1999) Knock-out of the *cyaY* gene in *Escherichia coli* does not affect cellular iron content and sensitivity to oxidants. *FEBS Lett. 456*, 13-16.

(36) Huynen, M. A., Snel, B., Bork, P., and Gibson, T. J. (2001) The phylogenetic distribution of frataxin indicates a role in iron-sulfur cluster protein assembly. *Hum. Mol. Genet. 10*, 2463-2468.

(37) Lutz, T., Westermann, B., Neupert, W., and Herrmann, J. M. (2001) The Mitochondrial Proteins Ssq1 and Jac1 are Required for the Assembly of Iron Sulfur Clusters in Mitochondria. *J. Mol. Biol. 307*, 815-825.

(38) Tokumoto, U., Nomura, S., Minami, Y., Mihara, H., Kato, S., Kurihara, T., Esaki, N., Kanazawa, H., Matsubara, H., and Takahashi, Y. (2002) Network of protein-protein interactions among iron-sulfur cluster assembly proteins in *Escherichia coli. J. BIochem. 131*, 713-719.

(39) Gerber, J., Mühlenhoff, U., and Lill, R. (2003) An interaction between frataxin and Isu1/Nfs1 that is crucial for Fe/S cluster synthesis on Isu1. *EMBO rep. 4*, 906-911.

(40) Bou-Abdalla, F., Adinolfi, S., Pastore, A., Laue, T. M., and Chasteen, N. D. (2004) Iron Binding and Oxidation Kinetics in Frataxin CyaY of *Escherichia coli. J. Mol. Biol. 341*, 605-615.

(41) Schoenfeld, R. A., Napoli, E., Wong, A., Zhan, S., Reutenauer, L., Morin, D., Buckpitt, A. R., Taroni, F., Lonnerdal, B., Ristow, M., Puccio, H., and Cortopassi, G. A. (2005) Frataxin in deficiency alters heme pathway transcripts and decreases mitochondrial heme metabolites in mammalian cells. *Hum. Mol. Genet. 14*, 3787-3799.

(42) Adinolfi, S., Trifuoggi, M., Martin, S., and Pastore, A. (2002) A structural approach to understanding the iron-binding properties of phylogenetically different frataxins. *Hum. Mol. Genet. 11*, 1865-1877.

(43) Cho, S.-J., Lee, M. G., Yang, J. K., Lee, J. Y., Song, H. K., and Suh, S. W. (2000) Crystal structure of *Escherichia coli* CyaY protein reveals a previously unidentified fold for the evolutionarily conserved frataxin family. *Proc. Nat. Aca. Soc. 97*, 8932-8937.

(44) Dhe-Paganon, S., Shigeta, R., Chi, Y.-I., Ristow, M., and Shoelson, S. E. (2000) Crystal Structure of Human Frataxin. *J. Biol. Chem. 275*, 30753-30756.

(45) Nair, M., Adinolfi, S., Pastore, C., Geoff, K., Temussi, P., and Pastore, A. (2004) Solution Structure of the Bacterial Frataxin Ortholog, CyaY: Mapping the Iron Binding Sites. *Struct. 12*, 2037-2048.

(46) Trotot, P., Sismeiro, O., Vivares, C., Glaser, P., Bresson-Roy, A., and Danchin, A. (1996) Comparative analysis of the cya locus in enterobacteria and related gram-negative facultative anaerobes. *Biochim. 78*, 277-287.

(47) Danchin, A., and Lenzen, G. (1988) Structure and evolution of bacterial adenylate cyclase: comparison between *Escherichia coli* and *Erwinia chrysanthemi. Second Messengers Phosphoproteins 12*, 7-28.

(48) Fleischmann, R. D., Adams, M. D., White, O., Clayton, R. A., Kirkness, E. F., Kerlavage, A. R., Bult, C. J., Tomb, J. F., Dougherty, B. A., Merrick, J. M., and al. (1995) Whole-genome random sequencing and assembly of *Haemophilus influenzae Rd. Science 269* 496-512.

(49) Jacq, C., Alt-Moerbe, J., Andre, B., Arnold, W., Bahr, A., Ballesta, J. P. G., and Bargues, M. (1997) The nucleotide sequence of *Saccharomyces cerevisiae* chromosome IV. *Nature 387*, 75-78.

(50) Andersson, S. G., Zomorodipour, A., Andersson, J. O., Sicheritz-Ponten, T., Alsmark, U. C., Podowski, R. M., Naslund, A. K., Eriksson, A. S., Winkler, H. H., and Kurland, C. G. (1998) The genome sequence of *Rickettsia prowazekii* and the origin of mitochondria. *Nature 396*, 133-140.

(51) Wood, V., Gwilliam, R., Rajandream, M. A., Lyne, M., Lyne, R., Stewart, A., Sgouros, J., and al. (2002) The genome sequence of *Schizosaccharomyces pombe. Nature 6874*, 871-880.

(52) Campuzano, V., Montermini, L., Molto, M. D., Pianese, L., Cossee, M., Cavalcanti, F., Monros, E., Rodius, F., Duclos, F., Monticelli, A., Zara, F., and Canizares, J. e. a. (1996) Friedreich's ataxia: autosomal recessive disease caused by an intronic GAA triplet repeat expansion. *Science 271*, 1423-1427.

(53) He, Y., Alam, S. L., Proteasa, S. V., Zhang, Y., Lesuisse, E., Dancis, A., and Stemmler, T. L. (2004) Yeast Frataxin Solution Structure, Iron Binding, and Ferrochelatase Interaction. *Biochem. 43*, 16254-16262.

(54) Lee, M. G., Cho, S.-J., Yang, J. K., Song, H. K., and Suh, S. W. (2000) Crystallization and preliminary X-ray crystallographic analysis of *Escherichia coli* CyaY, a structural homologue of human frataxin. *Acta Crystallographica 56*, 920-921.

(55) Guex, N., and Peitsch, M. C. (1997) SWISS-MODEL and the Swiss-PdbViewer: An environment for comparative protein modeling. *Electrophoresis 18*, 2714-2723.

(56) http://www.accelrys.com/.

(57) Chasteen, N. D., and Harrison, P. M. (1999) Mineralization in Ferritin: An Efficient Means of Iron Storage. *J. Struc. Biol. 126*, 182-194.

(58) Gakh, O., Adamec, J., Gacy, A. M., Twesten, R. D., Owen, W. G., and Isaya, G. (2002) Physical Evidence that Yeast Frataxin Is an Iron Storage Protein. *Biochem. 41*, 6798-6804.

(59) O'Neil, H. A., Gakh, O., and Isaya, G. (2005) Supramolecular Assemblies of Human Frataxin are Formed *via* Subunit-Subunit Interactions Mediated by a Non-conserved Amino-terminal Region. *J. Mol. Biol. 345*, 433-439.

(60) Cavadini, P., O'Neil, H. A., Benada, O., and Isaya, G. (2002) Assembly and iron-binding properties of human frataxin, the protein deficient in Friedreich ataxia. *Hum. Mol. Genet. 11*, 217-227.

(61) Adamec, J., Rusnak, F., Owen, W. G., Naylor, S., Benson, L. M., Gacy, A. M., and Isaya, G. (2000) Iron-Dependent Self-Assembly of Recombinant Yeast Frataxin: Implications for Friedreich Ataxia. *Am. H. Hum. Genet. 67*, 549-562.

(62) Yoon, T., and Cowan, J. A. (2004) Frataxin-mediated Iron Delivery to Ferrochelatase in the Final Step of Heme Biosynthesis. *J. Biol. Chem. 279*, 25943-25946.

(63) Park, S., Gakh, O., Mooney, S. M., and Isaya, G. (2002) The Ferroxidase Activity of Yeast Frataxin. *J. Biol. Chem. 277*, 38589-38595.

(64) Park, S., Gakh, O., O'Neil, H. A., Mangravitas, A., Nichol, H., Ferreira, G. C., and Isaya, G. (2003) Yeast Frataxin Sequentially Chaperones and Stores Iron by Coupling Protein Assembly with Iron Oxidation. *J. Biol. Chem. 278*, 31340-31351.

(65) Nichol, H., Gakh, O., O'Neil, H. A., Pickering, I. I., Isaya, G., and George, G. N. (2003) Structure of Frataxin Iron Cores: An X-ray Absorption Spectroscopic Study. *Biochem. 42*, 5971-5976.

(66) O'Neil, H. A., Gakh, O., Park, S., Cui, J., Mooney, S. M., Sampson, M., Ferreira, G. C., and Isaya, G. (2005) Assembly of Human Frataxin Is a Mechanism for Detoxifying Redox-Active Iron. *Biochem. 44*, 537-545.

(67) Labuda, M., Poirier, J., and Pandolfo, M. (1999) A Missense Mutation (W155R) in an American Patient with Friedreich Ataxia. *Hum. Mutat. 13*, 506-507.

(68) Ilari, A., Stefanini, S., Chiancone, E., and Tsernoglou, D. (2000) The dodacameric ferritin from *Listeria innocua* contains a novel intersubunit iron-binding site. *Nat. Struc. Biol. 7*, 38-43.

(69) Thompson, J. D., Gibson, T. J., Plewniak, F., Jeanmougin, F., and Higgins, D. G. (1997) The ClustalX windows interface: flexible strategies for multiple sequence alignment aided by quality analysis tools. *Nucleic Acids Res. 25*, 4876-7882.

(70) Cossee, M., Durr, A., Schmitt, M., Dahl, N., Pandolfo, M., and al. (1999) Friedreich's ataxia: point mutations and clinical presentation of compound heterozygotes. *Ann. Neurol. 45*, 200-206.

(71) Campuzano, V., Montermini, L., Molto, M. D., Pianese, L., Cossee, M., and al. (1996) Friedreich's Ataxia: Autosomal Recessive Disease Caused by an Intronic GAA Triplet Repeat Expansion. *Science 271*, 1423-1427.

(72) Lloyd, S. J., Lauble, H., Prasad, G. S., and Stout, C. D. (1999) The mechanism of aconitase: 1.8Å resolution crystal structure of the S642A:citrate complex. *Protein. Sci. 8*, 2655-2662.

(73) Rötig, A., de Lonlay, P., Chretien, D., Foury, F., Koenig, M., Sidi, D., Munnich, A., and Rustin, P. (1997) Aconitase and mitochondrial iron-sulphur protein deficiency in Friedreich ataxia *Nat. Genet. 17*, 215-217.

(74) Stryer, L. (1995) *Biochemistry*, 4 ed., Freeman, United States of America.

(75) Bulteau, A.-L., Ikeda-Saito, M., and Szweda, L. I. (2003) Redox-Dependent Modulation of Aconitase Activity in Intact Mitochondria. *Biochem. 42*, 14846-14855.

(76) Bulteau, A.-L., O'Neil, H. A., Kennedy, M. C., Ikeda-Saito, M., Isaya, G., and Szweda, L. I. (2004) Frataxin Acts as an Iron Chaperone Protein to Modulate Mitochondrial Aconitase Activity. *Science 305*, 242-245.

(77) Sellers, V. M., Wu, C.-K., Dailey, T. A., and Dailey, H. A. (2001) Human Ferrochelatase: Characterization of Substrate-Iron Binding and Proton-Abstracting Residues. *Biochem. 40*, 9821-9827.

(78) Wu, C.-K., Dailey, H. A., Rose, J. P., Burden, A., Sellers, V. M., and Wang, B.-C. (2001) The 2.0Å structure of human ferrochelatase, the terminal enzyme of heme biosynthesis. *Nat. Struc. Biol. 8*, 156-160.

(79) Hanahan, D. (1985) *in DNA Cloning: A Practical Approach*, Vol. 1, Glover, D.M., ed., IRL Press Ltd., Oxford.

(80) Rosenberg, A. H., Lade, B. N., Chui, D.-S., Lin, S.-W., Dunn, J. J., and Studier, F. W. (1987) Vectors for selective expression of cloned DNAs by T7 RNA polymerase. *Gene 56*, 125-135.

(81) Powlowski, J., Sealy, J., Shingler, V., and Cadieux, E. (1997) On the Role of DmpK, an Auxiliary Protein Associated with Multicomponent Phenol Hydroxylase from *Pseudomonas* sp. Strain CF600. *J. Biol. Chem. 272*, 945-951.

(82) Shingler, V., Franklin, C. H., Tsuda, M., Holroyd, D., and Bagdasrian, M. (1989) Molecular analysis of a plasmid-encoded Phenol Hydroxylase from *Pseudomonas* CF600. *J. Gen. Microbiol. 135*, 1083-1092.

(83) Ausubel, F. M., Brent, R., Kingston, R. E., Moore, D. D., Seidman, J. G., Smith, J. A., and Struhl, K. (1994-1998) *Current Protocols in Molecular Biology*, Vol. 1, John Wiley & Sons Inc., United States of America.

(84) Sambrook J, Fritsch, E. F., and Maniatis, T. (1989) *Molecular Cloning: A Laboratory Manual*, Cold Spring Harbor Laboratory Press, Cold Spring Harbor, NY.

(85) Ausubel, F. M., Brent, R., Kingston, R. E., Moore, D. D., Seidman, J. G., Smith, J. A., and Struhl, K. (1994-1998) *Current Protocols in Molecular Biology*, Vol. 4., John Wiley & Sons Inc., United States of America.

(86) Laemmli, U. K. (1970) Cleavage of a Structural Protein during the Assembly of the Head of Bacteriophage T4. *Nat. 227*, 680-685.

(87) Schägger, H., and Jagow, G. v. (1987) Tricine-sodium dodecyl sulfate-polyacrylamide gel electrophoresis for the separation of proteins in the range from 1 to 100 kDa *Anal. Biochem. 166*, 368-379.

(88) Ausubel, F. M., Brent, R., Kingston, R. E., Moore, D. D., Seidman, J. G., Smith, J. A., and Struhl, K. (1994-1998) *Current Protocols in Molecular Biology*, Vol. 2, John Wiley & Sons Inc., United States of America.

(89) Morrissey, J. H. (1981) Silver Stain for Proteins in Polyacrylamide Gels: A Modified Procedure with Enhanced Uniform Sensitivity. *Anal. Biochem. 117*, 307-310.

(90) Schuck, P. (2000) Size distribution analysis of macromolecules by sedimentation velocity ultracentrifugation and Lamm equation modeling. *Biophys. J. 78*, 1606-1619.

(91) Brown, R. E., Jarvis, K. L., and Hyland, K. J. (1989) Protein measurement using bicinchoninic acid: elimination of interfering substances. *Anal. Biochem. 180*, 136-139.

(92) Gill, S. C., and von Hippel, P. H. (1989) Calculation of protein extinction coefficients from amino acid sequence data. *Anal. Biochem. 182*, 319-326.

(93) Pace, C. N., and Schmid, F. X. (1998) *Structure: A Functional Approach* TE. Creighton Ed. IRL Press.

(94) Percival, M. D. (1991) Human 5-Lipoxygenase Contains an Essential Iron. *J. Biol. Chem. 266*, 10058-10061.

(95) Kobayashi, T., Ishida, T., Horiike, K., Takahara, Y., Naganori, N., Nakazawa, A., Nakazawa, T., and Nozaki, M. (1995) Overexpression of *Pseudomonas putida* Catechol 2,3-Dioxygenase with High Specific Activity by Genetically Engineered *Escherichia coli. J. BIochem. 117*, 614-622.

(96) Takemori, S., Komiyama, T., and Katagiri, M. (1971) Apo- and Reconstituted Holoenzymes of Metapyrocatechase from *Pseudomonas putida. Eur. J. Biochem. 23*, 178-184.

(97) Nozaki, M. (1970) Metapyrocatechase (*Pseudomonas*). *Methods in Enzymol 17A*, 522-525.

(98) Nelson, K. E., Weinel, C., Paulsen, I. T., and Dodson, R. J. (2002) Complete genome sequence and comparative analysis of the metabolically versatile *Pseudomonas putida* KT2440. *Environ. Microbiol. 4*, 799-808.

(99) Vincze, T., Posfai, J., and Roberts, R. J. (2003) NEBcutter: a program to cleave DNA with restriction enzymes. *Nucleic Acids Res. 31*, 3688-3691.

(100) Joardar, V., Lindeberg, M., Jackson, R., Selengut, J., Dodson, R., Brinkac, L. M., Daugherty, S. C., DeBoy, R. T., Durkin, A. S., Giglio, M. G., Madupu, R., Nelson, W. C., Rosovitz, M. J., Sullivan, S. A., Crabtree, J., Creasy, T., Davidsen, T. M., Haft, D. H., Zafar, N., Zhou, L., Halpin, R., Holley, T., Khouri, H. M., Feldblyum, T. V., White, O., Fraser, C. M., Chatterjee, A. K., Cartinhour, S., Schneider, D., Mansfield, J., Collmer, A., and Buell, R. (2005) Whole-genome sequence analysis of *Pseudomonas syringae* pv. phaseolicola 1448A reveals divergence among pathovars in genes involved in virulence and transposition. *J. Bacteriol. 187*, 6488-6498.

(101) Copeland, A., Lucas, S., Lapidus, A., Barry, K., Detter, J. C., Glavina, T., Hammon, N., Israni, S., Pitluck, S., Saunders, E. H., Schmutz, J., Larimer, F., Land, M., Kyripides, N., Anderson, I., and Richardson, P. Complete sequence of *Pseudomonas fluorescens* PfO-1. *Unpublished.*

(102) Blattner, F. R., Plunkett, G. I., Bloch, C. A., Perna, N. T., Burland, V., Riley, M., Collado-Vides, J., Glasner, J. D., Rode, C. K., Mayhew, G. F., Gregor, J., Davis, N. W., Kirkpatrick, H. A., Goeden, M. A., Rose, D. J., Mau, B., and Shao, Y. (1997) The complete genome sequence of *Escherichia coli* K-12. *Science 277*, 1453-1474.

(103) Stover, C. K., Pham, X.-Q. T., Erwin, A. L., Mizoguchi, S. D., Warrener, P., Hickey, M. J., Brinkman, F. S. L., Hufnagle, W. O., Kowalik, D. J., Lagrou, M., Garber, R. L., Goltry, L., Tolentino, E., Westbrook-Wadman, S., Yuan, Y., Brody, L. L., Coulter, S. N., Folger, K. R., Kas, A., Larbig, K., Lim, R. M., Smith, K. A., Spencer, D. H.,

Wong, G. K.-S., Wu, Z., Paulsen, I. T., Reizer, J., Saier, M. H., Hancock, R. E. W., Lory, S., and Olson, M. V. (2000) Complete genome sequence of *Pseudomonas aeruginosa* PA01, an opportunistic pathogen. *Nature 406*, 959-964.

(104) Findlay, W. A., Martin, S. R., Beckingham, K., and Bayley, P. M. (1995) Recovery of Native Structure by Calcium Binding Site Mutants of Calmodulin upon Binding of *sk*-MLCK Target Peptides. *Biochem. 37*, 2084-2094.

(105) Perozzo, R., Folkers, G., and Scapozza, L. (2004) Thermodynamics of Protein-Ligand Interactions: History, Presence, and Future Aspects. *J. Recept. Signal. Transduct. 24*, 1-52.

(106) Hogbom, M., Andersson, M. E., and Nordlund, P. (2001) Crystal structures of oxidized dinuclear manganese centres in Mn-substituted class I ribonucleotide reductase from *Escherichia coli:* carboxylate shifts with implications for O_2 activation and radical generation *J. Biol. Inorg. Chem. 6*, 315-323.

(107) Dailey, H. A., Michael, J., Finnegan, G., and Johnson, M. K. (1994) Human Ferrochelatase Is an Iron-Sulfur Protein. *Biochem. 33*, 403-407.

(108) Dailey, T. A., and Dailey, H. A. (2002) Identification of [2Fe-2S] Clusters in Microbial Ferrochelatases. *J. Bacteriol. 184*, 2460-2464.

(109) Orme-Johnson, W. H. (1973) Iron-Sulfur Proteins: Structure and Function. *Ann. Rev. Biochem. 42*, 159-204.

(110) Grabarek, Z., and Gergely, J. (1990) Zero-Length Crosslinking Procedure with the Use of Active Esters. *Anal. Biochem. 185*, 131-135.

(111) Gerber, J., and Lill, R. (2002) Biogenesis of iron–sulfur proteins in eukaryotes: components, mechanism and pathology *Mitochondrion 2*, 71-86.

(112) Millero, F. J., and Izaguirre, M. (1989) Effect of ionic strength and ionic interactions on the oxidation of Fe(II). *J. Sol. Chem. 18*, 585-599.

(113) Millero, F. J., Yao, W., and Aicher, J. (1995) The speciation of Fe(II) and Fe(III) in natural waters. *Marine Chem. 50*, 21-39.

(114) Cadieux, E., and Powlowski, J. (1999) Characterization of Active and Inactive Forms of the Phenol Hydroxylase Stimulatory Protein DmpM. *Biochem. 38*, 10714-10722.

(115) Nordlund, I., Powlowski, J., and Shingler, V. (1990) Complete Nucleotide Sequence and Polypeptide Analysis of Multicomponent Phenol Hydroxylase from *Pseudomonas* sp. Strain CF600. *J. Bacteriol. 172*, 6826-6833.

(116) Powlowski, J., and Shinger, V. (1990) In Vitro Analysis of Polypeptide Requirements of Multicomponent Phenol Hydroxylase from *Pseudomonas sp.* Strain CF600 *J. Bacteriol. 172*, 6834-6840.

(117) Qian, H., Edlund, U., Powlowski, J., Shingler, V., and Sethson, I. (1997) Solution Structure of Phenol Hydroxylase Protein Component P2 Determined by NMR Spectroscopy. *Biochem. 36*, 495-504.

(118) Cadieux, E., Vrajmasu, V., Achim, C., Powlowski, J., and Münck, E. (2002) Biochemical, Mössbauer, and EPR Studies of the Diiron Cluster of Phenol Hydroxylase from *Pseudomonas sp.* Strain CF600. *Biochem. 41*, 10680-10691.

(119) Shingler, V., Powlowski, J., and Marklund, U. (1992) Nucleotide Sequence and Functional Analysis of the Complete Phenol/3,4-Dimethylphenol Catabolic Pathway of *Pseudomonas sp.* Strain CF600. *J. Bacteriol. 174*, 711-724.